2011

An Approach to Improve the Failure Rate Model of a Solid State Laser by Utalizing the Physics of Failure Methodology

Omar L. Thompson
University of Central Florida

AN APPROACH TO IMPROVE THE FAILURE RATE MODEL OF A SOLID STATE LASER BY UTALIZING THE PHYSICS OF FAILURE METHODOLOGY.

by
OMAR L THOMPSON

B.S. University of Central Florida, 2001
M.S. University of Central Florida, 2003
M.S. University of Central Florida, 2010

A dissertation submitted in partial fulfillment of the requirements
for the degree of Doctor of Philosophy in Modeling and Simulation
in the College of Sciences
at the University of Central Florida
Orlando, Florida

Fall Term
2011

Michael Bass (Co-Chair) - CREOL

Peter Kincaid (Co-Chair) - IST

ABSTRACT

The ability to predict the failure rate of any military laser is very critical. In-field laser usage does not support the troubleshooting and repairing of a complex electro optical system. The only published laser failure rate model was last updated by the Department of Defense in 1975. Consequently, the failure rate predicted is inaccurate due to model deficiencies.

This dissertation has developed a laser failure rate model for diode pumped lasers with improved failure rate prediction accuracy. The model has surpassed the capabilities of the Department of Defense model by the inclusion of key performance attributes that are currently not taken into account. The scope of work completed was based on a tailored Physics of Failure methodology. The research approach implemented was:

1. Integration of Failure Mode and Effects Analysis to evaluate deployed laser failure.
2. Beam simulation for alignment tolerance analysis.
3. Thermal and vibration effects analysis on laser performance.
4. Analysis and development of a methodology to represent a resonator failure rate model.

A secondary contribution of this research effort is supporting the update of the current laser failure rate model. The success of revising the current model relies on leveraging the work of other organizations in the area of failure rate modeling and reliability predictions.

This dissertation is dedicated to my father and mentor, the late Maurice Keith Thompson Sr.

ACKNOWLEDGMENTS

There are many people who made commitments and sacrifices to support me on this journey to complete my course of study that began many years ago. Without them it would not be possible. At this junction I would like to take this opportunity to thank them for their continued guidance, advice and support over the years that has culminated in the successful completion of this course of study. I would like to acknowledge my committee members; Drs Michael Bass, Thomas Clarke, John Kincaid, Randall Shumaker and Rudolf Wiegand for investing their time and effort to support this research. A special note of thanks is extended to my committee co-chairs, Drs Michael Bass and John Kincaid for their critical insight, guidance, technical knowledge and positive criticism that guided my pen and focused my ideas to complete this research. Please accept my thanks and appreciation.

My family has been instrumental on my journey to complete my PhD. There were many instances during my academic career when their support and sacrifice was needed to enable the continuation of my education. I cannot express enough gratitude and thanks to them for their support and advice to succeed when there were challenges to overcome and for the times when I needed the motivation to carry on and complete the journey. To my wife, Heather thanks for your support in juggling our family life, my full-time career and working to complete this research. To my parents, Dannalin and the late Maurice Thompson Sr. words cannot express my gratitude for all that you have done in all aspects of my life and education. To my siblings Chandra, Maurice and Toni, please know that I truly appreciate your support over the years.

TABLE OF CONTENTS

LIST OF FIGURES

LIST OF TABLES

LIST OF ABBREVIATIONS/ACRONYMS

CND	Could Not Duplicate
DFMEA	Design Failure Modes and Effects Analysis
DoD	Department of Defense
DP	Diode Pumped
FEA	Finite Element Analysis
FMEA	Failure Modes and Effect Analysis
FR	Failure Rate
FY	Fiscal Year
GLAD	General Laser Analysis and Design Software package
M1	Mirror 1
M2	Mirror 2
MIL-HDBK-217	Military Handbook 217
MLE	Maximum Likelihood Estimation
MTBF	Mean Time Between Failures
MT	Mean Time
NFF	No Fault Found
NSRAM	New System Reliability Assessment Methodology
Nd: YAG	Neodymium Doped Yttrium Aluminum Garnet
PCM	Photonic Component Model
PDF	Probability Density Function
PFMEA	Process Failure Mode and Effect Analysis
PoF	Physics of Failure
RAC	Reliability Analysis Center
R&D	Research and Development
RIAC	Reliability Information Analysis Center
RPN	Risk Priority Number
RR	Rank Regression
SFMEA	System Failure Modes and Effects Analysis
TEM	Transverse Electromagnetic Modes
USAF	United States Air Force
VOA	Variable Optical Attenuators

CHAPTER ONE: INTRODUCTION

"The U.S. Army first began using military lasers in 1965. At that time, lasers were developed and used as range finders because of their extreme accuracy at measuring distances" (Ozberkmen 1989, p.16). Over the next several decades, military spending on lasers has increased significantly based on:

- The tactical advantage obtained using laser technology from several miles away for enemy detection and designation.
- The ability to reduce the number of casualties by increasing the distance between the solder and the enemy.

According to Ozberkmen (1989) during the three-year funding period from fiscal year, (FY) 87 to (FY) 89, the total defense-related research and development allocations were $164.5 billion. Over this period, the Department of Defense,(DoD) spent $795 million on laser research and development (R&D) with more than half of this going towards laser weapons technology, according to a budget report prepared by the American Association for the Advancement of Science. As a result, development and maintenance costs have evolved as the determinant for how much money the DoD is willing to invest into the advancement of new laser technologies. Compounding the expenditure calculations is the additional costs of maintaining deployed lasers when estimating their failure rate (FR) is unpredictable at best.

The DoD has continued funding the research and advancement of laser technology in an effort to develop and manufacture more precise, efficient and compact lasers. Yet the

methodology used to predict laser reliability, specifically the failure rate (FR) has not evolved in three and a half decades. There has been no published research that details or identifies any improvement to the first functional laser prediction model after 1975. The lack of model updates has resulted in inaccurate FR predictions and reliability over estimation.

The best method to increase the accuracy of the laser FR model should be viewed from a top down approach starting with the current model. Functionally, the current laser FR model located in Section 8.4 of MIL-HDBK-217F Notice 2 is the representative equivalent of a laser resonator. Functionally, a laser resonator is comprised of a pump source, a gain media and two mirrors that are optically aligned to each other as shown in Figure 1.

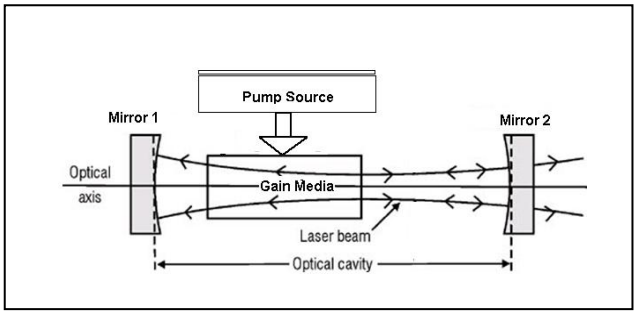

Figure 1: Optical Components of a Laser Resonator.

In solid state lasers, the pump source can be either a flash lamp, (technically identified as a discharge lamp) or diode lasers. The discharge lamp consists of a gas filled glass tube with a metallic electrode at each end, visually similar to a household fluorescent tube.

Diode lasers are semiconductor devices that provide that same functions as discharge lamps but are more efficient and reliable. In the resonator, the pump source generates light at specific wavelengths. This light excites the gain medium to achieve a population inversion

leading to lasing. In such a medium in a resonator, light can be amplified and reflected back and forth within the optical cavity formed by the mirrors. Oscillation occurs over several iterations until the desired energy level is achieved. The optical axis in a laser resonator is defined as the line going through the centers of the curvatures of the resonator mirrors.

The resonator is the most alignment sensitive subsystem within a laser; any unintended misalignment will cause resonator degradation. Research on resonator performance has indicated that all laser resonators are sensitive to misalignment; some are more sensitive than others based on the optical components chosen and resonator design implemented. "In any case, a resonator is very sensitive to a misalignment of the mirrors" (Hauck, Kortz & Weber 1980, p.598).

A misaligned resonator can be caused by several different sources such as:

- Temperature induced material changes that results in mirror movement.
- Environmental effects that aggravate design flaws that worsen over time resulting in mirror shifting.
- Workmanship when installing and aligning the optics and mirrors.

Mitchell, Griffith & Henderson (2001) research on beam stabilization methodologies has categorized beam movement into three sources: internal to the laser, the optical beam delivery system and the external environment of the laser. It was further stated that within the laser the collimated beam can be subjected to strong thermal gradients, vibration sources such as fans, shutters, cooling water flow, mechanical creep and aging optics. All are factors that contribute to

resonator misalignment. To address these factors, often times challenging design limits are imposed that increases production time (operator build time), material selection for the laser cavity and increased manufacturing processing costs. Rapaport, Weichman, Brickeen, Green & Bass (2001, p.1401) concluded that " cost effective manufacturing of laser and beam delivery systems requires a thorough optical and mechanical tolerance analysis to establish acceptable component parameters to properly balance alignment requirements and performance against unit produceability".

This document is comprised of five chapters. The first chapter provides an introduction to the research subject. The second is comprised of an introduction to reliability, acceleration models and FR modeling, a technical review of the current laser FR model, research on resonator misalignment and new FR models developed and the model methodology used. Third is the methodology used to create the laser FR model based on a tailored Physics of Failure (PoF) approach. The fourth chapter details the experiments completed and the results that were used to develop temperature and vibration acceleration models used to create the new FR model. Finally the fifth compares the results from the new FR model to field data to establish model credibility.

The PoF methodology is a science-based approach that uses modeling and simulation to improve the reliability of a design. Utilizing a tailored PoF approach provided the ability to focus the research on modeling the root cause of DP laser resonator failures. The main objective achieved was the creation of a FR model specifically focused on the thermal induced and vibration effects that ultimately cause premature resonator/ laser failures.

Model validation is critical if a model is to be accepted and used. The validation of the proposed laser FR model will be measured by comparative analysis against the MIL-HDBK217F

to calculate the predicted failure rate of a DP laser. Use of field data will support model validation of laser reliability and performance.

CHAPTER TWO: LITERATURE REVIEW

Reliability

A product's performance over its lifetime or over a defined period of time without an interruption is generally referred to as the reliability. "The most widely accepted definition states it is the ability or capability of the product to perform the specified function in the designated environment for a minimum length of time or a minimum number of cycles or events" (Grant, Coombs & Moss, 1998, p. 1.2). Complex electro optical systems such as DP lasers are designed for high reliability. Laser reliability is critical because performing unplanned repairs or maintenance is a very costly exercise and a significant inconvenience to the end user. Lasers for military applications are hyper-sensitive to failure since mission success in many instances is determined by equipment reliability. The reliability of any product is determined by three parameters: Operational time, the application environment and its intended function. Product usage outside the parameters can significantly impact the reliability either positive or negatively.

Reliability is often measured as a "Mean Time" (MT) ratio, based on the period of performance. One of the most commonly used methods of measuring product reliability is the Mean Time Between Failure, (MTBF) assessment. The MTBF can be simplified as the average time between product or component failures. It is calculated using the total time under evaluation divided by the number of failures over the evaluation period. The MTBF is measured in hours.

$$MTBF = \frac{Total\ Time\ (T)}{Number\ of\ Failures\ (F)} \quad (1)$$

The MTBF for a product can be calculated from one of three fundamental sources:

- Experimental or Test data.
- Field failure data.
- The use of prediction models such as or MIL-HDBK-217.

The three reliability parameters identified above are very critical to establishing an accurate MTBF figure. "Determination of an MTBF in test has little or no value if the test does not represent the correct use profile and duration with a proper margin to ensure reliability, especially if the items are not powered, or only a few performance attributes are monitored or checked before and after the test" (Krasich, 2009, p. 354).

The Failure Rate, (FR) is often commonly used in place of the MTBF. It is identified by the Greek letter λ (lambda) and it is simply the inverse of the MTBF (1/λ).

$$MTBF = \frac{1}{\lambda} \quad (2)$$

The failure rate of a product changes over its life span. There are three intervals that describe the failure zones of a product. The "Bath Tub Curve" was developed to represent the three life segments in a product's life: early failure period, constant failure rate period and the wear out failure period.

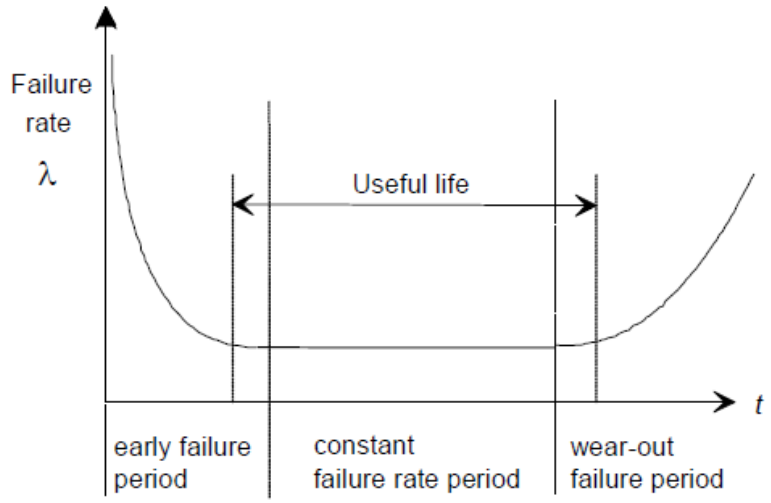

Figure 2: The Reliability Bath Tub Curve

The first segment is characterized by a decreasing failure rate termed as the early life failure or the infant mortality period. This period describes the section of the product life span where weaker units will fail thus leaving a population that is stronger. Next is the flat portion of the graph. It is called the normal life of the product or the constant failure rate period. Failures occurring during this section of the life span occur in random sequence in time. It is often difficult to predict which failure mode will manifest the product, but the rate of failures is known and predictable and as a result is represented as a constant slope.

The third period begins at the point where the constant failure rate ends and the failure rate begins to gradually increase and extend to the end of the graph. This describes the units that have aged and begin to fail at an increasing rate. This segment is referred to as the wear out period.

The useful life period begins in the early failure period as the failure rate decreases and ends in the wear out period before the increase in failures occur. The length of the useful life

period is referred to as the "system life" of a product. In reliability assessments, the useful life period is the most commonly used time frame for making reliability predictions. Failure rates calculated from reliability prediction models such as MIL-HDBK-217 is based on the useful life period.

Life Distributions

There are three life distributions that are generally used in reliability analysis: Exponential, Lognormal and the Weibull distribution. The most commonly used life distribution is the Weibull due to its applicability to the product's lifecycle. A Weibull distribution is used to describe the failure rates in all three phases of the bathtub curve. It was developed by the Swedish engineer Waloddi Weibull (1887-1979) who popularized its use for reliability analysis primarily because of its adaptability to model time the time to fail or repair and metallic material strength. The Weibull distribution has three parameters: the shape parameter (β), location parameter (*γ)* and scale parameter (η).

The Weibull density function is defined as

$$f\ x\ = \frac{\beta}{\eta}\left(\frac{x-y}{\eta}\right)^{\beta-1} \quad e^{-\left(\frac{x-y}{\eta}\right)\beta} \tag{3}$$

Where:

- $\beta > 0$
- $\eta > 0$
- $x \geq \gamma \geq 0$

The shape parameter is identified as Beta (β). It is the slope of the line used to represent the failure rate. A beta value less than 1 (β <1) models a failure rate that decreases with time, shown as the infant mortality period on the bath tub curve. A beta value equal to 1 (β = 1**)** models a constant failure rate period. The Weibull distribution approximates the exponential distribution when β = 1. An exponential distribution is the model for the useful life period, signifying that random failures are occurring. For beta values greater than 1 (β > 1) models an increasing failure rate shown as the wear-out period. The Weibull distribution approximates a Raleigh distribution for β = 2. For β values between 3 and 4, the Weibull distribution approximates the normal distribution.

The scale parameter is Eta (η). It determines the range of the distribution. A change in the scale parameter (η) has the same effect on the distribution as a change in the x axis of a graph provided that β is unchanged. Eta is also commonly referred to as the characteristic life of the product or when 63.2% of the population will fail when the location parameter is equal to zero.

The location parameter is called Gamma (γ). Gamma identifies the location of the distribution along the x axis. In reliability, Gamma is used to define a failure free zone on the x axis of a Probability Density Function, (PDF). Changing the value of Gamma has the effect of "sliding" the distribution and its associated function either to the right (if $\gamma > 0$) or to the left (if $\gamma < 0$).

Parameter Estimation

Several methods exist to define the parameters of the life distribution. The statistical methods include the Maximum Likelihood Estimation (MLE), Ranks Regression (RR) and graphical / probability plotting methods. The preferred method of parameter estimation in industry has been the maximum likelihood estimation method. "The advantages of the maximum likelihood method are all the more important in scenarios with suspensions (un-failed units) and time varying stresses" (Thiraviam, Foley & Malone, 2010 p.1). Each method of parameter estimation has its creditability and applicability to specific instances. Of the three methods identified earlier, the MLE is considered to be the most robust of the three with only limited exceptions since it can be applied to most models and to different types of data. A small sample size (<20 samples) is considered as a limitation. The parameters that are estimated from the MLE are considered to be statistically sound. This is primarily because the MLE is asymptotically consistent and asymptotically efficient. Asymptotically consistent means that as the sample size gets larger; the estimates converge to the correct values. Complementary is being asymptotically efficient for large samples, the MLE generates the most precise parameter estimates.

Acceleration models

Acceleration models or accelerated life models are used to analyze life data for products or components faster than traditional methods. Traditional methods of collecting and analyzing

field data over time is less preferred due to the inability of the design engineer to quickly implement changes to improve reliability. Accelerated life testing is the methodology employed to acquire life data for statistical analysis. It is performed by subjecting the test units to extreme conditions that exceed its normal intended conditions. The accelerated test conditions commonly used are temperature, voltage, pressure, vibration, humidity or cycling rate. Nelson (1972, p.2) stated "the results obtained at the more severe or accelerated conditions are then extrapolated to the normal conditions to obtain an estimate of the life distribution under normal conditions".

The useful life of any product or component is dependent on the stress that the product is exposed to during its life cycle. "The need to relate life and stress becomes a necessity in order to perform reliability predictions. In addition, the stresses experienced by a product in service are usually time-dependent" (Mettas 2002, p. 343).

Groebel, Mettas and Sun (2001, p. 59) in their research indicated, "once the accelerated life model has been defined, the objective is then to estimate the parameters of the failure distribution and life-stress relationship".

Acceleration models that are generally used to determine the life stress relationship were identified by Caruso and Dasgupta (1998) in their research. They included the Arrhenius and the Inverse Power Law models. Each acceleration model used in accelerated life testing is unique for determining the effects of a specific stressor on the product life. The selection of the correct model is based on the stress to be evaluated. The output of an acceleration model is an acceleration factor. Acceleration factors (or Pi factors) are utilized in the development of FR models that are based on the PoF methodology primarily because they estimate the effect of a specific stress and the resulting correlated effect on the failure rate.

Temperature and vibration are the two stresses evaluated in this research. The two acceleration models that were used are: The Inverse Power Law model to assess the effects of vibration and the Arrhenius Model to measure the temperature effects.

Inverse Power Law

The Inverse Power Law (IPL) is commonly used for non-thermal accelerated stresses. One common application of the model is to determine mechanical fatigue damage under constant stress. The Inverse Power Law model uses a power function to describe the life-stress relationship. Use of the IPL is based on the following assumptions:

- *L* represents a quantifiable life measure, such as mean life, characteristic life or median life.
- *V* represents the stress level.
- *K* and *n* are model parameters to be determined. They are characteristic of the material and the test method, where, ($K > 0$).

The IPL is defined as:

$$L\ V\ = \frac{1}{KV^n} \tag{4}$$

n is a measure of the effect of the stress on the life of the unit. If the value of *n* increases the resulting effect of stress on the unit is greater. Negative values of *n* indicate the effect of increasing the unit life with increasing stress. A value of *n* that approaches zero indicates that

there is a small effect of the stress on the life. In cases where $n = 0$, there is no effect of the stress on the life of the unit (constant life with stress). n is commonly referred to as exponent life.

The acceleration factor that is derived from the IPL equation refers to the ratio of the unit life between the use stress level (L_{use}) and a higher test stress level, referred to as the accelerated stress level ($L_{accelerated}$).

$$AF = \frac{L_{use}}{L_{accelerated}} \tag{5}$$

$$AF = \frac{L_{use}}{L_{accelerated}} = \frac{\frac{1}{KV_u^n}}{\frac{1}{KV_A^n}} = \left(\frac{V_A}{V_u}\right)^n \tag{6}$$

$$AF = \left(\frac{V_A}{V_u}\right)^n \tag{7}$$

V_u = Use stress level

V_A = Accelerated stress level

N = Exponent life

Arrhenius Equation

The Arrhenius equation is used to determine the acceleration factor where temperature is the only stress applied. It is a 2 parameter regression model that relates the scale parameter of

the failure distribution to the reciprocal of the absolute temperature. The life relationship is based on the Arrhenius equation which states that;

$$t = A_0 * e^{\frac{Ea}{KT}} \quad (8)$$

Where:

t = The nominal time to failure.

A_0 = A constant depending on the material characteristics.

E_a = Activation energy, dependent on the material.

K = Boltzmann constant. It is equal to 8.617 x 10^{-5} in Electron volts/Kelvin

T = Absolute temperature in Kelvin.

The activation energy, (E_a) represents the minimum energy that a molecule must have to participate in a reaction that produces the failure mode. A negative activation energy, ($-E_a$) indicates that the reaction is accelerated by temperature that is lower than the ambient temperature. If E_a is small, then the effect of a temperature change on the life of the product is slow. Conversely, a large E_a indicates that temperature has a significant effect on the life of the product.

The acceleration factor that is derived from the Arrhenius equation refers to the ratio of the life (or the acceleration characteristic) between the use level (L_{use}) and a higher test stress level, ($L_{accelerated}$). Hartler's (1986, p. 414) research on the Arrhenius model stated "the acceleration factor of the failure is given by the slope of the log Arrhenius equation, usually in terms of activation energy". The Arrhenius Acceleration Factor is represented as

$$AF = \frac{L_{use}}{L_{accelerated}} \quad (9)$$

The Arrhenius life equation is defined as:

$$AF = e^{\frac{Ea}{K}\left(\frac{1}{T_1}-\frac{1}{T_2}\right)} \quad (10)$$

AF = Acceleration factor

E_a = Activation Energy

K = The Boltzmann constant, (8.6171×10^{-5} in Electron volts/Kelvin).

T_1 = Design temperature in Kelvin.

T_2 = Stress temperature in Kelvin.

DP lasers are very sensitive to temperature changes or temperature swings. A significant increase in temperature can cause a laser diode to have a change in performance; a wavelength shift is one example of lowered performance. The most significant degradation effect on any laser is resonator misalignment. It can be caused by the thermal expansion and contraction of the resonator cavity at temperature extremes ultimately resulting in a misaligned resonator.

FR Modeling

FR Modeling has been the core tool available to predict the expected life of complex electronic and electro-optical systems. An electronic system can be considered to be a vast

network of various electronic and electro optical components all interconnected to one another creating a system model. Unfortunately, this model is unsuitable for reliability analysis in the networked state since it is far too complex to analyze without the use of FR modeling.

According to McLeish (2010, p.2), "the current version of MIL-HDBK-217 revision F defines two reliability predictions methods ("Part Count" and "Part Stress") to estimate the average life of electronic equipment in terms of their Mean Time To or Between Failures (MTTF/MTBF)". Both methods are represented by the addition of the individual component FR's to derive a total system FR. For each component FR, field failure data is gathered and a model is developed based on a statistical distribution coupled with additional analyses. "Unfortunately in many cases, field-failure data is often limited in terms of the number of failures in a given field environment and determination of the actual cause of failure is sometime unknown" (Cushing, Mortin, Staderman, & Malhotra, 1993, p. 542).

When conducting FR modeling there are key assumptions made at the inception of the analysis. One in particular is that the FR is constant which supports an exponential distribution and thus simplifies the mathematics involved in reliability calculations. "If distributions other than the exponential are used, the accuracy of the FR prediction may improve, but the mathematical complexity will increase significantly. On the contrary if constant FR methods are used and interpreted properly then the penalty of a slight inaccuracy of the predicted FR may worth the benefit of mathematical simplicity" (Manthos, 2004, p.353).

The reality is that the individual models within MIL-HDBK-217F cannot capture and represent every system parameter without becoming a complex computational effort that is resource hungry. Instead the FR models should be improved incrementally to achieve maximum

efficiency and the highest return on investment. Every method and process has advantages and limitations. There is no single method is that is a remedy for all problems. "Several methods should be employed at different points in time, or during the product lifecycle, to properly predict, assess, characterize and improve product reliability" (Manthos 2004, p. 352).

Research by Jones and Hayes (1998) on the comparison of the predicted failure rate of circuit boards using the parts count analysis across different prediction methodologies/ FR models including MIL-HDBK-217F was completed. When the FR model data was compared to the field return data for the circuit card assemblies, it was inconclusive with respect to acknowledging that MIL-HDBK-217F was worse than any other model. Instead the results indicated that each model had unique sensitivities to specific characteristics further supporting the proposal that a one fit solution does not exist within any model and adjustments must be made for improvement and application adaptability.

Laser FR model

The published DP laser FR model was created with limited availability of field failure data and manufacturer test data. Subsequently several assumptions were made that impacted the robustness and accuracy of the model. Key performance attributes are not represented in the model thus allowing an inaccurate FR assessment to be performed. None the less, there are specific fundamental attributes that are identified within the current laser FR model.

The pump source used in the FR model is a configured array of laser diodes. The pump FR (identified as λ_{pump}) is determined by the diode manufacturer using various reliability test

methods during the diode qualification and testing processes. The FR is provided to the laser designers along with other key performance parameters that are critical for diode use in the intended application.

Neodymium-Doped Yttrium Aluminum Garnet, Nd:YAG is the gain media available for use with the solid state laser FR model. The media FR (identified as λ_{media}) for Nd:YAG is documented in MIL-HDBK-217F Notice 2 as approximately equaling to zero.

Cleanliness factor (π_C) is the representation for the cleanliness level used in the FR model to address the impact of contamination. Range scores are assigned to represent the cleanliness level of the environment that supports laser build and repair. An open laser is very susceptible to contamination. If not properly controlled, airborne or human contamination can be easily introduced into the laser cavity which can lead to premature laser failure due to surface or coating damage, later identified as burns.

Active optical surfaces (π_{OS}) equates to the total number of optical surfaces that each has laser beam entry and exit. MIL-HDBK-217F identifies an active optical surface as one which interacts with the laser energy or beam. Internally reflecting surfaces are not considered as an optical surface for laser energy or beam interactions. All military equipment is operated in conditions not typical of a home or an office environment. Subsequently environmental factors (π_E) are used to represent specific types of harsh military environments that reflect the specific conditions of the intended applications. MIL-HDBK-217F identifies a list of military environments with specific values to equate to the condition of the intended application. Unfortunately, there is no explanation on the correlation or derivation of the assigned values for the environmental factors to either temperature or vibration.

The laser FR model is defined as:

$$\lambda_p = \lambda_{pump} + \lambda_{media} + 16.3\,\pi_c\,\pi_{os}\;\;\pi_E\,(\frac{failures}{10^6})hrs \quad (11)$$

Where;

λ_p = Laser FR

λ_{pump} = Pump Source

λ_{media} = Media FR ~ 0. (Nd:YAG) Neodymium-Doped Yttrium Aluminum Garnet

16.3 = Coupling Factor

π_C = Cleanliness Factor: 1(Rigorous), 30, 60 (Minimal).

π_{OS} = Number of Active Optical surfaces.

π_E = Environmental Factor.

The laser FR is defined as the total number of failures per million hours of operation. It is represented as *x* failures/ 10^6 hrs. The absence of a Q Switch FR within the current laser FR model further highlights its inability to accurately predict the FR of a DP laser. The authors of the MIL HDBK laser FR model indicated that the impact of the Q switch on laser reliability is represented within the coupling function factor which is "$16.3 * \pi_c * \pi_{os}$". This assumption is fundamentally incorrect since the function of a Q switch is more than an optical surface for laser energy or beam interaction. The function of a Q switch within a DP laser is dependent on the resonator design and the type of Q switch implemented. Koechner (2006, p.488) described the technique of Q switching as, "energy is stored in the amplifying medium by optical pumping while the cavity 'Q' is lowered to prevent the onset of laser emission". "Q" is the quality factor

defined as the ratio of the energy stored in the cavity to the energy loss per cycle. Koechner (2006) also identified four types of Q switches that are used in lasers: Acousto-Optical, Electro-Optical, Mechanical and Passive. Q Switches are designed and manufactured with performance and design limitations that are directly tied to a FR that cannot simply be represented within an optical coupling factor.

Resonator Misalignment

Burger and Forbes (2008) indicated the property of insensitivity to misalignment is an essential requirement whenever a laser is designed for a field application. Lasers that are less sensitive to misalignment are used in military applications for range-finding and target designation systems.

Research by Perkins and Jones (1984) on the root causes of misalignment has confirmed that actual lasers are not likely to be perfectly aligned for various practical reasons. There are several practical causes for resonator misalignment:

- Temperature induced material changes that results in mirror movement.
- The effect of environmental vibration that ultimately leads to mirror shifting.
- Workmanship when installing and aligning the optics and mirrors.

The most common effect observed from a misaligned resonator is a loss of power. "In a conventional spherical mirror resonator, tilting of a mirror always leads to a tilt of the laser beam in the same direction due to cylindrical symmetry" (Lee & Leung, 1988, p. 2701).

"Misalignment of a resonator mirror causes a lateral displacement and angular tilt of the output beam which causes an increase in the diffraction losses and therefore a reduction in output power". A loss of power in the resonator causes a cascade effect that leads to a total laser failure.

According to Perkins and Jones (1984), the ranges of power loss can be significant with the maxima of power loss corresponding to either a mode loss crossing or mode cusping behavior. As a result, mode distortion is the observed defect of resonator misalignment.

The resonator mode is described as the variation of the electromagnetic field after one round trip in the laser cavity discounting a power loss. Magni (2004, p.1965) states "the axis of the resonator modes is the ray that retraces itself after one round trip around the resonator. For a perfectly aligned resonator this ray obviously coincides with the optical axis of the system between mirrors and is perpendicular to the mirror surfaces".

There are two types of resonator modes and three traditional resonator configurations. "Resonator modes are classified as either longitudinal or transverse. Longitudinal modes differ from each other only by their respective oscillation frequency. Transverse modes differ in oscillation frequency in addition to their field distribution in a plane perpendicular to the direction of propagation" (Koechner, 2006, p.210). Resonators are functionally equivalent to multi mode oscillators by design. Mode control is critical to sustain resonator stability. There are three traditional resonator configurations:

- Flat – Flat
- Flat – Curve
- Curve – Curve

Within each resonator configuration, there are multiple design variations that are possible. A flat - flat configuration utilizes two flat mirrors to form the resonator and has been proven to be very sensitive to misalignment. The standard resonator misalignment sources are design, temperature or workmanship induced as earlier identified. There are specific applications that require the use of a flat – flat resonator. High power laser applications typically use a flat – flat resonator at the expense of the induced thermal lens. Thermal lensing is fundamentally the creation of a lensing effect induced by temperature gradients (heat buildup) within the gain medium. Thermal lensing is typically resolved by the correct selection of the gain medium, intra cavity corrective optics or improvement to the laser cooling capability. Junhai, Li, Wang, Shao and Jiang (1999, p.267) explained, "the misalignment sensitivity that is characteristic of a flat-flat resonator can be considerably improved by stabilizing the effect of the pump (pump source) induced thermal lens".

The flat – curve resonator in comparison to a flat-flat resonator is less sensitive to resonator misalignment. Conversely, a plano concave resonator (as representative of a flat – curve resonator) is more sensitive to misalignment than a resonator with two curved mirrors. "In addition it was also observed that the alignment tolerances become less stringent for higher order modes in curve –curve resonators" (Koechner, 2006). The variations and sensitivities of unique resonator designs significantly limit the ability for the one to one comparison of different resonator designs. Hauck et al. (1980, p.599) proved misalignment sensitivities of different resonator configurations may be compared only if their gains are about the same.

For a Curve- Curve resonator, the resonator consists of two spherical mirrors with radii of curvature R_1 and R_2 separated by a distance L. R_1 and R_2 can vary depending on the resonator

design. Koechner (2006, p. 220) states that "a resonator comprising mirrors having a radius of curvature that is several times longer than the length of the resonator, (L) is one of the most commonly employed configuration. Primarily because a large radius mirror resonator has reasonable alignment stability and a good utilization of the active medium". The active medium (gain medium) is identified with a length (*l*) and a refractive index of (n). It is assumed to be homogeneous. The mode properties of the resonator are characterized by the effective length (L*) and g_i parameters;

Where the effective length (L*) = $L - \frac{l}{n}$ (12)

Where the g_i parameters (g_i) = $1 - \frac{L^*}{R_i}$ (13)

Hauck et al. (1980) explained, "that the misalignment sensitivity of any spherical resonator can be characterized by one parameter D, which again is a function of effective resonator length L* and the g_i parameters. The reciprocal value of D is the tilt angle". Any increase in the tilt angle will result in a reduction of resonator output power.

New FR Models

The MIL-HDBK-217 Rev F failure rate data and models are a frozen snapshot of conditions from over 15 years ago that are well out of date. "While the faultfinders claim that MIL-HDBK-217 is inaccurate and costly, to date no viable replacement methods are available in

the public domain" (Denson, Keene & Caroli, 1998, p. 414). As a result, a concerted effort was initiated by several organizations to mitigate the risk of using outdated models by developing and releasing several alternate models that supports performing reliability calculations/FR modeling on electronic systems. (Manthos 2004).

The effort for improved FR modeling to overcome the inherent limitations of MIL-HDBK-217 resulted in the development of the two new FR models within the last decade: 217 PLUS FR Models (a 2nd Generation Reliability Analysis Center, (RAC) SW tool called PRISM) and the Photonic Component FR Model. The models can be used on either military or commercial electronic equipment. They are application specific and complement each other with respect to component type. Unfortunately neither of the models includes a laser FR model.

PRISM™ and 217 PLUS™ FR Models

The New System Reliability Assessment Methodology, (NSRAM) was initiated in 1996 and published in 1998. NSRAM provided the basis for adopting a "systems level" reliability assessment approach to estimating system reliability. The PRISM FR Models were developed and released by RAC with the support from the United States Air Force, (USAF) Rome Laboratory in January 2000. The PRISM FR models, referred to as the PRISM tool is the trade mark used to identify the new FR models and was a direct result of the NSRAM initiative.

PRISM was considered as the most significant and long awaited change to modeling electronic systems and component failure rates (Nicholls 2007). It provided an improved method of performing reliability predictions based on the new failure mode causes that were represented

in the FR models. Those failure modes were not measured using the outdated MIL-HDBK-217 models. Concurrently the new FR models that were developed were able to obtain the credibility of the MIL-HDBK-217 models by using the same data sources, (field failure and manufacturing test data). This promoted user acceptance.

The research and analysis performed by the RAC team that developed PRISM, showed that contrary to MIL-HDBK-217's theory that the component failure was the sole determinant in system reliability and performance; several other key factors were present and contributed more to the overall systems reliability than just component failure rates. "RAC data showed that more than 78% of failures stem from non-component causes, namely: design deficiencies, manufacturing defects, poor system management techniques such as inadequate requirements, wear out, software induced, and no-defect found failures. These failure modes were not explicitly addressed in previous FR models" (Dylis & Priore, 2001).

In June 2005, the Reliability Information Analysis Center (RIAC), formerly known as the RAC was awarded another DoD contract to improve upon the gains that were derived from the PRISM tool and the associated models. The culmination of the contract effort resulted in the July 2006 release of the 217PLUS models. The 217 PLUS was the identified replacement for PRISM. RIAC for the first time also published the 217Plus FR models in their reliability model handbook. The handbook was created in a MIL-HDBK-217 style format, detailing the 217Plus methodology and models as a current replacement for the early 1990's vintage MIL-HDBK-217 (Nicholls 2007). Similar to the PRISM methodology, the elements of 217Plus are a component FR and system FR model. The component FR model provides the lower level data to support the system level FR assessment just as before. Within the 217Plus methodology is continued use of

process grading factors, a carryover from the PRISM methodology which is critical to accurately represent the application environment.

The only difference between PRISM and 217Plus is the addition of six component failure rate models that were previously unavailable in PRISM. The methodology, process, model attributes and philosophy remain unchanged from PRISM to the 217 PLUS. A complete comparison list of component FR models is identified in Table 1.

Table 1: PRISM vs. 217 Plus Component FR Models
(Reference Nicholls 2007)

PRISM Component FR Models	217 Plus Component FR Models
Capacitors	Capacitors
	Connectors
Diodes	Diodes
	Inductors
Integrated Circuits	Integrated Circuits
	Opto-Electronic Devices
	Relays
Resistors	Resistors
	Switches
Thyristors	Thyristors
Transistors	Transistors
	Transformers

A system level reliability assessment requires use of the component FR models initially to determine the component level FR similarly to the MIL-HDBK-217 methodology. The individual component FR's are then summed to the assembly level. The assembly level is then fed into the system level FR model.

The 217 PLUS component FR model has expanded FR representation capability beyond the traditional models that were primarily based on statistical analysis of failure data. Use of statistical analysis coupled with distribution mapping and data correlation, results in a multiplicative model which is not the most accurate representation of the problem space. This is

an inherent limitation of a traditional FR model and is primarily due to the fact that the individual failure mechanisms, or classes of failure mechanisms, are not explicitly accounted for**.** **"**A better approach is the combination of an additive and multiplicative model that predicts a separate failure rate for each generic class of failure mechanisms" (Dylis & Priore 2001).

A traditional component FR model is defined as:

$$\lambda_p = \lambda_b \pi_e \pi_q \pi_s \quad (14)$$

Where:

λ_p = Component failure rate.

λ_b = Base Failure rate.

π_e = Environmental Factor.

π_q = Quality Factor

π_s = Stress Factor.

When compared, the 217 PLUS component FR model accounts for several factors that were not represented in a traditional component FR model. A typical 217 PLUS component FR model is defined as:

$$\lambda_p = \lambda_o \pi_o + \lambda_e \pi_e + \lambda_c \pi_c + \lambda_i + \lambda_{si} \pi_{si} \quad (15)$$

Where:

λ_p = Predicted failure rate.

λ_o = Failure rate from operation stress

π_o = Product of failure rate multiplier for operational stresses

λ_e = Failure rate from environmental stress.

π_e = Product of failure rate multiplier for environmental stresses.

λ_c = Failure rate from power or temperature cycling stresses

π_c = Product of failure rate from power or temperature cycling stresses.

λ_z = Failure rate from induced stresses, including electrical overstress/ ESD.

λ_{sj} = Failure rate from solder joints.

π_{sj} = Product of failure rate multipliers for solder joint stresses.

The fundamental differences between the component FR models are:

- The inclusion of individual product FR's for each failure category (stress categories).
- The addition of a solder joint FR to represent the contribution of failures that are associated with solder joint fractures and failures.

Dylis and Priore (2001) identified the failure mode categories by nominal percentage for failure contribution at the system level. This analysis is presented as a pie chart referenced as Figure 3. The data indicated that component failures were only 22% of the failure contribution at the system level and runs counter to the philosophy of traditional FR modeling (MIL-HDBK-217 FR models) that is only focused on component failures as the primary failure mechanism. There were significant percentages (35% combined) attributable to No Defect Found failures and Manufacturing Induced failures. For both failure modes, they are beyond the control of the design engineer.

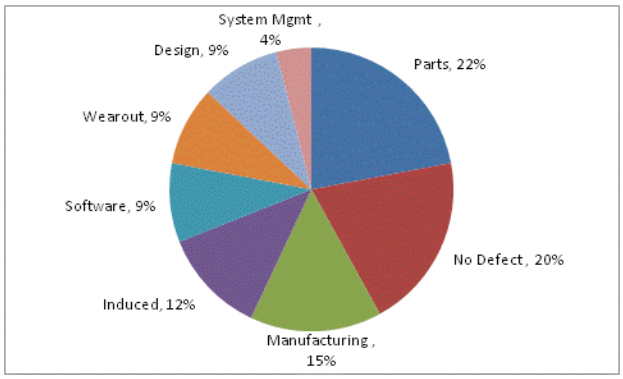

Figure 3: RAC Data: Failure Cause Distribution of Electronic Systems (nominal %) (Reference Dylis et al 2001)

Research by Nicholls (2007) on the 217 Plus methodology for component and system level FR modeling complement the research performed by Dylis & Priore (2001). Nicholls also identified seven elements that affect system level reliability that are measured in the 217 PLUS methodology:

- Design
- Manufacturing
- Parts quality
- Systems Management
- Can Not Duplicate failures
- Induced
- Wear-out

The seven elements are referred to as Process Grading Factors and are assessed independently within the FR model via a grading scheme. Process grading factors allows the user to address and account for non component failure induced effects which are considered to

be significant and ultimately contribute to a high number of the actual failures modes. The grading scheme measures the associated process for each of the failure modes in comparison to the corrective action plan that was implemented by the organization to prevent a failure recurrence. "This grading is accomplished by assessing the processes in a self-audit fashion" (Dylis & Priore, p.22).

The basic form of the 217 PLUS system FR model is defined as:

$$\lambda_p = \lambda_{IA}\ \pi_p\pi_{IM}\pi_E + \pi_D\pi_G + \pi_M\pi_{IM}\pi_E\pi_G + \pi_S\pi_G + \pi_I + \pi_N + \pi_W + \lambda_{SW} \qquad (16)$$

Where:

λ_p = Predicted failure rate of the system.

λ_{IA} = Initial assessment of the failure rate.

π_p = Parts process multiplier

π_{IM} = Infant mortality factor.

π_E = Environmental factor.

π_D = Design process multiplier.

π_G = Reliability Growth factor.

π_M = Manufacturing process multiplier.

π_S = System management process multiplier.

π_I = Induced process multiplier

π_N = No defect process multiplier.

π_W = Wear out process multiplier.

λ_{SW} = Software failure rate prediction.

The 217 PLUS FR models have the capability to address and account for factors (Pi factors or Acceleration factors) that contributed to the underestimation in the predicted FR using traditional FR models; specifically the MIL-HDBK-217.

Photonic Component FR Model

The Photonic Component Model (PCM) was developed as a result of the growing use of photonic and opto-electronic components in military applications. This was a direct result from the inability of MIL-HDBK-217F to support deterministic reliability calculations for various photonic and opto-electronic components and their anticipated FR in military environments.

"Electronics that are used in military platforms have applicable standards, such as MIL-HDBK-217, for predicting their reliability. However, photonic components are not addressed in MIL-HDBK-217" (Nicholls, Avak & Mazurowski, 2008, p.48). Driven by the need for high data transfer rates to support super fast communications speeds, the use of photonic component in military applications offers significant advantages over other electronic components. The advantages range from the immunity to electromagnetic interference to the compact size and weight that photonic and opto-electronic components offer when used in high speed, light weight, low power electronic systems.

An assessment of the FR models available was performed by Nicholls, Mazurowski, Avak & Hackert (2010). It identified significant gaps within the two prediction models available; MIL-HDBK-217F and Telecordia: (the telecommunication model for optical component application). MILHDBK- 217F, Notice 2 contained point estimate failure rates for

fiber optic cables and connectors, but no other passive photonic component. "While Telcordia contains failure rate prediction models on a wide variety of photonic electronic, fiber, connector and selected passive optical components, the data supporting these models comes from relatively benign telecommunication environments, not the more severe military environments" (Nicholls et al 2010).

The PCM methodology that was developed is very similar to the 217PLUS methodology. The primary motivator for the methodology adoption is that the traditional prediction models uses statistical analysis of failure rate data that ultimately generates a model that is purely multiplicative. On the other hand, the 217 Plus methodology is an additive and multiplicative model that is not limited by the failure rate data because it takes into account various operating conditions such as normal, non-operating and cycle related failures. This limits the instances where failure rate values become unrealistically small or large in certain conditions, i.e. military applications.

The PCM offers the following advantages over MIL-HDBK-217F:

- End users have the ability to account for individual failure mechanisms or failure modes that are critical to establishing a representative model.
- Use of quantitative stresses rather than qualitative environmental categories.
- Actual component failure rates are modeled.
- Ability to be tailored with test or field use data if available.

The components that are applicable to the PCM FR model are identified in Nicholls et al (2010) research as:

- WDMs (Thin film and Fiber based)
- Couplers (fiber)
- Taps
- Band-splitters
- Isolators
- Optical Fiber
- Laser pump modules
- Photodiodes
- Transmitters
- Receivers
- Transceivers
- Filters
- Variable Optical Attenuators (VOAs)
- Fiber connectors
- Cable assemblies
- Splices

A review of the traditional FR model identifies a model that is purely multiplicative such as MIL-HDBK-217. The PCM FR model is an additive and multiplicative model that allows the system designers to account for failure mechanisms outside a standard statistical model that is based solely on failure rate data.

A traditional multiplicative model is represented as:

$$\lambda_p = \lambda_b \pi_e \pi_q \pi_s \quad (17)$$

Where:

λ_p = Predicted failure rate

λ_b = Base failure rate

π_e = Environmental factor

π_q = Quality Factor

π_s = Stress factor

The Photonic component FR model general form is:

$$\lambda_p = \pi_Q \left(\lambda_{OB} \pi_{DCO} \pi_{TO} \pi_V + \lambda_{EB} \pi_{DCN} \pi_{TE} \pi_{RH} + \lambda_{TCB} \pi_{CR} \pi_{DT} + \lambda_{ind}\right) \quad (18)$$

Where:

λ_p = Predicted failure rate

π_Q = Multiplier for quality

λ_{OB} = Base failure rate from operational stress

π_{DCO} = Failure rate multiplier for duty cycle

π_{TO} = Factor for operating temperature

π_V = Vibration factor

λ_{EB} = Base failure rate from environmental stresses

π_{DCN} = Failure rate multiplier for non-operating duty cycle

π_{TE} = Non-operating temperature factor

π_{RH} = Humidity factor

λ_{TCB} = Base failure rate from power or temperature cycling stresses

π_{CR} = Cycling rate factor

π_{DT} = Delta temperature factor

λ_{ind} = Failure from induced stress

Nicholls et al (2010) identified that by modeling the FR as represented in the PCM, intrinsic factors can be applied that account for application and component specific variables that affect reliability.

The additional advantages for using the PCM are:

- Operating, non-operating and cycling related failure rates are measured.
- Actual component failure causes are empirically modeled.
- Based on quantitative stresses rather than qualitative environmental categories.
- Assesses the average stress conditions as a function of environment.

The review of the PCM indicates a significant improvement in the ability to accurately calculate the FR of photonic and opto-electronic components. A result of the fundamental shift in the FR modeling methodology used when compared to traditional models. There is also a secondary gain in FR modeling since the PCM support new photonic and opto-electronic components.

CHAPTER THREE: RESEARCH METHODOLOGY

The purpose of the dissertation is to develop an improved laser FR model with increased FR prediction capability by measuring and representing the contribution of temperature and vibration induced failures. The current laser FR model identified in MIL-HDBK-217 Revision F Notice 2 was used as the foundation for the improved FR model because it contains all the fundamental components for a DP laser.

The modeling methodology used during the experiment is very similar to other proven methodologies used in the development of new component FR models such as the 217 PLUS and the PCM. The methodology focuses on the failure mode of the product and the circumstances that induces the failure within the design. Adopting the failure cause approach is very similar to the Physics of Failure, (PoF) methodology but it has been specifically tailored for a DP resonator. "The PoF focuses on understanding the cause and effect of the physical processes and mechanisms that cause degradation and failure of materials and components" (McLeish 2010, p.1).

A tailored PoF approach evaluated the potential causes that contributed to resonator failure (specifically mirror misalignment) due to:

- Temperature: Unintended laser cavity motion over temperature that may lead to misalignments of the mirrors during lasing.
- Vibration: Extended use of the laser where momentary or extended exposure to conditions that can cause opto-mechanical parts to temporarily shift, causing beam misalignment.

Researchers including McLeish (2010) have shown that component failures represent less than 25% of the failures modes observed at the system level. Using the PoF methodology overcomes the limitation of the MIL-HDBK-217 FR modeling methodology which does not adequately measure and represent the effects of temperature and vibration.

The average power referenced in the model development is the output power measured from the DP resonator. The wavelength identified within the analysis is selected to be 1064 nano-meters, (1064 nm), a common wavelength used in laser resonators. The wavelength is defined as the distance between two points having the same phase in consecutive cycles of a wave. The wavelength is measured in the direction of propagation.

The resonator that will be evaluated during this research is a flat - curve, (Plano Concave) resonator. There are immediate advantages from using a flat - curve resonator to develop a FR model:

- Curve - curve resonators are considered to be almost insensitive to misalignment in comparison to a flat - curve resonator. A flat - flat resonator is very sensitive to misalignment in comparison to a flat - curve resonator. The flat - curve is the midpoint with respect to misalignment sensitivity.
- Flat - flat resonators are used in high power application but the beam quality/ beam characteristics are sacrificed. A flat - curve resonator maintains the beam quality but the power generated from the resonator is less.

The data (experimental, simulation and fielded) used within the model was filtered. Several data attributes were unavailable or not assessable. These attributes were considered to

be insignificant and do not affect the research nor compromise the intent. Specifically the unavailable data attributes are the total numbers of units fielded, end user data, fielded environment/ location, specific resonator design details and experimental data that may include design details. The use of experimental analysis will be limited within this research since a substantial amount of research has already been performed on the various types of resonators designs and their correlated behavior.

Research Requirements and Support

The research focuses on the analytical and experimental analysis to support the FR model development. The experimental data requirement to support the research will be satisfied primarily from experiments and research.

To support the research, Northrop Grumman Corporation has granted controlled data access to review field and experimental data under specific conditions. The data is critical to the research since data availability on fielded lasers, resonator failure, thermal effects analysis (FEA) and GLAD simulations on resonator designs is not available in academia. Furthermore, literature research on the development of component and systems level FR models has identified the importance and criticality user and field data.

Resonator FR Model Development

The work steps that were used to develop the resonator FR model were segmented into the following research phases.

- PoF of the Resonator
    I. Defining the PoF methodology.
    II. The identification of the Key Performance Parameters, (KPP) of the DP resonator.
- FMEA:
    I. Defining the FMEA process and applicability to the PoF model.
    II. Resonator FMEA.
        A. Resonator Description.
        B. Identification of failure mode to failure causes.
        C. Occurrence and percentage rank.
    III. Field data analysis.
- GLAD Simulations: Simulation analysis on resonator performance for change in the resonator output power versus misalignment ,(angular and linear change):
    I. Use of the General Laser Analysis and Design, (GLAD) software package to simulate resonator misalignment @1064 nm versus changes in average output power.
    II. Experimental analysis on changes to the average power versus misalignment @ 1064nm. Experiments conducted at room temperature.
- Temperature Acceleration Model: Formulation of a PoF Temperature Model for the resonator.

I. FEA impact analysis on the resonator to assess the effect of temperature versus misalignment.

II. Temperature experiments to quantify misalignment versus temperature.

III. Estimate of temperature acceleration factor using the ALTA software.

- Vibration Model: Formulation of a PoF vibration Model for the resonator.

I. Mode Frequency analysis to assess the effect of vibration versus misalignment.

II. Vibe experiments to quantify misalignment versus vibration.

III. Estimate of vibration acceleration factor using the ALTA software.

- FR model composition using Mil HDBK 217F Laser FR model as a baseline model to develop an improved FR model.
- Model validation by comparative analysis of the improved DP laser FR to Mil HDBK 217F to field data.

These work phases described above are presented in a work flow diagram as Figure 4:

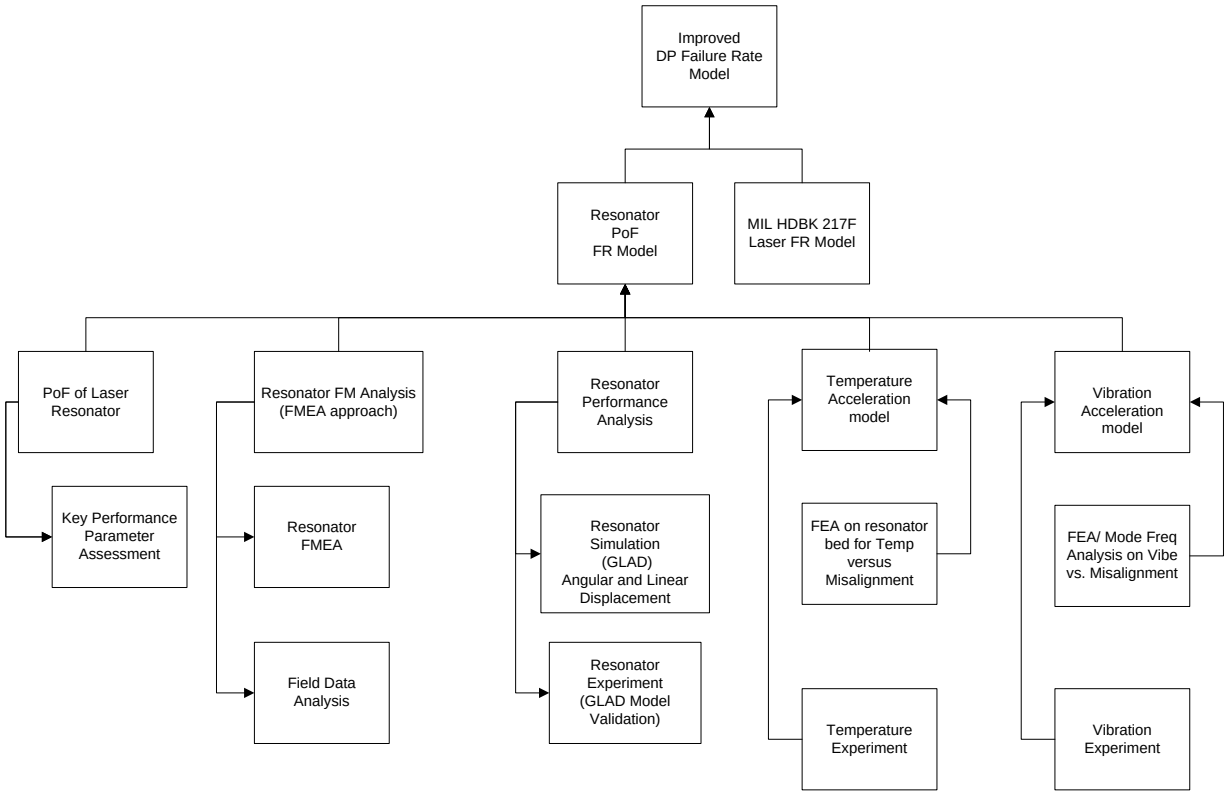

Figure 4: Work flow diagram for model development and research phases.

CHAPTER FOUR: DATA COLLECTION AND ANALYSIS

The following chapter provides an in-depth assessment of the work completed including the experiments completed to derive and develop the first resonator FR model for a DP laser using a PoF approach. At the conclusion of this chapter, two acceleration models are derived. Both acceleration models were then used to create the improved DP resonator FR model.

Physics of Failure

Physics of Failure, (PoF) is a science and engineering based methodology recently adopted by reliability practitioners due to the paradigm shift at the DoD regarding improved system and product reliability. "Attempts, which began during the 1970s, to include physics of failure into military handbooks were not very successful, although the need for a physics of failure methodology was realized in the 1970s" (White and Bernstein, 2008, p.16).

Commonly termed as "Reliability Physics", the methodology is applied early in the design phases to assess the reliability of a design to reduce the number of failure mechanism to support designing a more stable and reliable product. "PoF focuses on understanding the cause and effect of physical processes and mechanisms that cause degradation and failure of materials and components" (McLeish 2010). Initially, the methodology was not supported since the use of structural and strength analysis was not widely exercised during the design stages of electrical and electronic components in the early 1970's. McLeish (2010) stated that " by adapting the techniques of mechanical and structural engineering, computerized durability simulations of the

electrical and electronic devices using deterministic physics and chemistry, models are now possible and becoming more practical and cost effective every year". The use of PoF has greatly expanded outside of electrical and electronic devices. Mechanical designers have begun to embrace the PoF methodology to address their reliability concerns since design improvements will result in an improvement in the reliability. The PoF methodology can be implemented in the following steps:

- Identification of potential failure mechanisms or processes. Specifically whether a chemical, electrical, physical, mechanical, structural, or thermal effect causes the failure.
- Exposing the product to highly accelerated stresses such as temperature, vibration or humidity to find the dominant root cause of failure.
- Identify the dominant failure mechanism.
- Model the dominant failure mechanism.
- Combine the data gathered from acceleration tests and statistical distributions.
- Develop an equation for the dominant failure mechanism at the failure site

McLeish (2010) stated that by using the PoF methodology there were three generic root cause failure categories: Errors and Excessive variation, Overstress Mechanisms and Wear out Mechanisms. Errors and Excess variation induced failures in a PoF reliability environment are the generic equivalent to the traditional infant mortality failures observed during the product life cycle. Within a population of units there is a small group of units with defects that will not fail the various built-in manufacturing tests. They will fail when exposed to a stress that would otherwise be normal to a good unit such as a thermal or electrical stress. "These types of failures

are the most diverse and challenging categories: diverse, random, stochastic events are involved. These types of failures cannot be modeled or predicted using a deterministic PoF cause and effect approach" (McLeish 2010). The methods used to address the infant mortality failures should be based on the analysis performed during the PoF evaluation.

Overstress failure are common to both reliability philosophies; traditional and the PoF methodology. These failures occur when the device is used outside of its intended design limits and as a result an over stress condition is created that ultimately leads to failure. Typically the failures are random in nature. PoF load-stress analysis is used to determine the strength limits of a design for stresses like shock and electrical transients and to assess if they are adequate. In McLeish (2010) research was it stated that "PoF load-stress analysis is used to determine the strength limits of a design for stresses like shock and electrical transients and to assess if they are adequate".

Wear out failures occur in the product lifecycle typically at the end of the device lifecycle due to the aging of devices from wear, tear and fatigue. The failure rate increases rapidly in this period. Utilizing a PoF assessment, a wear out failure is defined as the stress driven damage accumulation for failure modes such as fatigue or corrosion. The wear-out period does not occur at one time for all components. The shortest-lived device will determine the location of the wear-out time. To determine the wear out time, long term testing is required in most cases. There are inherent benefits of using the PoF wear out analysis. "Device failures are ranked with time to failure and fallout rates for the various wear out mechanisms" (McLeish 2010). The identified wear out mechanism can then be addressed within the design phase to increase the device's useful life.

Laser failure is very important to the military. As a result, critical design decisions are made to ensure that Infant Mortality or Error and Excess variation failures are removed from the manufactured population.

Lasers that are employed in military systems such as range finders and target designators have to operate in a totally different environment (specifically temperature and vibration) when compared to commercial or laboratory lasers. There are several compounding factors that contribute to military laser failure. Temperature, shock and vibration are the most significant environmental contributors to military laser reliability. Koechner (2006) indicated that a temperature and alignment insensitive optical resonator is a key feature of a military laser. He further stated that the three most critical attributes to designing an efficient and practical laser system is;

- The diameter of the TEM_{00} should be limited by the active material.
- The resonator should be dynamically stable.
- The resonator modes should be fairly insensitive to mechanical misalignments.

The most significant attribute identified, the insensitivity to mechanical misalignment has not be fully assessed using a PoF methodology where the effects of temperature and vibration on mirror misalignment was researched.

Key Performance Parameters

An optical resonator for a military laser by design should be insensitive to temperature, vibration and shock to certain levels. However, the simulation models used by design engineers cannot simulate all environmental conditions perfectly. Using PoF as a reliability tool provides the ability to perform reliability tests on military lasers to determine failure mechanisms that are accelerated by temperature and vibration. The effects of temperature and vibration that lead to resonator misalignment will be measured and modeled in this research.

In an optical resonator, maintaining the optical axis is the most critical parameter for laser reliability. Any variation in the optical axis due to mirror misalignment causes a degradation of laser performance. Resonator output power is the most significant and critical laser performance attribute that is impacted by a change in the optical axis. The change in the average output power is either negative or positive. There are additional parameters beyond resonator output power that are also affected the mirror misalignment; diffraction losses and mode volume. When mirror misalignment occurs, the net effect on the resonator performance will be significant. "The diffraction losses are increased leading to higher a higher laser threshold and the cross sectional area of the laser beam in the gain medium is decreased resulting in a lower mode volume" (Hodgson & Weber 2005).

Output Power

When either of the resonator mirrors (M1 or M2) is misaligned or tilted the immediate effect is a change in the resonator output power. There are two classes of resonators: Stable and unstable. Hodgson and Weber (2010) identified the relationship between the angle of rotation to small mirror tilts as $V(\alpha)$. They stated that, "for all linear resonators, stable as well as unstable, the loss factor decreases parabolically with the angle of rotation for small mirror tilts".

$$V\ \alpha\ =\ V\ 0\ [1 - 0.1\ [\frac{\alpha}{\alpha_{10\%}}]^2] \quad (19)$$

Where

- $\alpha_{10\%}$ denotes the angle of misalignment, at which the loss factor has decreased by 10% and consequently the losses have increased by 10%
- $V(0)$ is the loss factor for the aligned resonator.

Resonator configuration is directly related to change in output power. A common misconception is that mirror misalignment equates to a reduction in output power. This is not always the case. In a stable resonator, the output power decreases due to the tilt of the mirror which was causes a shift in the optical axis. The shift in the optical axis then clips/ cuts the beam at the intra cavity aperture resulting in decreased mode volume; reduced output energy per round trip. In an unstable resonator a mirror tilt in the resonator may cause an increase in output power. This occurs when an aligned resonator is under-coupled, "the output coupling is too low for the given small signal gain of the active medium" (Hodgson & Weber 2005).

Referring to Figure 5, Hodgson and Weber (2005) validated the loss of output power versus mirror tilt as a parabolic function. The measured loss factor per round trip of a stable resonator as a function of the angle of misalignment of mirror 2 was compared to output power. It was found by that a typical value of $\alpha_{10\%}$ for a stable resonator in the fundamental mode, ranged up to 50 µrad of mirror tilt for a specific resonator design.

If a comparison of different resonators sensitivity to misalignment was performed, then a new parameter D, the misalignment parameter would be introduced. The new parameter D, is required primarily due to Kirchhoff's integral for misaligned resonators that relates the angle of misalignment to the resonator length and the aperture radius. Hence for different resonators, the misalignment sensitivity, D_i is calculated from:

$$D_i = \frac{L}{a}\alpha_{10\%\, i} \qquad i = 1,2 \tag{20}$$

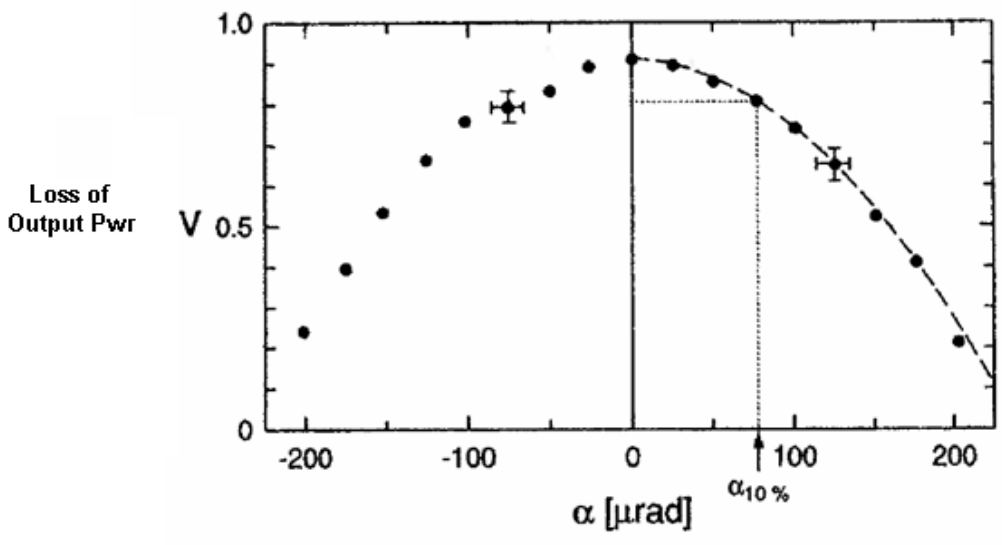

Figure 5: Loss of Output Power versus Mirror Tilt (Hodgson & Weber 2005)

Diffraction Losses

Within a laser resonator, diffraction loss is inevitable. During the lasing process, a section of the laser beam will be lost either from spillover at the mirrors or from the intra- cavity limiting aperture in the resonator. The amount of loss is controllable by design. "The loss is determined by the diameter of the laser beam in the plane of the aperture and the aperture radius" (Koechner, 2006, p.223).

A resonator aperture can be either of two forms. One variant is an optical component that is installed in the laser beam path to select/ limit beam modes present and for decreasing beam diameter in a certain axis. Alternatively utilizing the dimensions of the gain media, specifically the width, an aperture can be designed within the resonator since only certain mode will be allowed to be generated. The net effect of mirror misalignment with respect to diffraction loss within the resonator can be catastrophic dependent of resonator configuration and their correlated performance response to mirror misalignment; flat - curve, flat - flat and curve-curve. With a curve - curve resonator it has been shown to be misalignment insensitive when compared to a flat - flat resonator that is ultrasensitive.

Koechner (2006) identified the diffraction losses in a resonator as the relationship of the ratio of the acceptance angle (a/L) of one mirror from the center of the opposing mirror to the diffraction angle (λ/L). This ratio is referred to as the Fresnel number (*N*)

$$N = \frac{a^2}{\lambda L} \tag{21}$$

For Fresnel numbers that are greater than 1, those resonators will experience minimal diffraction losses. Resonators that have Fresnel numbers that are less than 1 will experience high diffraction losses because only a fraction of the beam will be intercepted by the mirrors.

Mode Volume

A laser beam is comprised of beam modes which are standing oscillating electromagnetic waves that are defined by the laser cavity geometry. The oscillating modes interfere with each other forming the transverse standing wave pattern. The pattern of the output waves based on the aperture plane is termed as the Transverse Electromagnetic Modes (TEM) of the laser beam

Transverse modes are identified by the designation TEM_{mn} for Cartesian coordinates. "M and N represent the number of nodes of zeros of intensity transverse to the beam axis in the vertical and horizontal direction" (Koechner, 2006, p.211). TEM_{00} is considered the fundamental mode. It has the smallest beam radius and divergence in the resonator. Higher order modes have increasingly larger beam diameters and are identified by higher TEM designations. In an aligned resonator, the mode volume fills the gain medium, the beam cross sectional area is maximized and specific beam modes may be selected depending on the intra-cavity aperture installed.

When a resonator is misaligned, the cross sectional area of the laser beam in the gain medium is reduced. The optical axis becomes rotated at the misaligned mirror and the mode structure is reduced at the other end of the gain medium which causes a decrease in mode volume. Hodgson and Weber (2005) identified that the optical axis remains the center of gravity

of the mode structure but the beams gets clipped on both sides of the medium, indicative of diffraction losses. The cross sectional area of the misaligned beam $A_b(\alpha)$ can be calculated to determine the impact on the resonator.

$$A_b(\alpha) = \pi b^2 \quad 1 - \frac{4 \max\ h1,h2}{\pi b} \tag{22}$$

Perkins and Jones (1984) defines b as the radius of the active material (gain medium), and the function "max" chooses the maximum of the beam shifts; h1 and h2 at either end of the gain media.

Defining the FMEA process and its applicability to a PoF model

A Failure Mode and Effects Analysis, (FMEA) is a tool that is utilized in reliability to identify failure modes, failure causes and associated risks at the lowest level within a system during the design phase. The failures are assessed using a bottom to top or "Bottoms Up" approach. The process involves each component being reviewed for their associated failure mode and impact at the next higher level. The failure analysis process is repeated over several iterations ultimately ending at the top level. "FMEA is a key tool used to prevent problems from occurring and is a vital part of the upfront engineering discipline" (Ireson et al, 1988, p.6.3).

The FMEA was developed for the US Military and was released in 1949 as Mil-P 1629 in the "Procedures for performing a Failure Modes Effects and Critically Analysis". Over the

years, there have been revisions to the Military Standard, (Mil Std). The most current version is Mil Std 1629A which was released on 24 November 1980.

Using a FMEA to support the development of a PoF model is very applicable in this situation. Primarily because the fundamental principle of the FMEA is to evaluate the product based on the possible failure mechanism coupled with the PoF intent of evaluating the failure mechanism and understanding how the environment accelerates or induces the failure.

There are three types of FMEAs. There is a System FMEA, (SFMEA) which is conducted at the system level. It is the highest level FMEA that can be performed. It is primarily used to identify system and sub system level failures and their associated risk to ensure a failure free system operation. Next is the Design FMEA, (DFMEA) or the product level FMEA which is performed on the product or a lower level assembly within a subsystem. A design FMEA is "intended to validate the design parameters selected for a given functional performance requirement" (Ireson et al, 1988, p.6.4). Finally, there is the Process FMEA (PFMEA). It is used to evaluate the manufacturing or assembly process to identify any potential process or procedural failures or deficiency that may lead to a failure.

A FMEA can be performed by an individual but it is recommended that a team approach is used. A team approach is preferred since it provides the ability for the team to share product or process knowledge that can be used in the failure identification stages. "Teams that are driven to analyze product performance are often the best and most complete source of information about product failure modes and their effects" (Ireson et al, 1988, p.6.7). There are specific steps to perform a FMEA. Ireson et al (1988) defines the steps as follows:

1. Start at the lowest level that is feasible for the analysis. This includes the part level.
2. Determine the functional specification for the part including measurable parameters that describe functionality.
3. Determine the failure mode for each function.
4. Determine the cause for each failure mode including the root causes for key design failure modes that relate to critical part function.
5. Determine the effects of each failure mode/ consequence on the next higher level up to the system level.

A FMEA measures the net effect or consequence of the failure on the system. The failure is measured as the Risk Priority Number, (RPN). It is the product of three FMEA risk assessment parameters. The likelihood of a failure occurring within the system is referred to as the occurrence, (O). Impact of the failure on the system is termed as the severity, (S). The detection (D) rating of the system is the ability of the system to detect and identify a failure.

The goal of the FMEA is to identify the risks using the RPN where the scores will be ranked from 1 to 1000. Each of the FMEA parameters are ranked on a 1 to 10 scale where 1 represents the lowest risk or least impact to a high of 10 representing the highest risk or worst outcome. Based on the calculated values, "where there are calculated high RPN's, the FMEA team must undertake efforts to reduce the risks through corrective actions" (Ireson et al, 1988, p.6.19). The RPN is calculated from:

$$RPN = S * O * D \tag{23}$$

The FMEA form is the method for presenting the FMEA analysis. There are many software packages available that identifies the different types of failure modes for specific component that will assist in completing a FMEA. The actual process of completing the FMEA form remains a manual effort. FMEA form complexity is dependent on the type of FMEA being performed. There are certain key elements that are common for all FMEA forms, specifically:

- The failure mode observed.
- The effect of failure.
- Severity of failure.
- The potential cause of failure.
- Occurrence of failure.
- Design control or evaluation techniques.
- RPN
- Recommended action.
- Action taken
- Revised RPN

Resonator Failure Mode and Effect Analysis

Resonator performance is deterministic for laser reliability. When a resonator failure occurs, the predominant effect observed is a reduction in output power or in some cases there is no output power from the resonator. Critical investigative techniques are deployed in a clean

room environment to isolate and identify the reasons for resonator failure. The ultimate outcome of the investigation is the clear identification of the root cause for failure.

A modified FMEA approach was used to identify the most common failure modes that occur on deployed lasers. A FMEA team concept was used to establish the knowledge base which is a key requirement for understanding laser design and production failure modes. "The core FMEA team should be cross functional in nature and include product engineers, manufacturing or assembly process engineers, reliability engineers ,quality engineers" (Ireson et al, 1988, p. 6.18). The FMEA team may also include other members from different disciplines such as purchasing, customer services members, legal department research and materials engineering. The resonator FMEA team chosen was comprised of an Opto-Mechanical engineer, Laser Design/ Optical Engineer, laser repair technician, manufacturing engineer and the reliability engineer.

The first step completed in the analysis was a product description and system level assessment. The resonator was determined to be at the lowest system level within the laser. The resonator chosen for the experiment is described in the following categories:

- Laser Pump Source: Diode Pumped.
- Diode Configuration: 2 diode bars.(8mm long with 40 emitters)
- Diode Power: 40W per bar at nominal current.
- Central Wavelength: 808nm.
- Power Output: Low Power. (Resonator output power (@ 1064nm) is approximately 5 W)
- Resonator Mirror Configuration: Flat-Curve.
- Gain Media: ND YAG.

- Resonator length (mirror to mirror): 15 cm.
- Mirror Configuration:
    a. Curved Mirror (M1) – Radius of Curvature = 50 cm.
    b. Flat mirror (M2) = 12.5 mm.

A functional layout diagram was used to represent the resonator with component layout is shown in Figure 6.

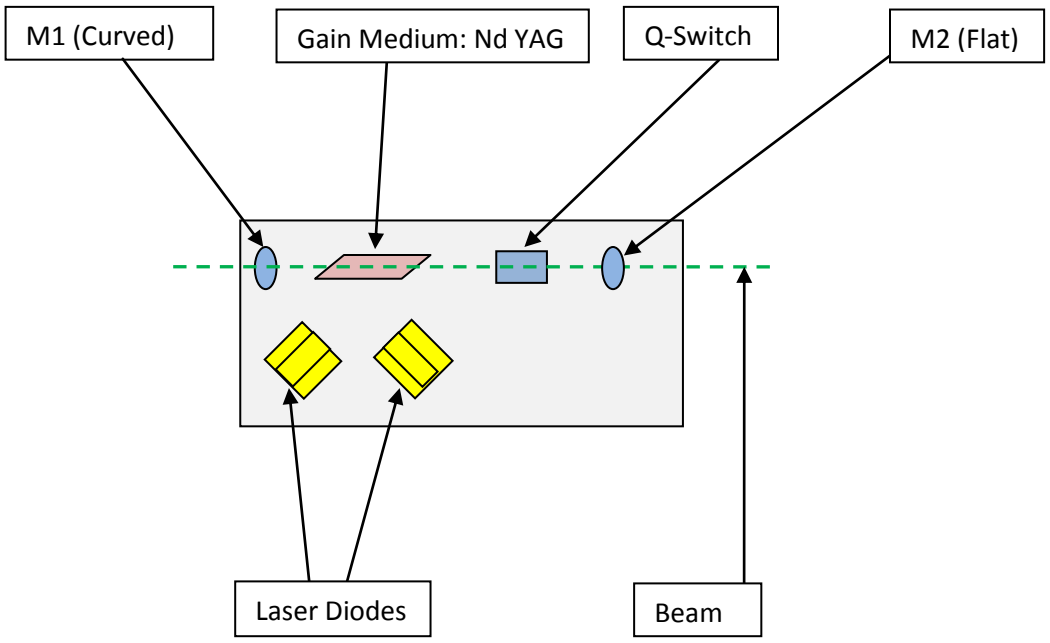

Figure 6: Resonator functional layout diagram.

The next step in the FMEA process was the identification of failure modes and the causes of failure. This process utilized the inputs from the FMEA core team based on their level of experience, technical knowledge and product support for the resonator. Additionally, a review of applicable laser literature did not yield any new failure modes beyond the identified failure mode list. Table 2 lists the failure modes identified for the resonator in Figure 6

Table 2: Resonator Failure Modes Observed

System/ Assemby	Failure Mode Observed
	Misalignment
	Burns - Contamination
Resonator	Burns - Fluence
	Pre-Lasing
	Diode Degradation
	EO Component Failure (Q- Switch)
	Optic Bonding Failure
	Diode Accessory Component Failure (Diode heater, Temp sensors , Wiring)

Using the observed failure mode list, a determination of the likelihood of a failure occurring within the resonator was performed. This task is referred to as determining the occurrence, (O). "Occurrence is the likelihood that a specific cause/ mechanism listed in will occur. The likelihood of occurrence ranking number has a meaning rather than a value" (Ireson et al, 1988, p.6.18). If a ranking scale of 1 to 10 is utilized, a rank of 1 indicates that the failure occurrence is remote, in comparison to a ranking score of 10 where the failure occurrence is determined in evitable.

A rank of the likelihood of occurrence for the different resonator failure modes was completed. Instead of using the standard 1 to 10 individual likelihood probabilities, an alternative approach was used that focused the ranks to three specific groups as they pertain to DP lasers. The likelihood of occurrence categories was defined as:

- High likelihood – Score = 9
- Medium Likelihood – Score = 3

- Low Likelihood – Score = 1

Determining the percentage occurrence per failure mode, ($\% FM_o$) is critical. The percentage occurrence provides the ability to assess the individual percentage in comparison to all the failure modes based via their ranked probability.

$$\%FM_o = \frac{R_o}{\sum Ro} * 100 \quad (24)$$

Where R_o = Rank of the individual failure mode occurrence

A percent and occurrence table was generated for the resonator used in the experiment. Identified within Table 3, are the results from the analysis. Misalignment was identified as the highest likelihood for resonator failure with a corresponding percent occurrence.

Table 3: Likelihood and Occurrence Percentage by Failure Mode Rank

System/ Assemby	Failure Mode Observed	Occurrence (Likelihood) R_o	% Occurrence
	Misalignment	9	50.00
	Burns - Contamination	3	16.67
Resonator	Burns - Fluence	1	5.56
	Pre-Lasing	1	5.56
	Diode Degradation	1	5.56
	EO Component Failure (Q- Switch)	1	5.56
	Optic Bonding Failure	1	5.56
	Diode Accessory Component Failure (Diode heater, Temp sensors , Wiring)	1	5.56

Utilizing the data compiled in Table 3, a failure mode to failure cause relationship was established. This provided the ability to determine the base FR percentages for specific categories. Using a primary and secondary weight assignment of 3 and 1 respectively, where the occurrence of a failure was classified as either a primary or a secondary effect based on the failure mode categories, Table 4 was developed. The data indicated the operational base FR % was approximately 60.16%. A similar approach was adopted in the PCM model.

Table 4: Laser Failure Mode to Failure Cause

	Failure Mode Observed and %	Misalignment = 50%	Burns (Contamination) = 16.67%	Burns (Fluence) = 5.56%	Prelasing = 5.56%	Diode Degradation = 5.56%	EO Component Failure = 5.56%	Optic Bond Failure = 5.56%	Diode Accessory Component Failure = 5.56%	**Individual Cause Percentage**	
ENVIRONMENTAL OPERATION	Temperature	P	S		P	S	P	S		25.79	
	Vibration	P	S			S	S	P	S	24.12	
	Duty Cycle (Laser Modulation)					P	P			4.87	
	Humidity		S			S		P		5.37	
MANUFACTURING	Alignment (Dynamic & Static)	P		P	P					25.01	
	Handling		P				S	P	P	14.87	

Field Data Analysis

The resonator used in this experiment is from a fielded laser with a deployed population of greater than 500 units. The laser can be used across a wide temperature range from -55^0C to 70^0C. The specific number of units deployed was deemed as classified due to the application and the end user. The data limitation on total fielded laser is inconsequential since the number of units that are field is significantly large and as a result, failures that are observed are representative of the population.

The laser failure data analyzed was over a 12 month period beginning April 1st 2010 to March 31st 2011. There were 141 lasers that were returned during the period of evaluation. The standard repair process requires all failures to be evaluated with an incoming Functional Test Procedure, (FTP). All production and manufacturing processes utilizes a test block approach. All return units are routed through a standard test process. The test process was developed based on the unit specification and environmental use. Figure 6 is the repair test process used for return lasers. Units are identified on their associated work order with the customer reason for return.

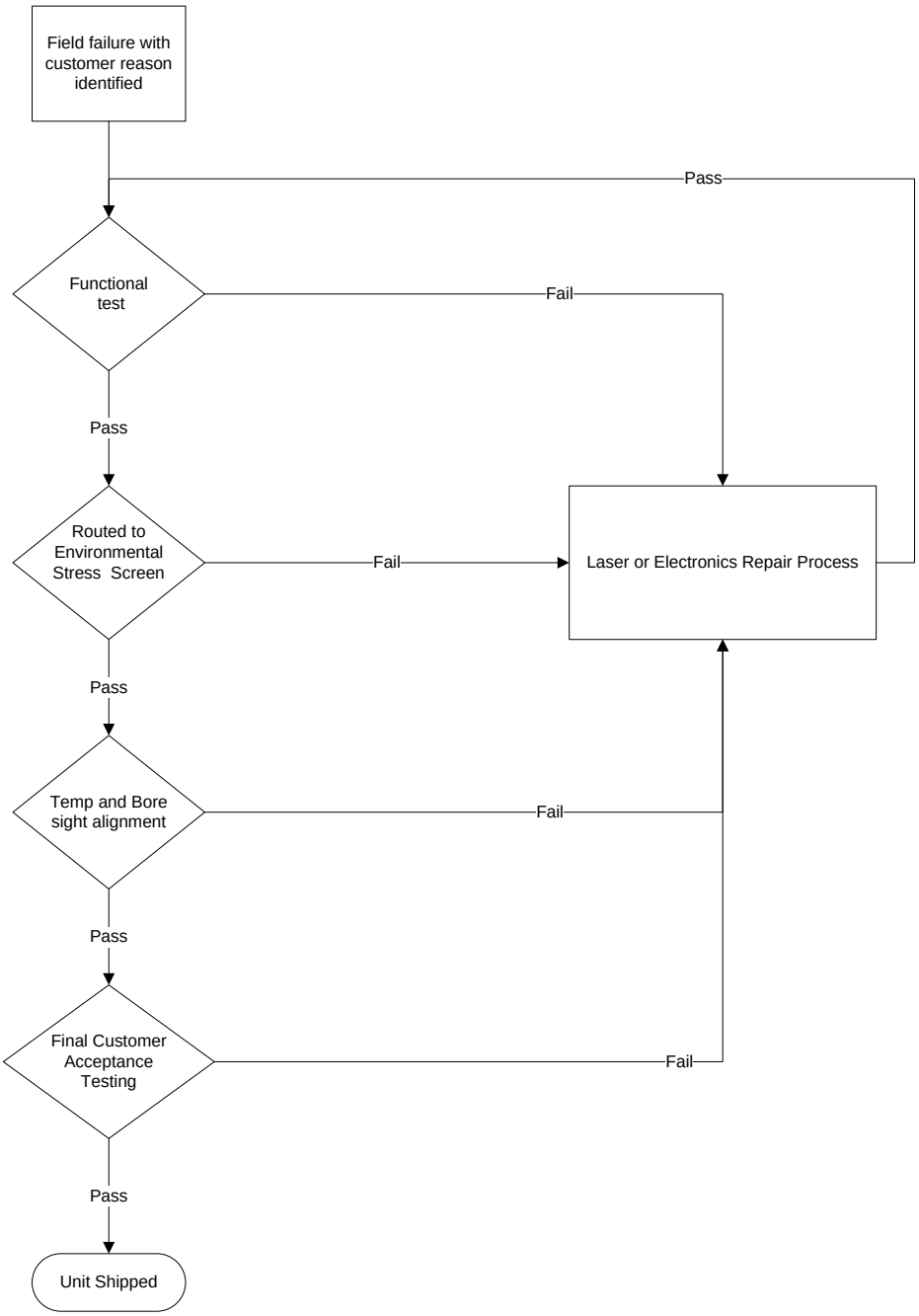

Figure 6 : Laser Test and Repair Process

The repair and troubleshooting process classified the failures into three primary groups:

- Verified Failures: Lasers that were returned by the user with a reason for return. The lasers were sent through the incoming evaluation and repair test process and the failure reason for return was verified.
- No Fault Found (NFF): These lasers were returned for repair without any defect data supplied by the end user. The lasers were routed through the test process without any defect being detected.
- Could Not Duplicate (CND): This set of lasers was returned with a failure reason. Unfortunately the reason for return could not be verified but these lasers could have displayed a different failure mode other than what was reported.

Figure 7 identifies the number of failures by return failure categories.

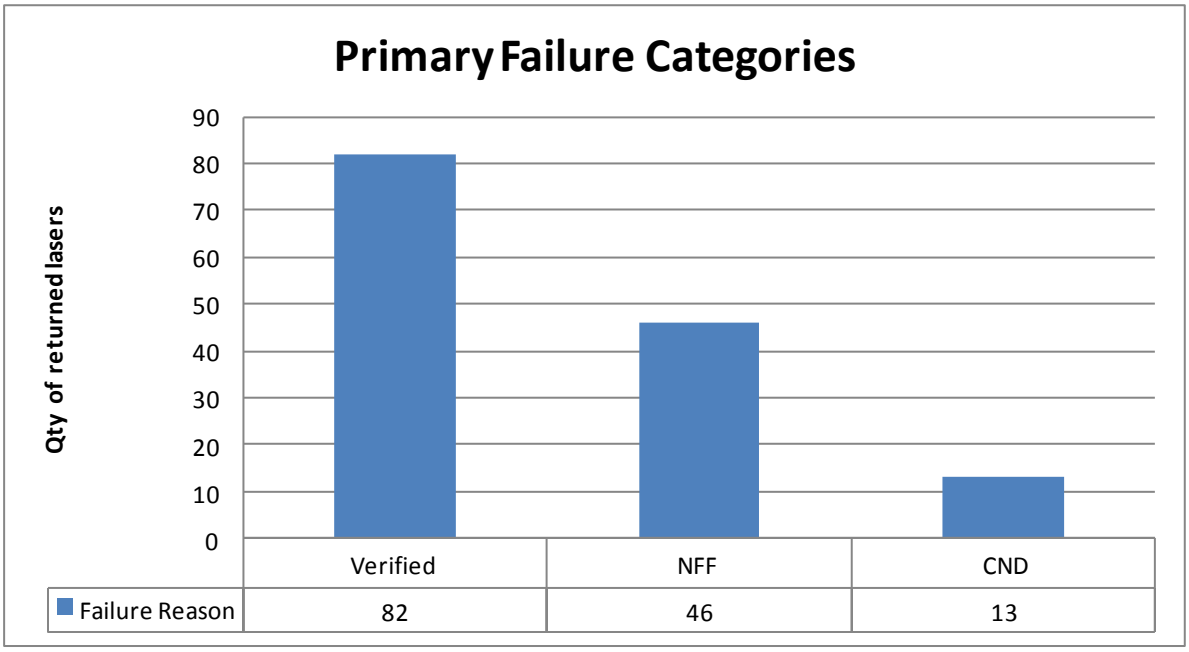

Figure 7: Return Laser Failure Categories

The failure modes for the 82 verified laser failures were analyzed to determine the contribution of resonator failures in comparison to the other failure modes identified. The laser under evaluation utilizes a secondary system of optics and optical devices before the beam exit the laser cavity. The secondary subsystem is not considered a part of the resonator and was not treated as such.

The breakdown of laser failures modes indicated that approximately 34% of all failures (28/82) were attributable to the resonator. Figure 8 identifies the number of failures by primary laser failure mode categories.

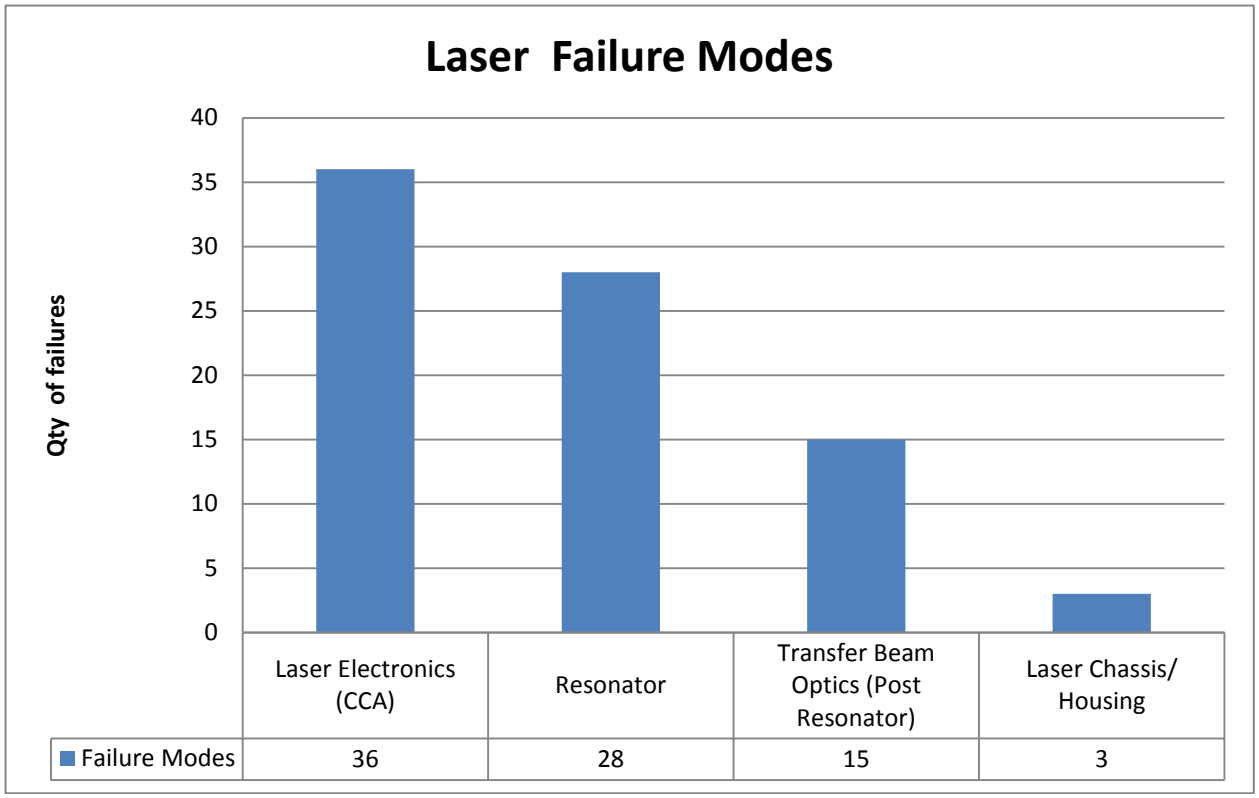

Figure 8: Laser Failure Mode Categories

Resonator failure was identified as the highest contributor to laser failure based on the field return laser data prompting the need to model and simulate these factors. The PoF methodology is an appropriate reliability analysis tool that can be used to determine under which environmental condition; temperature or vibration accelerates the failures. Figure 9 identifies the number of failures by resonator failure mode categories for a population size of 28 units. Referring to Table 3, the percent by failure mode rank identified resonator misalignment as having a very high likelihood/ occurrence.

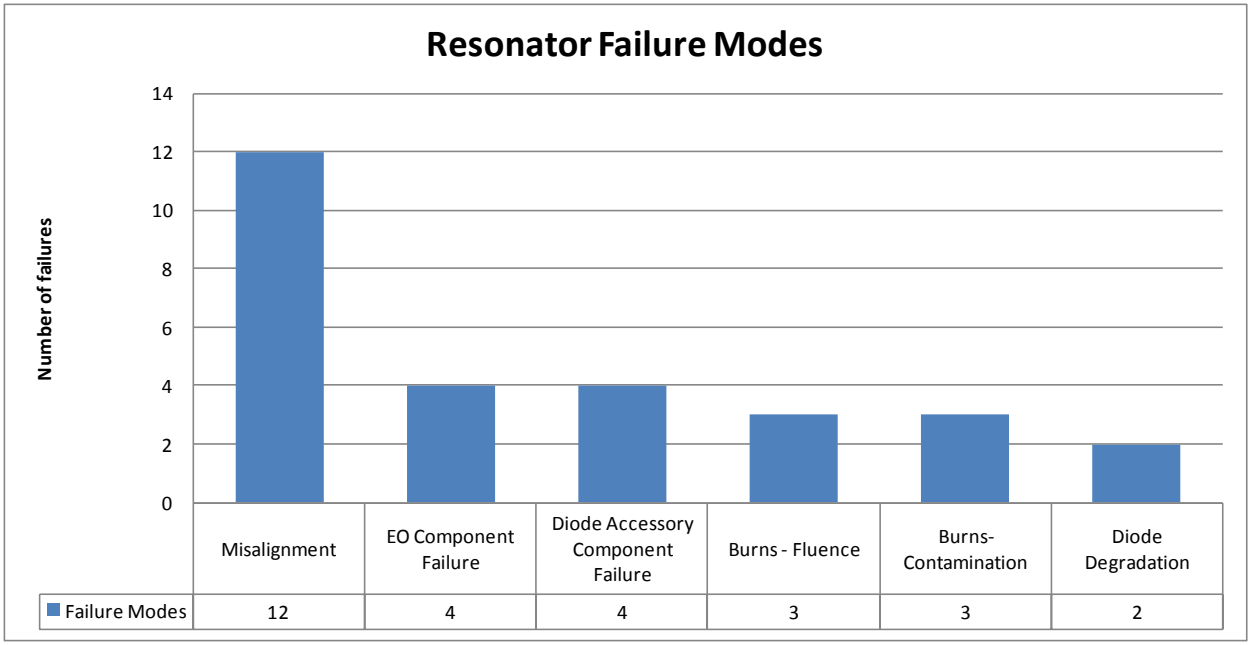

Figure 9: Resonator Failure Mode Categories

. A review of the twelve resonator failures identified in Figure 9, indicated that in all cases the final action taken to repair the laser was a re-alignment of the resonator. As a result, a resonator deficiency table was created to identify the specific resonator deficiency, the associated quantities and repair actions taken. The data indicates that resonator misalignment was the

primary root cause for laser failure. In all instances a realignment of the resonator was able to return the laser to a functional state. Table 5 identifies resonator deficiencies observed from the laser repair process.

Table 5: Resonator Deficiency Table for 12 Month Analysis

Deficiency Observed	Qty	Action Taken
Resonator output pwr decreased:	5	Realign Resonator
Suspect mirror movement	4	Realign Resonator
Beam Shift	3	Realign Resonator

This analysis supports the conclusion that resonator misalignment, specifically mirror movement/ mirror tilting is not uncommon in lasers and requires further research.

Resonator Simulation using GLAD

The General Laser Analysis and Design, (GLAD) Software package was used to simulate the effects of mirror misalignment to a reduction in the average output power. The GLAD resonator model used in the simulation is a custom application designed to support resonator modeling. GLAD has the configuration flexibility laser design engineers utilize to model critical attributes when designing lasers. "GLAD has been applied to a wide variety of the most advanced physical optics modeling applications including commercial laser systems, laser research experiments, stable and unstable laser design, transient laser response, photolithography, high-performance phase plates for beam control, diffraction effects, and single and multiple mode waveguides" (Applied Optics Research). To accurately determine the effects

of mirror misalignment as a result of a thermal or vibration distortion on a production laser is very important to laser reliability analysis specifically the MTBF.

A review of test data for the flat – curve resonator indicated that mirror misalignment has a significant impact on resonator output power including beam direction. Figure 10 shows the relationship of the average output power to the degree of misalignment (tilt in the y direction) of Mirror 2 (M2- Flat). The numbers within the graph are the associated power loss in percentage.

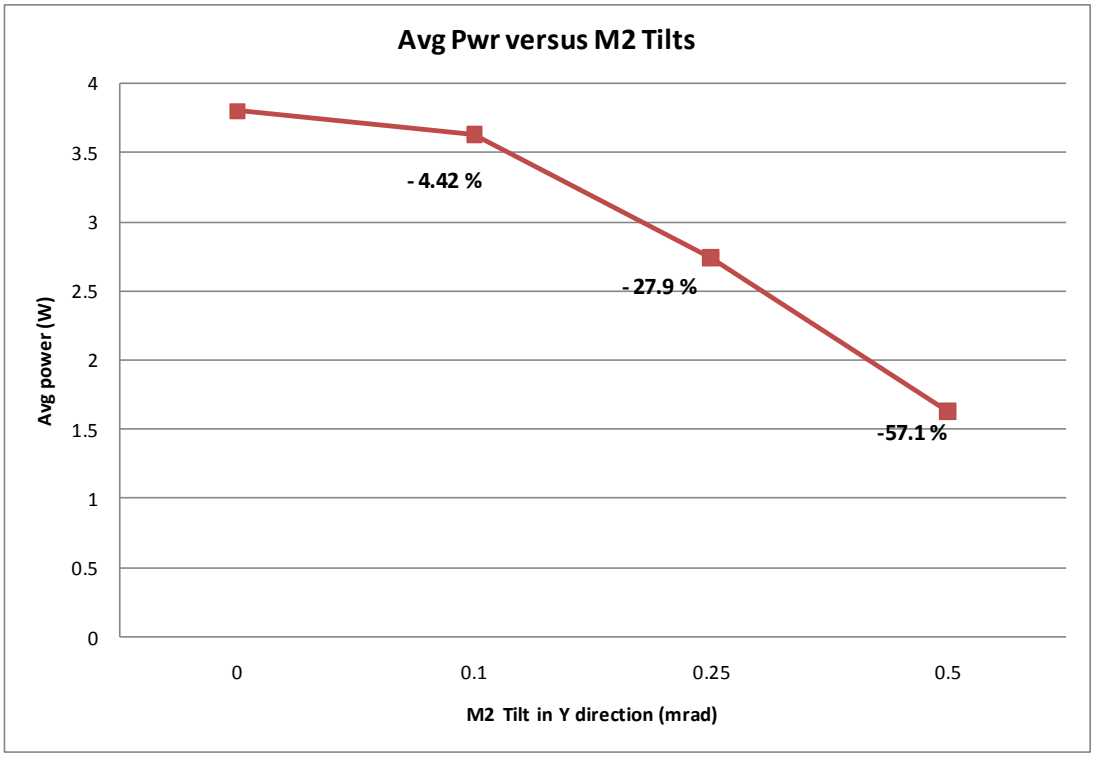

Figure 10: Average Output Power versus M2 tilt (Y-Rotations)

An optical layout of the simulated resonator used for the analysis of average power versus tilt versus bore sight shift is shown in Figure 11.

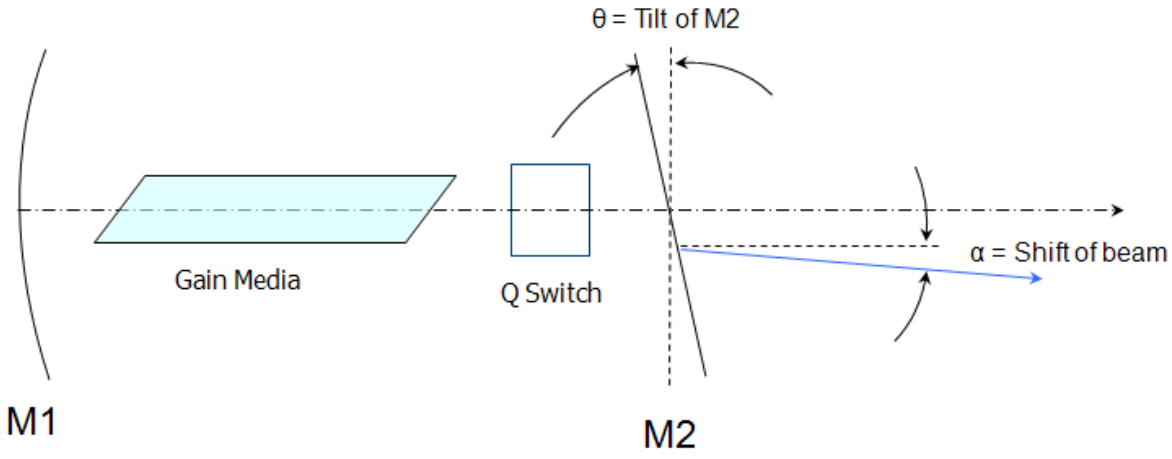

Figure 11: Configuration of the Simulated Resonator

A tilt of M2 (θ) results in a shift in the beam point direction (α) or the bore sight of the beam. In this case the beam shift was significant. A beam shift from the laser's internal reference when built and aligned causes an inaccurate range designation in military lasers. In a military laser, a beam shift (shift in bore sight) can result in failure to achieve the mission goal. Identified in Figure 12, is the bore sight versus M2 tilts (Y Rotations).

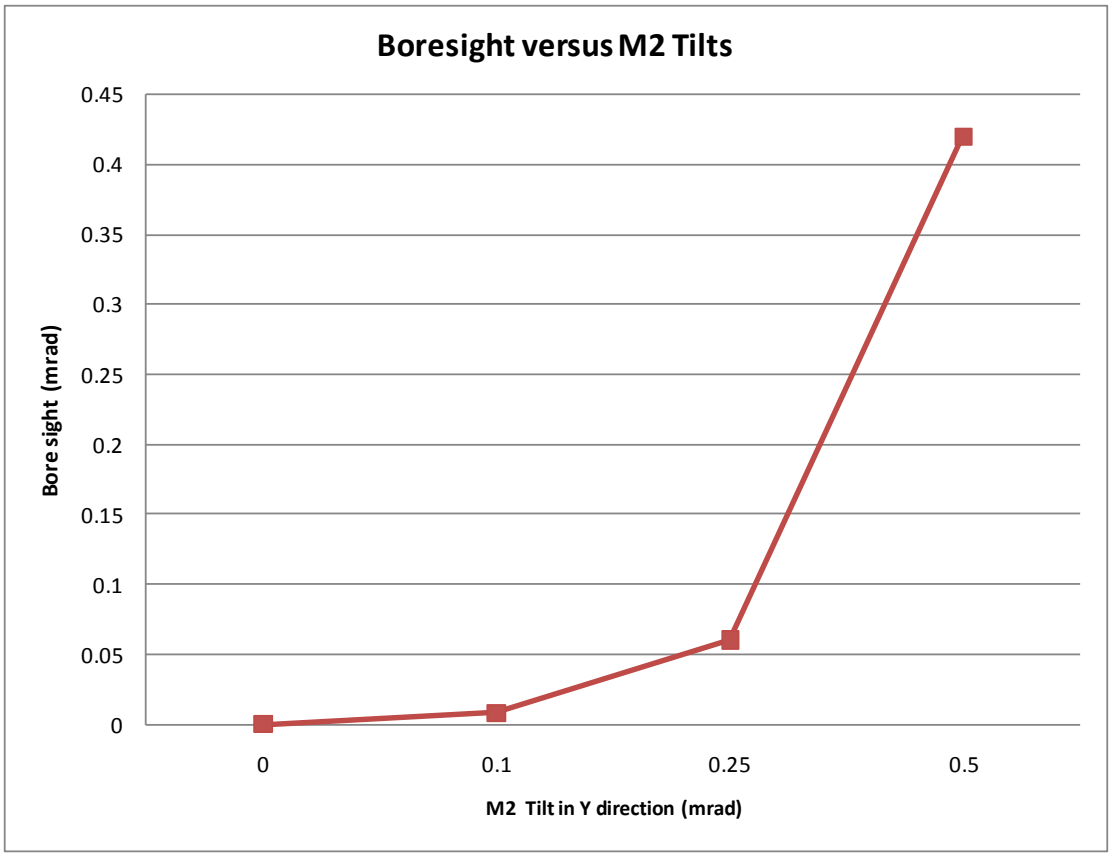

Figure 12: Boresight versus M2 tilts (Y-Rotations).

Glad Model Definition

The resonator used in the simulation to determine the impact of mirror misalignment was a flat - curve resonator. The simulation model was created using the following resonator parameters, representative of a fielded design:

- Mirror Configuration :
    - M1 - Curved. Radius of curvature ~ 50 cm.
    - M2 - Flat.

        - Diameter of clear aperture ~ 1.25cm.
        - 80% Reflectivity.
- Gain Medium: Nd YAG Slab
    - Length = 25 mm.
    - Width = 1.2mm.
    - Height = 2.2mm.
    - Orientation = Beam direction in air = Z axis (Optical Axis).
    - Beam Reflection = X-Z plane.
- Diodes:
    - Quantity = 2
    - Power = 40W Peak Power.
    - Wavelength = 808nm.
- Q-Switch:
    - 2cm long.
    - RF power = 3.5W.
- Resonator cavity length ~ 15cm.

Angular Displacement Simulation

The simulation was divided into the following sections to determine the impact of each mirror adjustment over a specified misalignment range. The events simulated were:

- Tilt of Mirror 1 in the X direction from 0.1 mrad to 1mrad in Table 5.

- Tilt of Mirror 1 in the Y direction from 0.1 mrad to 1mrad in Table 5.
- Tilt of Mirror 2 in the X direction from 0.1 mrad to 1mrad in Table 6.
- Tilt of Mirror 2 in the Y direction from 0.1 mrad to 1mrad in Table 6.

Critical reference points were required to define the direction of the laser beam utilizing a three point coordinate system. There are three axes used when referencing optical systems; X, Y and Z axis. For this research the Z axis will be defined as the optical axis in which the light travels. Below in Figure 13, the optical axes used in the experiment are identified.

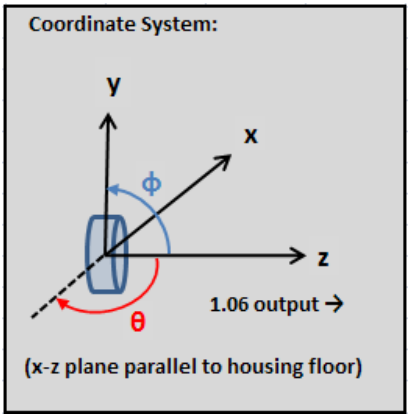

Figure 13: Optical Axis Definition

All simulations were performed for the system using an ambient temperature of 25^0C. The simulation made the following assumptions:

- A thermal algorithm, (temperature control to ensure diode wavelength compliance) was implemented and consequently it did not require a thermal profile to be supported within the resonator model.

- The slab was properly cooled to reduce the effect of heating the slab that could cause beam distortion/ bending.
- Thermal lensing was not a factor that required modeling in this analysis primarily because the effect of thermal lensing results in degradation in beam properties. Koechner (2006) stated that the effect of thermal lensing, "leads mainly to changes in mode structure and beam divergence. Whereas a misalignment of a resonator mirrors causes a lateral displacement and angular tilt of the output beam which causes an increase of the diffraction losses and therefore a reduction of output power".

Table 6 presents the calculated average output power for various tilts of M1 mirror in both X and Y Axis (Horizontal and Vertical Tilts). Table 7 presents the calculated average output power for various tilts of M2 mirror in both X and Y Axis (Horizontal and Vertical Tilts).

Table 6: Calculated Average Output Power for Various Tilts of M1in both X and Y Axis

X - Direction			Y - Direction	
M1_Tilt (mrad)	Avg Pwr (W)		M1_Tilt (mrad)	Avg Pwr (W)
-1	2.99		-1	0.46
-0.9	3.12		-0.9	0.72
-0.8	3.27		-0.8	0.90
-0.7	3.25		-0.7	1.14
-0.6	3.42		-0.6	1.42
-0.5	3.46		-0.5	1.81
-0.4	3.63		-0.4	2.30
-0.3	3.69		-0.3	2.76
-0.2	3.74		-0.2	3.25
-0.1	3.73		-0.1	3.60
0	3.74		0	3.74
0.1	3.73		0.1	3.60
0.2	3.74		0.2	3.25
0.3	3.69		0.3	2.76
0.4	3.63		0.4	2.30
0.5	3.46		0.5	1.81
0.6	3.42		0.6	1.42
0.7	3.25		0.7	1.14
0.8	3.27		0.8	0.90
0.9	3.12		0.9	0.72
1	2.99		1	0.46

Table 7: Calculated Average Output Power for Various Tilts of M2 in both X and Y Axis

X - Direction			Y - Direction	
M2_Tilt (mrad)	Avg Pwr (W)		M2_Tilt (mrad)	Avg Pwr (W)
-1	3.23		-1	0.70
-0.9	3.20		-0.9	0.99
-0.8	3.26		-0.8	0.93
-0.7	3.25		-0.7	1.24
-0.6	3.39		-0.6	1.67
-0.5	3.51		-0.5	1.89
-0.4	3.66		-0.4	2.34
-0.3	3.73		-0.3	2.84
-0.2	3.75		-0.2	3.27
-0.1	3.73		-0.1	3.61
0	3.74		0	3.74
0.1	3.73		0.1	3.61
0.2	3.75		0.2	3.27
0.3	3.73		0.3	2.84
0.4	3.66		0.4	2.34
0.5	3.51		0.5	1.89
0.6	3.39		0.6	1.67
0.7	3.25		0.7	1.24
0.8	3.26		0.8	0.93
0.9	3.20		0.9	0.99
1	3.23		1	0.70

The simulation results indicated that the calculated average output power was sensitive to horizontal tilting of either M1 or M2. The sensitivity to mirror tilts resulted in a significant loss in average output power as observed when either mirror was tilted. Conversely, the net effect on the calculated average output power was very insignificant for changes in the X axis or the vertical tilting of either mirror.

These results are expected since the resonator design dictates the alignment profile for the resonator. Referring to Figure 12, the clear aperture of the slab controls the beam clipping effect. Specifically the width of the gain medium used is only 1.4mm of clear aperture and as a result introduces design sensitivity to the resonator. This unfortunately results in misalignment sensitivity in the Y axis.

A comparative analysis on the calculated average output power versus changes in the alignment of the M1 and M2 was completed. Figure 14 shows the simulated (calculated) average output power versus horizontal tilting of M1 and M2. The data indicates that output power is sensitive to horizontal changes to both M1 and M2 when misaligned in the y direction. A power loss of 0.49W was caused by a tilt of M1 by 0.25 mrad.

Figure 15 shows the simulated (calculated) average output power versus vertical tilting of M1 and M2. The data indicates that output power is insensitive to vertical changes to both M1 and M2 when misaligned in the x direction. The data also indicates there is no reduction in the average output power for mirror tilts up to 0.2mrad. A power loss of 0.28W was caused by a significant tilt of M2 of 0.5 mrad. A similar behavior was displayed by M1.

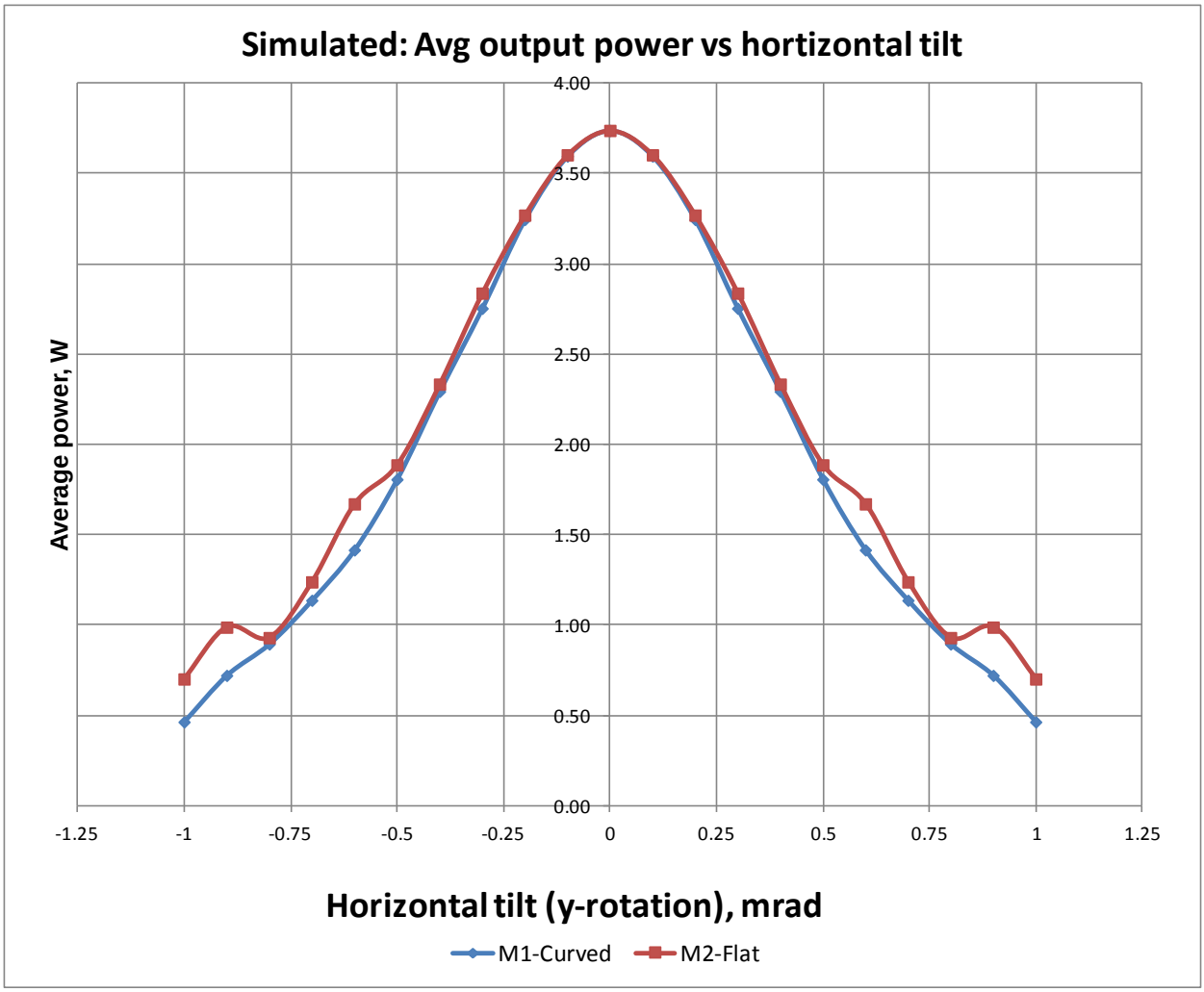

Figure 14: Simulated Average Output Power versus Horizontal Tilts of M1 and M2.

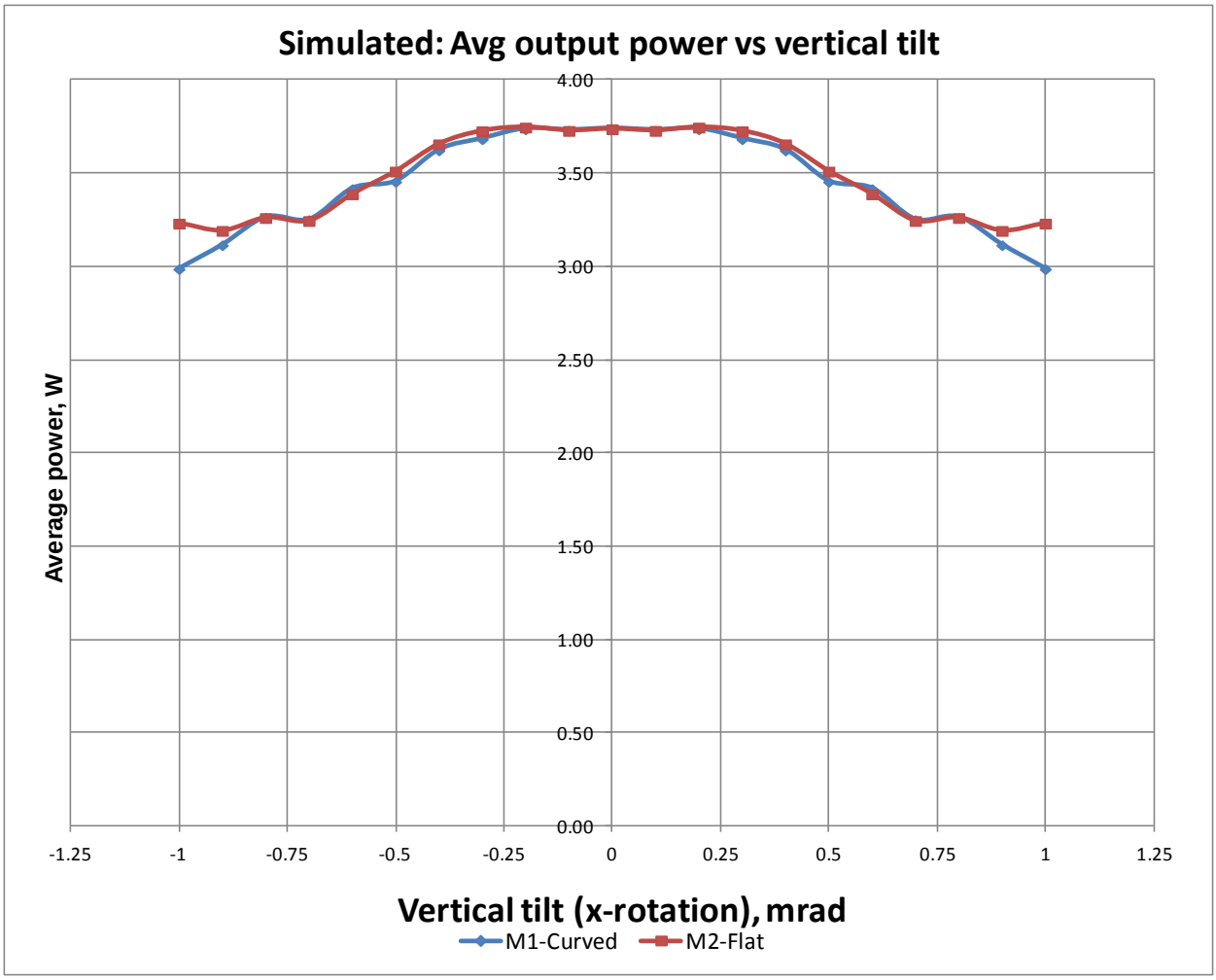

Figure 15: Simulated Average Output Power versus Vertical Tilts of M1 and M2

Resonator Experiment (Angular)

A functional resonator was evaluated at the typical room temperature of approximately 25^0 C. The scope of the experiment was to monitor the output power from the resonator when incremental tilts in the X and Y direction of M1 and M2 were performed independently. Changes in the alignment of M1 and M2 was achieved using a sensitive optical adjustment tool; a three axis rotary stage. Using a modified laser cavity allowed mirror manipulation while lasing via the rotary stage, without experimental compromise, (false data). Figure 16 shows the experimental layout used in the research.

To eliminate the possibility of variation in the experimental process, the following steps were implemented to ensure repeatability and experimental consistency:

- Resonator was initially aligned with fixed/ installed M1 and M2.
    - Stable output power ~ 3.9W measured.
- Removed in-place M1 and inserted M1 attached to rotary stage.
- Static alignment of M1 using a HeNe laser.
- Dynamic alignment of M1 to obtain optimum power (baseline) ~3.9W.
- Performed zeroing of the autocollimator at reference mirror position to identify mirror and static reference.
- Measured output power versus M1 tilt changes.
- Removed M1 positioning apparatus and reconfigured into a vertical suspension arrangement.
- Repeated steps to collect data for vertical rotation of M1.
- Steps were duplicated for M2 assessments.

- Measurement Accuracy:
    - Rotational displacements were made in increments of 50 urad away from the zero reference position, first in the “positive” direction until reaching the upper limit, and then resetting back to zero and moving in the “negative” direction until reaching the lower limit.

Note: Variations in the output power caused by intermittent fan cooling operation in addition to autocollimator reading errors were mitigated by taking both power and angle measurements as average values over a 100 second interval. This was done at each rotational displacement for both M1 and M2.

Tables 8 and 9 present the measured average output power versus angular tilts of M1 and M2 in the X and Y directions.

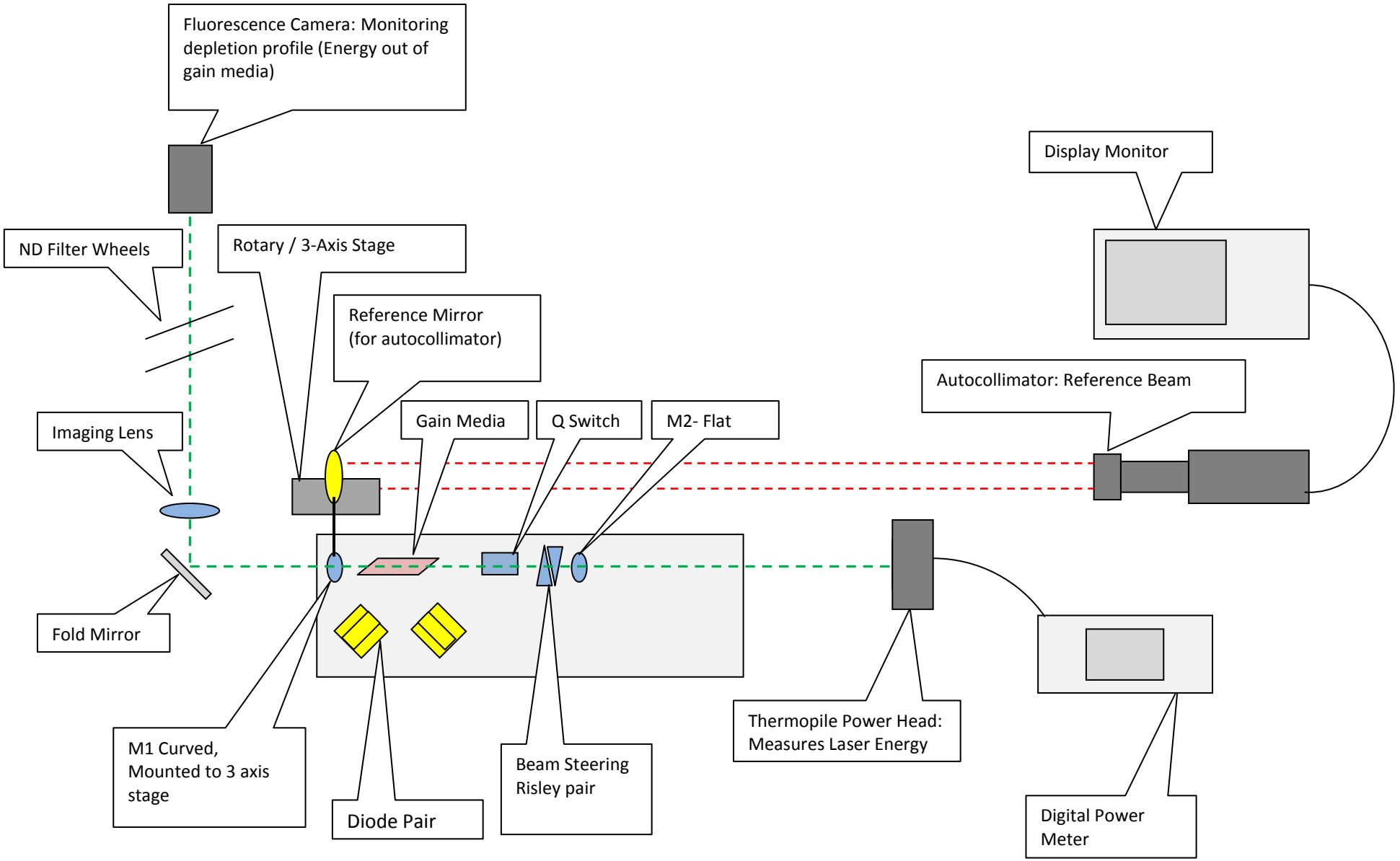

Figure 16: Resonator Experimental Test Layout

Table 8: Measured Average Output Power for Angular Tilts of M1 (X and Y Rotations)

X - Direction			Y - Direction	
M1_Tilt (mrad)	Avg Pwr (W)		M1_Tilt (mrad)	Avg Pwr (W)
-1.17	3.593		0.459	1.835
-1.097	3.6		0.409	2.091
-1.03	3.657		0.352	2.353
-0.996	3.64		0.308	2.609
-0.968	3.733		0.25	2.939
-0.911	3.788		0.211	3.135
-0.856	3.82		0.151	3.37
-0.797	3.754		0.096	3.589
-0.758	3.79		0.044	3.833
-0.706	3.847		-0.003	3.93
-0.671	3.864		-0.063	3.842
-0.612	3.87		-0.115	3.747
-0.55	3.862		-0.174	3.564
-0.499	3.882		-0.219	3.422
-0.46	3.866		-0.27	3.212
-0.408	3.901		-0.315	2.998
-0.362	3.949		-0.372	2.717
-0.333	3.979		-0.394	2.49
-0.309	3.969		-0.45	2.246
-0.262	3.965			
-0.221	3.933			
-0.172	3.927			
-0.123	3.897			
-0.074	3.962			
-0.024	3.943			
-0.018	3.952			
-0.014	3.902			
0.056	3.961			
0.101	3.916			
0.153	3.934			
0.195	3.921			
0.245	3.924			
0.301	3.879			
0.354	3.814			
0.397	3.805			
0.454	3.784			
0.508	3.811			
0.56	3.813			
0.611	3.772			
0.657	3.702			
0.709	3.65			
0.765	3.614			
0.805	3.669			
0.82	3.59			
0.857	3.625			
0.918	3.594			
0.968	3.524			
1.025	3.477			

Table 9: Measured Average Output Power for Angular Tilts of M2 (X and Y Rotations)

X - Direction			Y - Direction	
M2_Tilt (mrad)	Avg Pwr (W)		M2_Tilt (mrad)	Avg Pwr (W)
-1.1	3.403		-0.468	1.982
-1.042	3.419		-0.421	2.132
-1	3.433		-0.362	2.422
-0.955	3.46		-0.312	2.683
-0.924	3.437		-0.261	2.849
-0.869	3.462		-0.215	3.094
-0.811	3.51		-0.161	3.289
-0.753	3.539		-0.106	3.495
-0.706	3.583		-0.059	3.642
-0.657	3.62		0.04	3.743
-0.606	3.647		0.066	3.74
-0.551	3.672		0.096	3.711
-0.505	3.685		0.14	3.645
-0.451	3.682		0.2	3.509
-0.395	3.663		0.252	3.323
-0.35	3.642		0.306	3.121
-0.299	3.658		0.357	2.905
-0.258	3.659		0.406	2.651
-0.218	3.64		0.449	2.446
-0.169	3.652			
-0.124	3.677			
-0.066	3.693			
-0.03	3.706			
-0.008	3.711			
0.045	3.707			
0.102	3.697			
0.151	3.687			
0.201	3.679			
0.256	3.667			
0.306	3.64			
0.363	3.604			
0.399	3.573			
0.449	3.546			
0.503	3.506			
0.54	3.457			
0.573	3.443			
0.606	3.418			
0.653	3.408			
0.706	3.415			
0.759	3.389			
0.816	3.413			
0.854	3.375			
0.906	3.315			
0.964	3.319			
1.018	3.282			
1.07	3.233			
1.103	3.184			
1.169	3.093			

A comparative analysis was completed on the measured average output power versus tilting of M1 and M2 in both the X and Y directions. Figure 17 shows the measured average output power versus horizontal tilts of M1 and M2. The data indicates that both M1 and M2 are equally sensitive to horizontal tilting. A small horizontal tilt to either M1 or M2 resulted in a significant power loss. The tilting effect observed during the experiment was approximately equivalent to the simulated tilting effect. In the simulation a decrease of approximately 0.49W in output power was observed when either M1 or M2 was horizontally tilted by 0.2 mrad.

In Figure 18, the measured average output power versus the vertical tilting of M1 and M2 is presented. The data indicated that both M1 and M2 are equally insensitive to vertical tilts as earlier presented in the simulation experiment. For example, a reduction in the average output power of 0.205W was observed by a significant tilt of M2 of 0.511mrad.

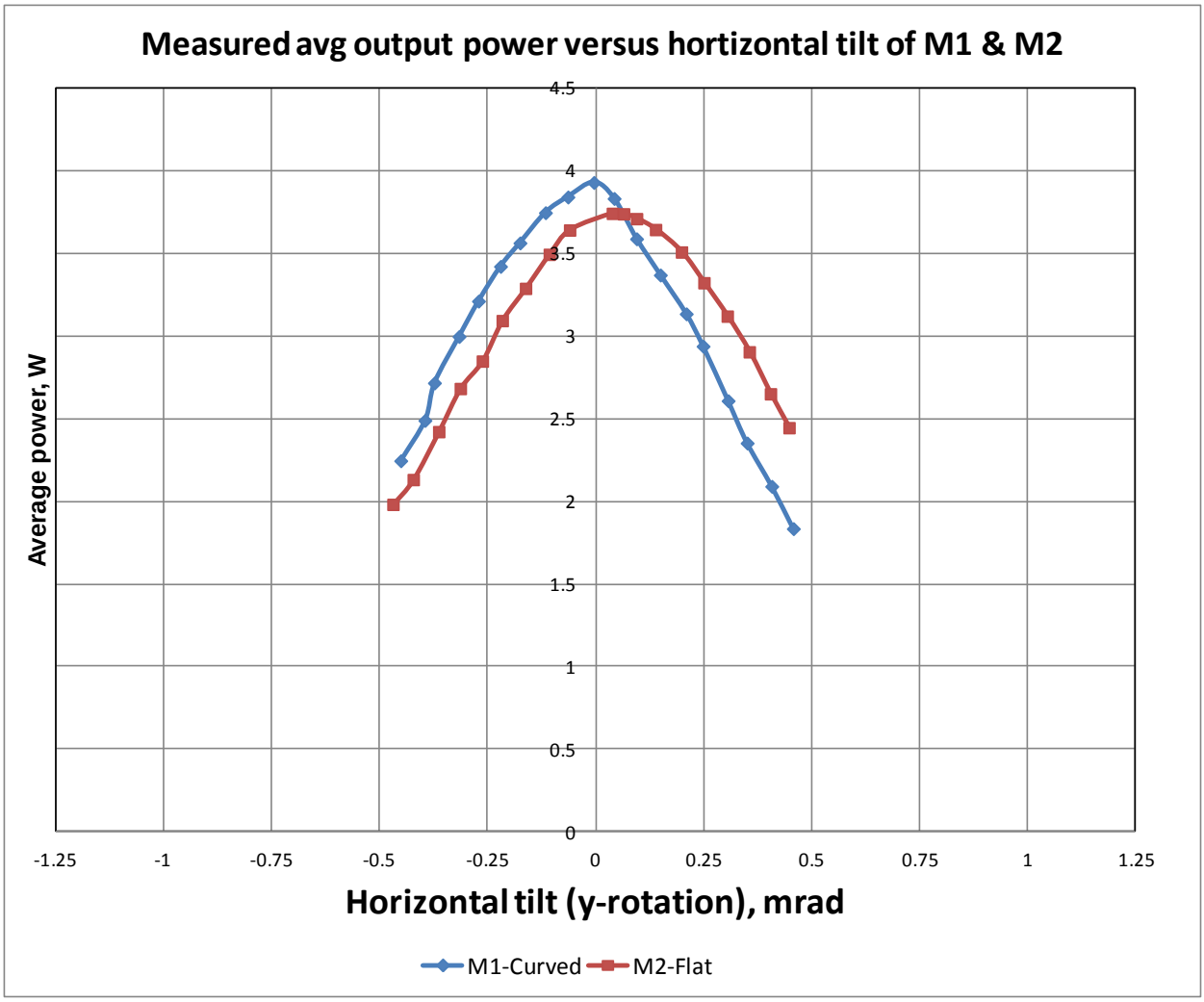

Figure 17: Measured Average Output Power versus Horizontal Tilts (Y Rotations) of M1 and M2

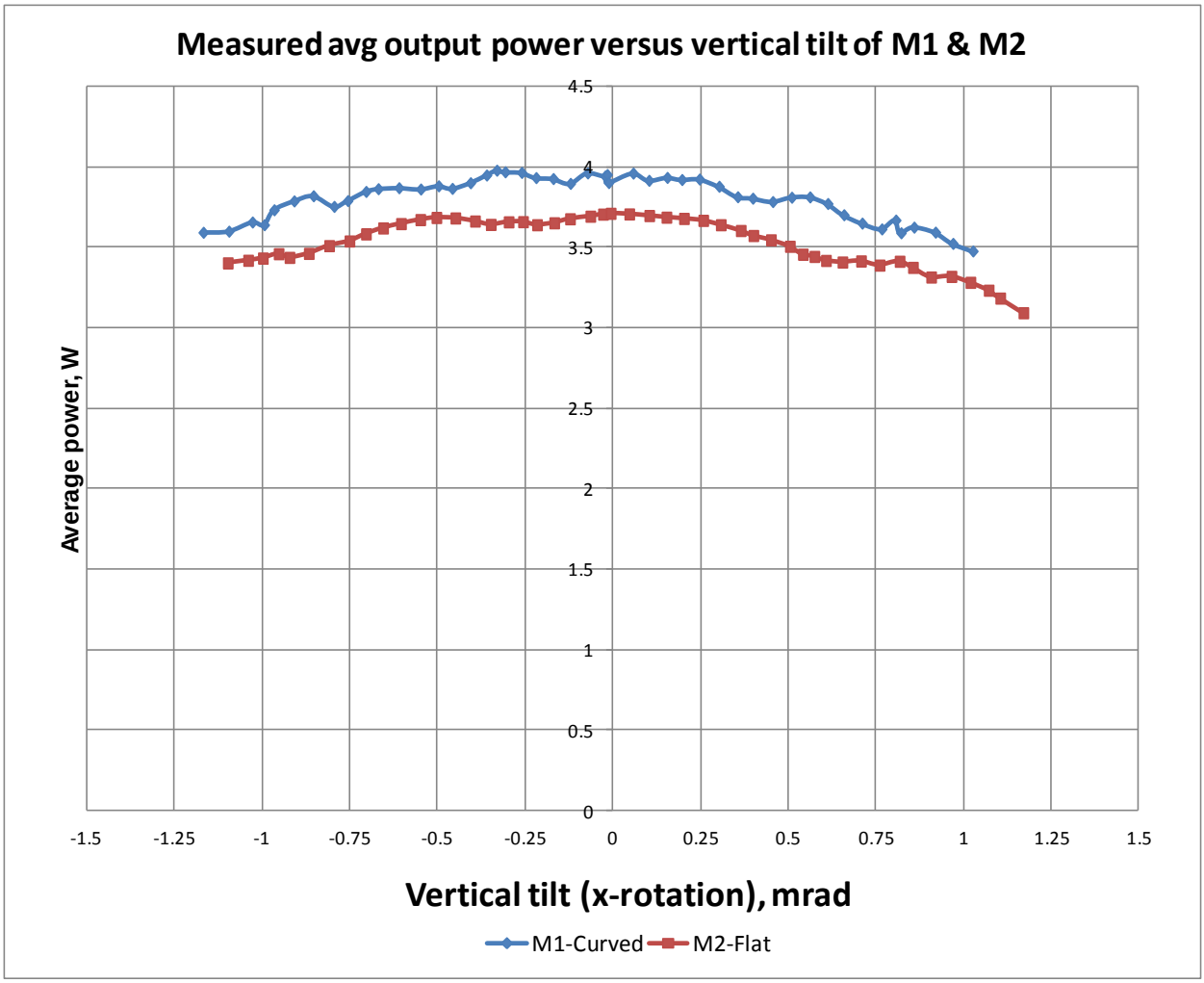

Figure 18: Measured Average Output Power versus Vertical Tilts (X Rotations) of M1 and M2

A combined graphical assessment was performed to show the correlation of the simulated (calculated) data in comparison to the experimental (measured) data. The analysis indicated that the behavior of the simulated resonator is very representative of the actual performance response to tilts for M1 and M2 experimentally. In figures 19 through figure 22, the comparison is presented for each mirror for different tilts (directional rotations). As anticipated the simulation and experimental both indicate a common sensitivity; a reduction in average output power for both M1 and M2 when horizontal tilting, (y rotations) is present.

The power loss observed when either M1 or M2 was horizontally tilted was due to the "A-Symmetrical" design of the resonator; specifically induced by component selection. When either mirror was tilted in the horizontal plane (y- rotations), beam movement was limited by the width of the gain medium. The net effect is the width of the gain medium effectively became an aperature that limited the amount of movement allowed in the horizontal plane before beam clipping occurred that caused a decrease in the average output power. Conversely the height of the gain medium allowed more vertical movement (x-rotations) since there was a larger surface. This phenomenon was observed in both the simulated and measured experiments.

Adopting an acceptable average power drop tolerance limit of a 10% decrease in average output power to determine the correlated response to individual mirror tilt indicated:

- An average simulated output power of 3.74 W, the impact of a 10% drop in output power was 3.36W for M1 in the Y axis. The tilt effect on the resonator was approximately equal to a 0.170 mrad deviation from the optical axis.

- An average simulated output power of 3.74 W, the impact of a 10% drop in output power was 3.36W for M2 in the Y axis. The tilt effect on the resonator was approximately equal to a 0.175 mrad deviation from the optical axis.

The rationalization for using a 10% power drop as the tolerable limit has been a generally established limit within the Engineering and Optics disciplines. A decrease or degradation that is greater than 10% is generally unacceptable within a design and as a result, performance and reliability are usually considered compromised and unpredictable. Conservatively, the limit that will be used going forward is a misaligned limit of 0.170 mrad for M1 or M2 without an appreciable decrease in average output power, bore sight or beam characteristics since there is no data to prove otherwise.

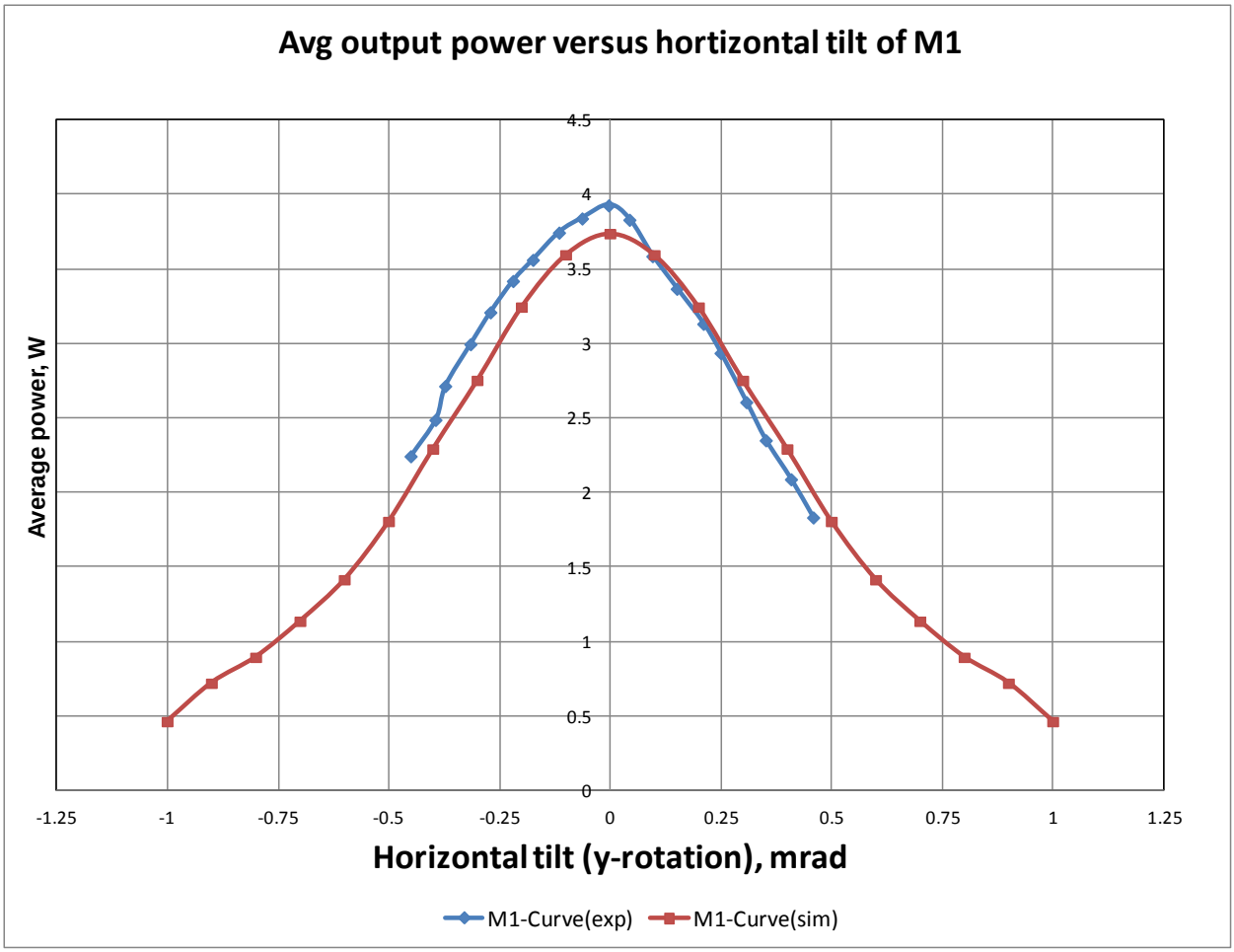

Figure 19: Average Output Power versus Horizontal Tilt (Y Rotations) of M1.

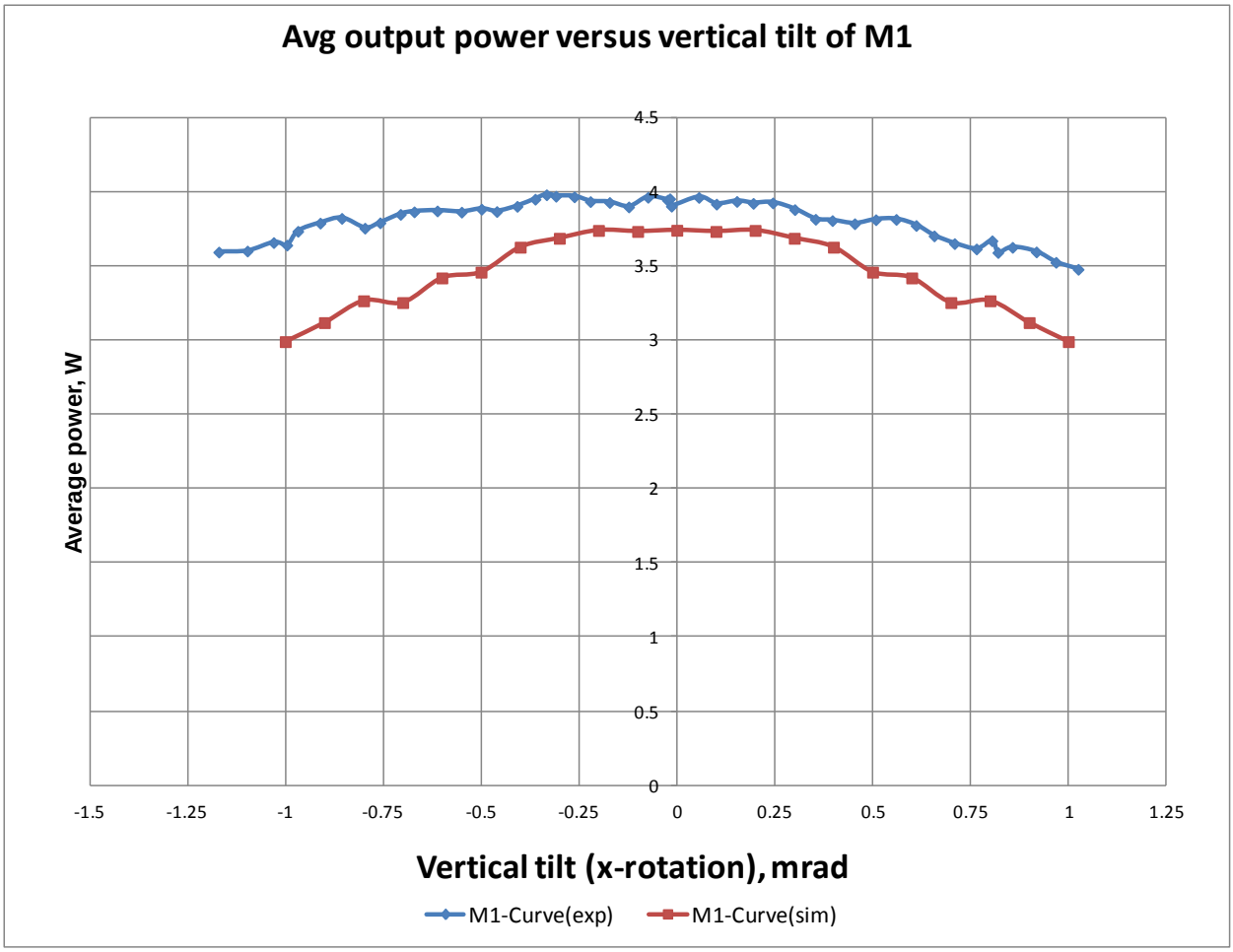

Figure 20: Average Output Power versus Vertical Tilt (X Rotations) of M1.

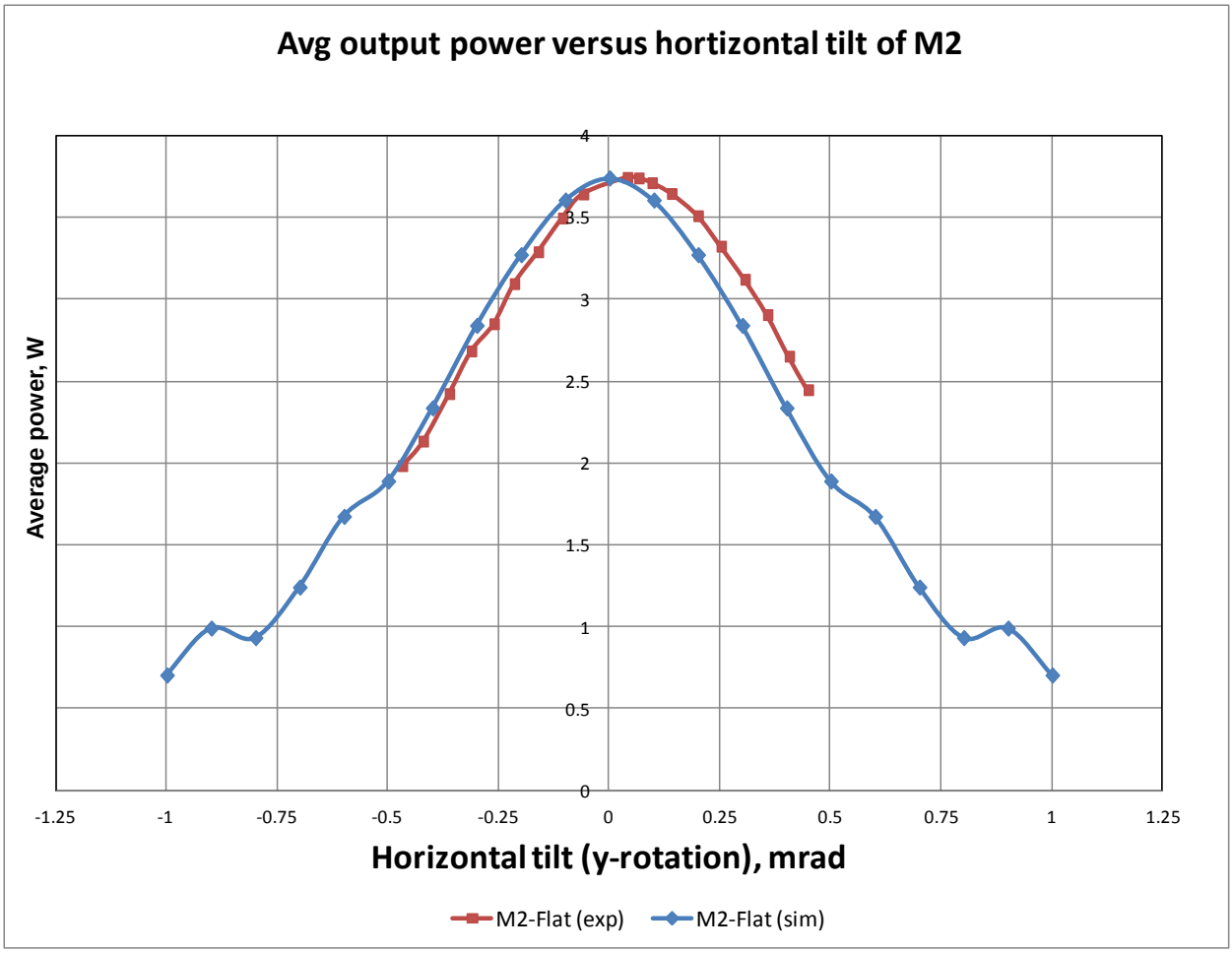

Figure 21: Average Output Power versus Horizontal Tilt (Y Rotations) of M2.

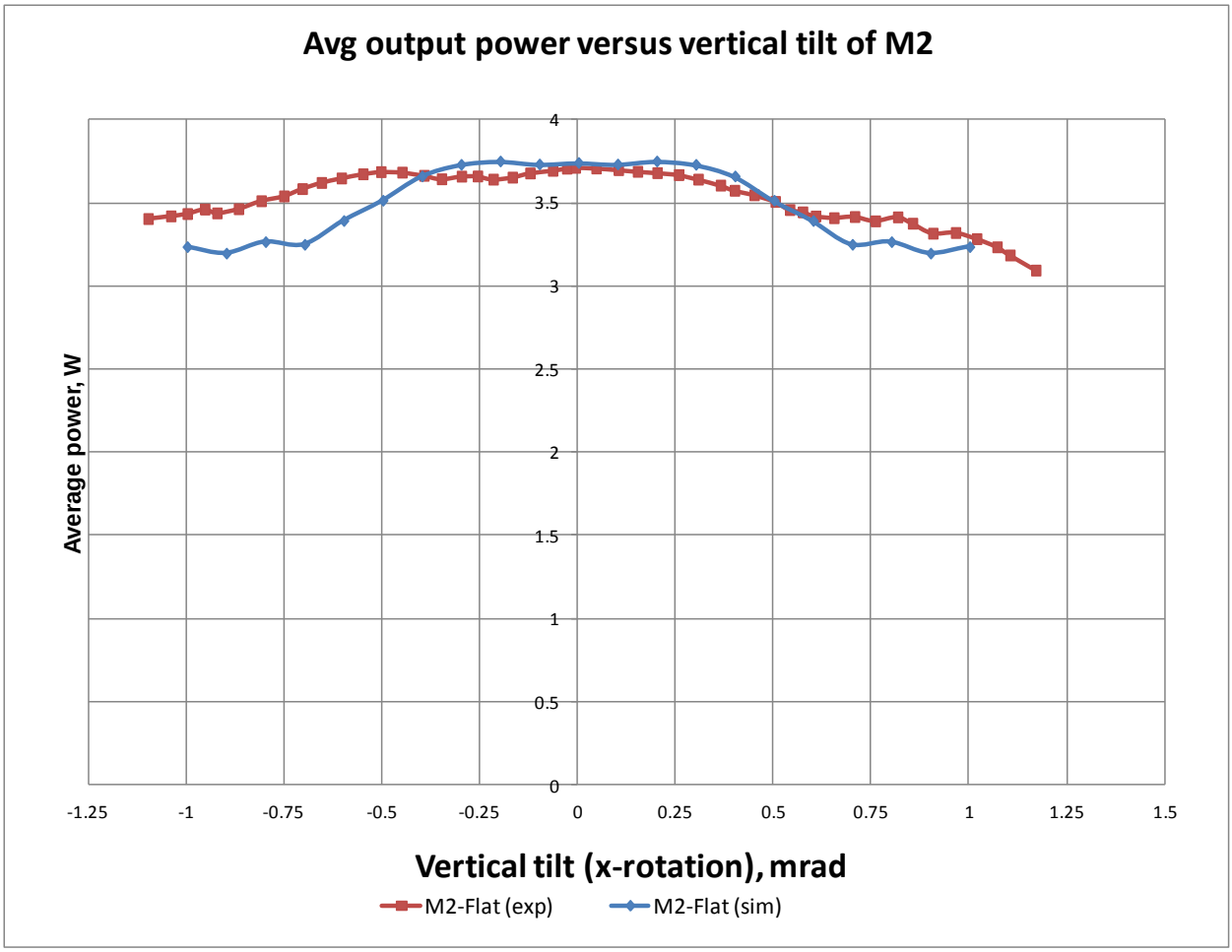

Figure 22: Average Output Power versus Vertical Tilt (X Rotations) of M2

Linear Displacement Simulation

The GLAD resonator model was proven to be very accurate in simulating the effect of changes in the average output power to mirror tilts (angular displacement). Based on earlier successes, the GLAD Model was utilized to simulate the effect of mirror misalignment in terms of a linear displacement of the resonator mirrors beyond the initial resonator alignment and the resulting change in the average output power. The first analysis completed in this research was to quantify the angular displacement due to environmental temperature changes. Subsequent simulations were performed to understand the possible relationship of M1 and M2 linearly shifting from the aligned optical axis as it relates to a vibration induced shift

The next phase of the research is to analyze the effect of a linear shift/displacement of either mirror due to the effect of an environmental vibration. Lasers are used in multiple environments on different applications by various users. The effect of a vibration input (stimulation) to a laser while in operation can be significant if the laser cannot withstand the input. A resonator that is exposed to vibration stimulation beyond the design specification can ultimately result in misaligned mirrors. As proven earlier, a misaligned resonator leads to a reduction in average output power ultimately causing a decrease in laser performance.

Some resonator designs are more sensitive to mirror misalignment than others. A resonator that utilizes a flat – curve mirror configuration has been shown to be more sensitive in one axis in comparison to another axis for tilts (angular displacement) of the mirrors. Conversely, the flat – curve design allows the flat mirror to be shifted (linearly displaced) in both X and Y axes without a significant reduction in average output power. In this resonator, M2 is a flat mirror and as a result a linear displacement will have a negligible effect on the average

output power. Table 10 presents the values of the calculated (simulated) average output power using the GLAD Resonator model when mirror M1 is displaced along the X and Y axes.

Table 10: Simulated Average Output Power for Different Displacements of M1 along the X and Y Axis.

M1 Shift in X (μm)	Avg Power (W)		M1 shift in Y (μm)	Avg Power (W)
-500	0.46		-500	2.99
-450	0.75		-450	3.12
-400	0.9		-400	3.27
-350	1.14		-350	3.25
-300	1.42		-300	3.42
-250	1.81		-250	3.46
-200	2.3		-200	3.63
-150	2.76		-150	3.69
-100	3.25		-100	3.74
-50	3.6		-50	3.73
0	3.74		0	3.74
50	3.60		50	3.73
100	3.25		100	3.74
150	2.76		150	3.69
200	2.30		200	3.63
250	1.81		250	3.46
300	1.42		300	3.42
350	1.14		350	3.25
400	0.90		400	3.27
450	0.72		450	3.12
500	0.46		500	2.99

The simulation results indicated that the average output power was very sensitive to vertical shifts/displacements (x axis shifts). When M1 was linearly displaced greater than 82µm, the result was a significant loss in average output power greater than 10%.

Most importantly is the comprehension of the net effect of a vertical shift/displacement of M1. Since M1 is a curved mirror, it is crucial that there is no movement of M1 since it is the focusing mirror that is primarily used to collect and focus/ re-focus the laser beam within the resonator cavity. Any shift will cause a reduction in the average output power.

The data also indicated the following M1characterstics:

- A linear displacement of M1 by 500µm in the x direction resulted in a significant decrease in power from 3.74W to 0.46W, a reduction of 88.7% in average output power.
- A linear displacement of M1 by 500µm in the y direction resulted in a decrease in power from 3.74W to 2.99 W, a reduction of 20.1% in average output power.
- By comparison, there is greater than 4:1 sensitivity for changes in the x axis versus the y axis.

Figure 23 shows the average output power versus the vertical shift (X Direction) of M1.

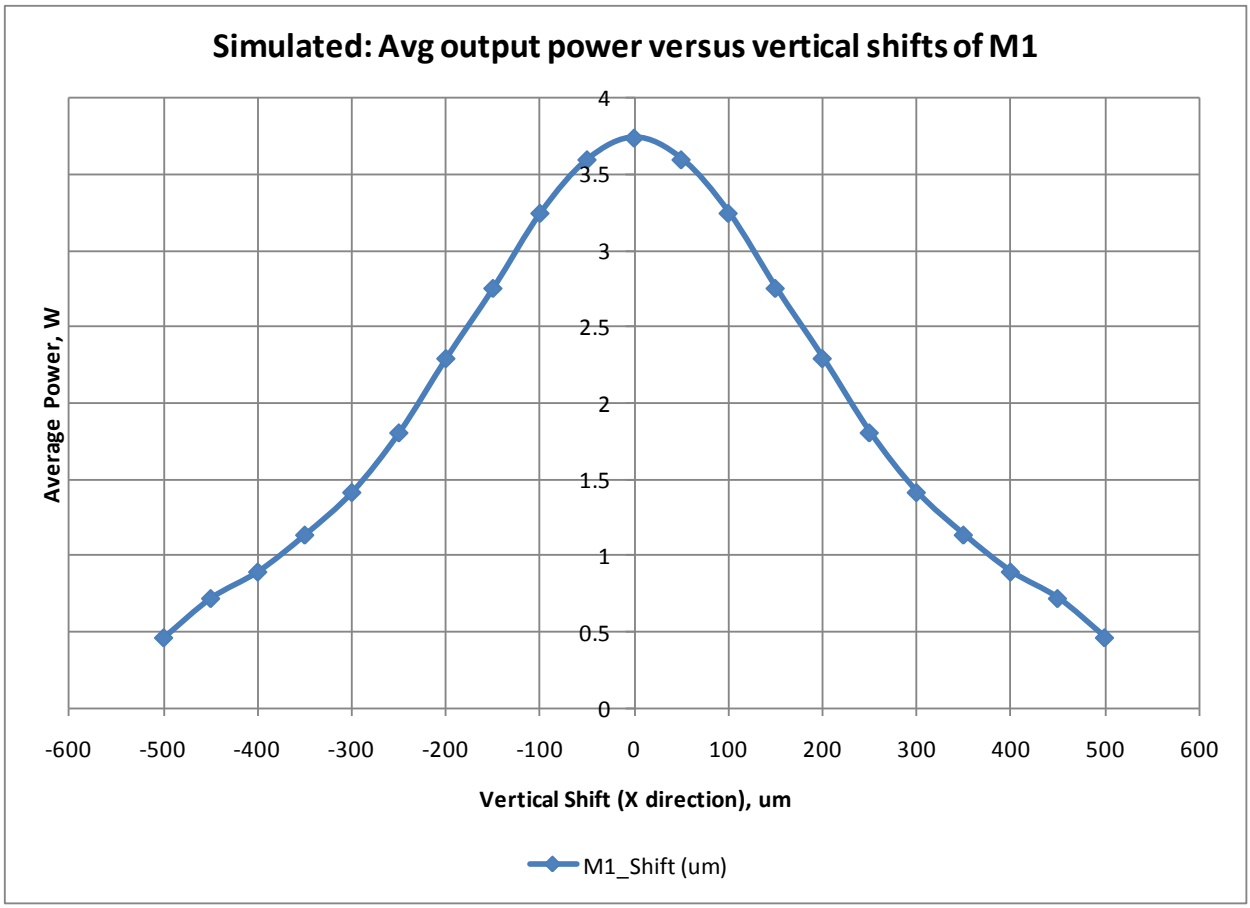

Figure 23: Average Output Power versus Vertical Shift (X Direction) of M1.

Temperature Model Development

The development of a PoF temperature model is based on an acceleration model that uses experimental temperature data to generate an accurate representation on the correlation of temperature to misalignment of the resonator mirrors. "The aim of such testing is to quickly obtain data when, properly modeled and analyzed yield desired information on product life under normal use" (Nelson, 1990, p. 3).

Long term resonator performance is temperature dependent. Lasers are designed to operate at specific temperatures. Use in an environment outside of the design temperature range can result in decreased laser performance and reliability. The driving factor for laser performance is maintaining the alignment of the resonator over different temperatures since all resonators are built within an encased cavity that is composed of various materials. As a result, the effects of thermal induced movements are analyzed using computer modeling methods to determine whether a change in the thermal environment can cause unintended tilt or shift of the resonator mirrors. Primarily driven by the fact that the optical components used for beam steering, resonator alignment and mounting are sensitive to thermal distortions of the resonator bed.

FEA of Temperature Contribution to Misalignment.

Finite Element Analysis, (FEA) is a computer modeling application commonly used by mechanical engineers to determine the stress limits for a product. "Finite Element Analysis is a tool used to support thermal design analysis. A design analysis is a process of investigating

certain properties of parts, assemblies, or structures. Design analysis can be conducted on real objects or on models that represents certain aspects of a real object" (Kurowski, 2004, p.1).

The FEA also provides useful information on the interaction of temperature and the stability of the design. A FEA study is very valuable in new design analysis since it provides critical data that can be used to improve the structural integrity of the design. Kurowski (2004) stated that if models are used instead of real objects, the analysis can be conducted earlier in the design process, before the final product or even the prototypes are built. The use of an FEA model in the development of a resonator PoF temperature model is applicable since the interaction of temperature and resonator misalignment will be established.

A FEA software package is used to provide a close end model solution to problems involving stress and strain in materials under analysis. "Linear static analysis in two and three dimensions which is necessary to analyze stress concentrations is a basic part of all such programs. Some of the well-known products are NASTRAN (1994), ANSYS (1992), and ABAQUS (1995)" (Pilkey, 1997, p. 441).

A complete FEA study using the ANSYS software was not required for this research since a historical analysis was completed on the laser cavity in a three dimensional model and the data was available. Utilizing this data, a resonator analysis based on node assignment to specific points within the laser cavity to assess the misalignment of either M1 or M2 over the temperature range from -55^0C to 75^0 C was completed. The data is considered valid since there was no change to the structural integrity of the laser cavity.

Shown in Tables 11 and 12 are the ANSYS analysis of temperature changes versus M1 and M2 tilts in the X and Y axes. The data indicates at -55^0C the temperature induced horizontal

tilt of M1 and M2 was 45 and 10 μrad respectively. Indicating minimal mirror movement/ resonator misalignment thus the anticipated loss in average power loss was insignificant.

Table 11: ANSYS Analysis of the Effect of Temperature Change on the Alignment of M1 (X and Y axis)

	M1	
	Vertical	Hortizontal
Temp °C	RX (mrad)	RY (mrad)
75	0.05462	0.02895
65	0.043698	0.02316
55	0.032775	0.01737
45	0.02185	0.01158
35	0.01093	0.00579
25	0	0
15	-0.01092	-0.005794
5	-0.02184	-0.0115841
-5	-0.03277	-0.017374
-15	-0.04369	-0.02316
-25	-0.05461	-0.02895
-35	-0.06554	-0.03474
-45	-0.07644	-0.04053
-55	-0.08634	-0.04575

Table 12: ANSYS Analysis of the Effect of Temperature Change on the Alignment of M2 (X and Y axis)

	M2	
	Vertical	Hortizontal
Temp °C	RX (mrad)	RY (mrad)
75	-0.0424335	-0.00643049
65	-0.033947	-0.005144
55	-0.02546	-0.003858
45	-0.01697	-2.572
35	-0.00849	-0.001286
25	0	0
15	0.008489	0.001286
5	0.01697	0.002572
-5	0.02546	0.003857
-15	0.03394	0.005147
-25	0.04243	0.006427
-35	0.05092	0.007717
-45	0.05938	0.009007
-55	0.06708	0.010157

Resonator Temperature Analysis

The intent of the temperature analysis was two fold. The first was to validate the FEA analysis and secondly to quantify mirror misalignment across multiple test units at an accelerated stress temperature. The hypothesis presented is that misalignment of the resonator occurs primarily at cold temperatures because the thermal deformation of the laser cavity occurs at cold temperatures as indicated by the FEA. The hypothesis is supported by the following conditions:

- All testing and alignment of the resonator is performed at an ambient clean room temperature of approximately 24^0C to 26^0C. The internal laser temperature range from 80^0 to 120^0 C across the laser housing. As a result, the thermal distortion occurring at high temperatures does not contribute the mirror misalignment.
- A thermal interaction/ distortions at low temperature is possible between the different metal parts that are used to hold and align the resonator to the laser chassis.

The test data was gathered utilizing an accelerated test plan. There are several factors that drive the selection of an accelerated test plan such as sample size, test temperature, test cycle duration and test equipment availability. These factors contribute directly to the decision to use a particular test plan versus another. A poor test plan can ultimately waste a significant amount of time and money and not yield the required data to support any useful analysis.

Nelson (1990, p.317) describes three fundamental types of accelerated test plans that are available for use when performing an accelerated test.

Optimal plans yield the most accurate estimate of life at the design stress. Traditional plans consist of equally spaced test stress levels, each with the same number of specimens. Good compromise plans run more specimens at low stress than at high stress.

The optimal test plan was chosen primarily since it provides the most accurate estimate of device life at the design stress. An accelerated life test plan was generated using the ALTA™ software to determine the allocation of test units and other critical test requirements. Selection of an applicable stress temperature effect was critical to test success. The normal operating temperature of the laser is from -55^0C to 70^0C. A lower stress level of -70^0C was chosen since there has been no studies performed at -70^0C and the test chamber used to simulate hot and cold environments can supply a -70^0C environment. In addition there was no risk of introducing any new failure modes outside of resonator misalignment.

The temperature test was performed utilizing a functional resonator built in a standard laser cavity with representative heat loading sources equivalent to production units. For experimental purposes, the heat source installed is not a resonator component but does interact with the output from the resonator.

Consideration was given to the selection of a stress temperature of -70^0C versus the impact to the bond strength of the optics, laser diode performance, wiring harness assemblies and other internal laser components. There was no immediate risk identified by exposing the resonator to a stress temperature of -70^0C. ALTA™ requires specific test assumptions to support the model such as stress factors and probability data. Typically, the source of this data is usually from an engineering assessment or field data driven. The stress factor assumptions made were:

- An Arrhenius model is used for the life-stress relationship since temperature is the stressor.
- The design stress is measured in Kelvin and ranges from 218 to 343K (-55^0 to 70^0C).
- A maximum stress temperature of 203 K (-70^0C) was used to avoid the introduction of new failure modes.

Data Distribution Assumption:

- The laser reliability is expected to follow a Weibull distribution with the beta value of 3.
- A reasonable probability of failure at the upper temperature design stress (218 K/-55^0C) was chosen to be 20% (0.2) based on the production yield data that showed that the First Time through Test yielded an averaged pass rate of 80 % over a 1 year period.
- The probability of failure for the resonator is expected to be 90% when tested for 7 cycles at 203K since this temperature exceeds the operating stress limit of 218 K.
- Test cycle time was established at 390 minutes or 6.5 hours per unit.

Test Cycle

Test cycle time is the time required by the resonator to reach the stress temperature from a non-powered state to an operational state and vice versa. The time measured was 30 minutes from a cold soak temperature of 203 and 218 K to reach the operating temperature of 80^0 and 120^0C respectively for the diodes and the internal heat source. Production lasers are subjected to

multiple cycles of Environmental Stress Screening, (ESS) to eliminate early life failures. A similar methodology was implemented utilizing 7 cycles of On/Off temperature excitation to replicate an equivalent the amount of induced thermal shock. The rationalization for using 7 cycles is based on the current test process where 6 cycles are used. The additional cycle was added to ensure measurements stability in addition to determining whether further resonator degradation was occurring.

Presented next is the output data from the ALTA™ software for test plan execution.

Input

Test Plan	2 Level Statistically Optimum Plan
Use Level Unreliability Criterion	0.1
Distribution	Weibull
Beta	3
Stress Count	1
Test Duration	6.5
Allocated Units	24

Stress 1

Stress Relation	Arrhenius
Use Stress	218
Highest Stress	203

Probabilities of Failure

P(Test Duration, Use Stress)	0.2
P(Test Duration, Highest Stress)	0.9

Results

	Stress Level	**Portion Units**	**Units on Test**
Low Stress Level	217.6301	0.923	22.152
High Stress Level	203	0.077	1.848

Tp (Time at Unreliability)	5.0615

ALTA ™ indicated that with a test sample size of 24 samples the test plan was statistically sound. The quantity of units for test at each stress levels were:

- 22 units at 218 K (92.3 % of the population).
- 2 units at 203 K (7.7% of the population).

ALTA ™ uses two critical attributes for determining the accuracy of a test plan. The Confidence level and Bounds Ratio are used to determine the test plan effectiveness for detecting failures that are representative of device performance.

The Confidence Level is defined as the ratio of upper confidence bound to lower confidence bound based on the amount of test samples used. In this case, *the calculated confidence level was 85%*. This confidence value indicates that the number of samples proposed will accurately represent the attribute under evaluation, (resonator misalignment).

The Bounds Ratio was determined based on the number of the samples tested and a confidence level desired. The goal is to obtain a number that is close to one. This indicates the tighter the confidence bounds the greater certainty. *The calculated Bounds Ratio was 1.68.* This calculated value was accepted since lowering the confidence bound required approximately twice as many test samples which were unavailable.

Temperature Study

The temperature experiment was performed in a Thermotron Environmental Chamber Model 5400. All 24 samples were cycled for 7 On/Off cycles. Data measurements were documented when the internal resonator component temperatures were stabilized at design set points. The required temperature set points of 80^0 C (diode operating temperature) and 120^0 C (heat load temperature) were monitored and recorded during the experiment. Additional data points were captured to ensure temperature stability specifically the temperature of the chamber and the external surface temperature of the resonator cavity.

The resonator components used were representative of fielded hardware. A mirror configuration change was required to support testing and data gathering. The resonator under evaluation utilized a flat - curve mirror configuration. In this configuration it was not feasible to measure the misalignment of the mirrors using an autocollimator.

An autocollimator is an optical instrument used for the non-contact measurement of angles. In optical engineering it is used to align optical components and measure their movement. An autocollimator works by projecting an image onto a target mirror and measuring the movement of the returned image against a scale.

In principle a flat mirror reflects collimated light back to the origin but a curve mirror focuses the collimated light to a point. The focused light would not be returned to the autocollimator for measurement via the reticule. As a result, a second flat mirror (M2) was used in place of a curved mirror, M1. This change did not affect the results of the experiment since the laser was not emitting photons but was only powered for actual heat loading effects. The following steps were implemented to measure the misalignment:

- All optical components were inspected and cleaned prior to install to reduce the possibility of contamination burns.
- A HeNe laser was used to statically align both mirrors. A HeNe laser is an inexpensive Helium Neon gas laser that is commonly used in laboratories. It operates at 632.8nm.
- Each test resonator/laser was installed in the chamber within a specially designed housing with shock absorption feet to negate the effects of chamber vibration during operation.
- The autocollimator used in the experiment provided angular displacement measurement increments of arc minutes. The measurement sensitivity was established to be 0.5 arc minute per graduation.
- Performed zeroing of the autocollimator to M2 to identify a mirror reference while the chamber was at ambient temperature.
- Chamber temperature was cycled and mirror misalignment measurements were captured over iterations.

Figure 24 is one of measurements taken using the autocollimator with the image capture software (Spiricon) used to obtain still images of angular displacement. The sample being measured is #22 during cycle 2 at -55^0 C.

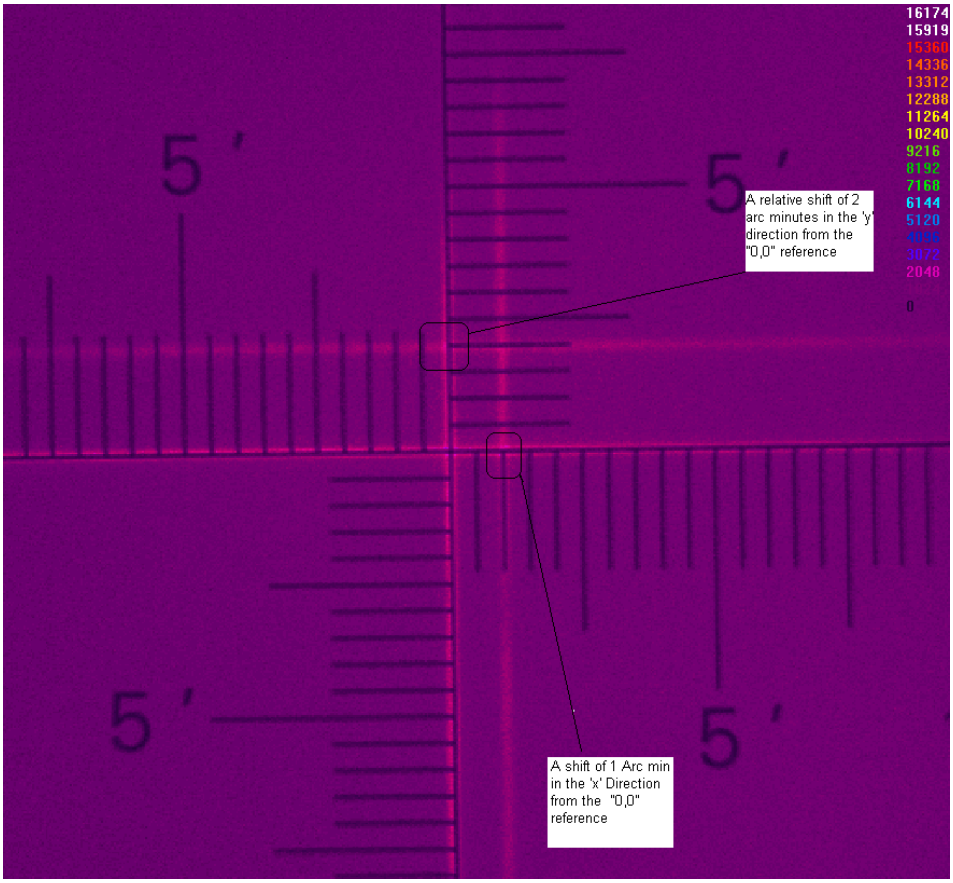

Figure 24: Spiricon Image Capture through the Autocollimator of Test Sample 22 during cycle 2 at -55^0 C showing the Angular Displacement Observed.

Utilizing this measurement accuracy required the use of a conversion factor since the simulation data collected was measured in micro-radians, (µrad). The conversion factor used was 1 arc minute = 290.88 µrad. All misalignment measurements were taken and then compared to the reference point established for both states, (On/Off) of the temperature controller. The misalignment was then calculated by taking the new position relative to the reference position at the specified temperature controller state.

To establish experimental creditability since all test samples were partial lasers, essentially only complete resonators installed within the laser cavity. Two fully functional lasers

were included within the sample groups (1 for each temperature) to prove that using only completed resonators did not compromise the test data. The complete lasers were identified as Sample one (1) in both test groups. For both temperature studies, the misalignment data gathered from the complete lasers (Samples #1) were representative of the units that were partially completed, (resonator only installed). Tables 21 through 44 located in the Appendix are the individual temperature test reports for the 24 units that were subjected the temperature study.

The angular displacement values used for all analyses were horizontal tilts (y rotations) primarily because of the a-symmetrical design of the resonator. A test data summary is presented in Table 13. The measured data indicates that horizontal tilting of the mirrors occurred at both low temperatures but was more significant at -70^0 versus -55^0C as expected

Table 13: Temperature Test Report Summary

			Hortizontal Tilt (Y Rotations)			
Sample #	**Temp (^{0}C)**	**Build State**	**Min Ang Disp (µrad)**	**Max Ang Disp (µrad)**	**Mean Ang Disp (µrad)**	
Sample 1	-70	Complete	145.44	218.17	206.05	
Sample 2	-70	Resonator	290.89	290.89	290.89	
Sample 1	-55	Complete	72.72	72.72	72.72	
Sample 2	-55	Resonator	72.72	72.72	72.72	
Sample 3	-55	Resonator	145.44	145.44	145.44	
Sample 4	-55	Resonator	145.44	145.44	145.44	
Sample 5	-55	Resonator	72.72	145.44	133.32	
Sample 6	-55	Resonator	72.72	145.44	133.32	
Sample 7	-55	Resonator	145.44	145.44	145.44	
Sample 8	-55	Resonator	72.72	72.72	72.72	
Sample 9	-55	Resonator	72.72	72.72	72.72	
Sample 10	-55	Resonator	72.72	145.44	133.32	
Sample 11	-55	Resonator	72.72	145.44	84.84	
Sample 12	-55	Resonator	72.72	72.72	72.72	
Sample 13	-55	Resonator	145.44	145.44	145.44	
Sample 14	-55	Resonator	72.72	72.72	72.72	
Sample 15	-55	Resonator	145.44	145.44	145.44	
Sample 16	-55	Resonator	145.44	145.44	145.44	
Sample 17	-55	Resonator	72.72	145.44	121.2	
Sample 18	-55	Resonator	72.72	72.72	72.72	
Sample 19	-55	Resonator	72.72	72.72	72.72	
Sample 20	-55	Resonator	72.72	72.72	72.72	
Sample 21	-55	Resonator	72.72	72.72	72.72	
Sample 22	-55	Resonator	72.72	145.44	133.32	

Temperature Modeling

To model the temperature versus misalignment of the resonator to establish an Arrhenius relationship was achieved using the ALTA SW package. ALTA provides life distribution optimization based on the input test data. Use of this feature allows the user to select the most acceptable life model to be applied via a comparative analysis of the test data to model fit that is generated. ALTA indicated that the Weibull distribution was the best match based on the test data set supplied.

The correlation between an independent variable and temperature is best described using the Arrhenius equation as identified in Chapter 2 of this research. It is the fundamental acceleration model that predicts the relationship of how time to failure varies with temperature. "Once a model is specified with its parameters, and data have been collected, one is in a position to evaluate its goodness of fit, that is, how well it fits the observed data. Goodness of fit is assessed by finding parameter values of a model that best fits the data" (Myung 2003, p.90).

Based on the test data collected, ALTA recommended the MLE as the most applicable for use to estimate the parameters of the Weibull distribution. Identified in Table 37 are the results generated by ALTA where;

- Model: Arrhenius. The model selected to measure the thermal accelerated stresses.
- Distribution: Weibull life distribution selected.
- Analysis: MLE, life distribution parameter estimation method.

- Beta (β) = 3.62. Slope of the line used to represent the failure rate of the Weibull distribution. This indicates that the failure rate increases with time which is an expected behavior since lasers do not have an infinite life.
- B and C = Model constants generated by the ALTA from fitting the test data to the Weibull distribution.
- Ea = Activation Energy measured in Electron Volts (Ev).
- LK Value: Used to determine test data to model fit. A value close to zero is preferred when comparing different life distributions.
- Fail\ Susp: Number of test points entered and the associated test state (pass or fail)

Table 14: ALTA Results for Distribution Fitting of Misalignment Data over Temperature.

Model:	Arrhenius
Distribution:	Weibull
Analysis:	MLE
Beta:	3.625615409
B:	2227.218386
C:	0.004487319
Ea:	0.191927983
LK Value:	-120.44546
Fail \ Susp:	24 \ 0

Further analysis was completed to understand the effect of temperature and time to fail. A life versus stress graph was generated using ALTA to determine the effect of temperature versus resonator life. With proper interpretation, the model and data supports the hypothesis that laser usage at cold temperatures can result in mirror misalignment due to the thermal movement/

bending of the resonator bed, the potential shifting of the mirrors and the coefficient of thermal expansion of different materials used in the laser.

Figure 25 is the Life versus Stress graph that represents laser life (represented as mirror misalignment) versus temperature, (Kelvin). The data indicates that lowering the temperature of the resonator results in an increase in life. Unfortunately this is the inverse to the experimental data since life is equated to misalignment. An increase in misalignment results in a decrease in laser life. A more realistic relationship would be misalignment versus temperature, (Kelvin). This would clarify and support the data being presented. Unfortunately ALTA is designed with a defined set of models to represent the time to failure data, ultimately transferring interpretation to the end user.

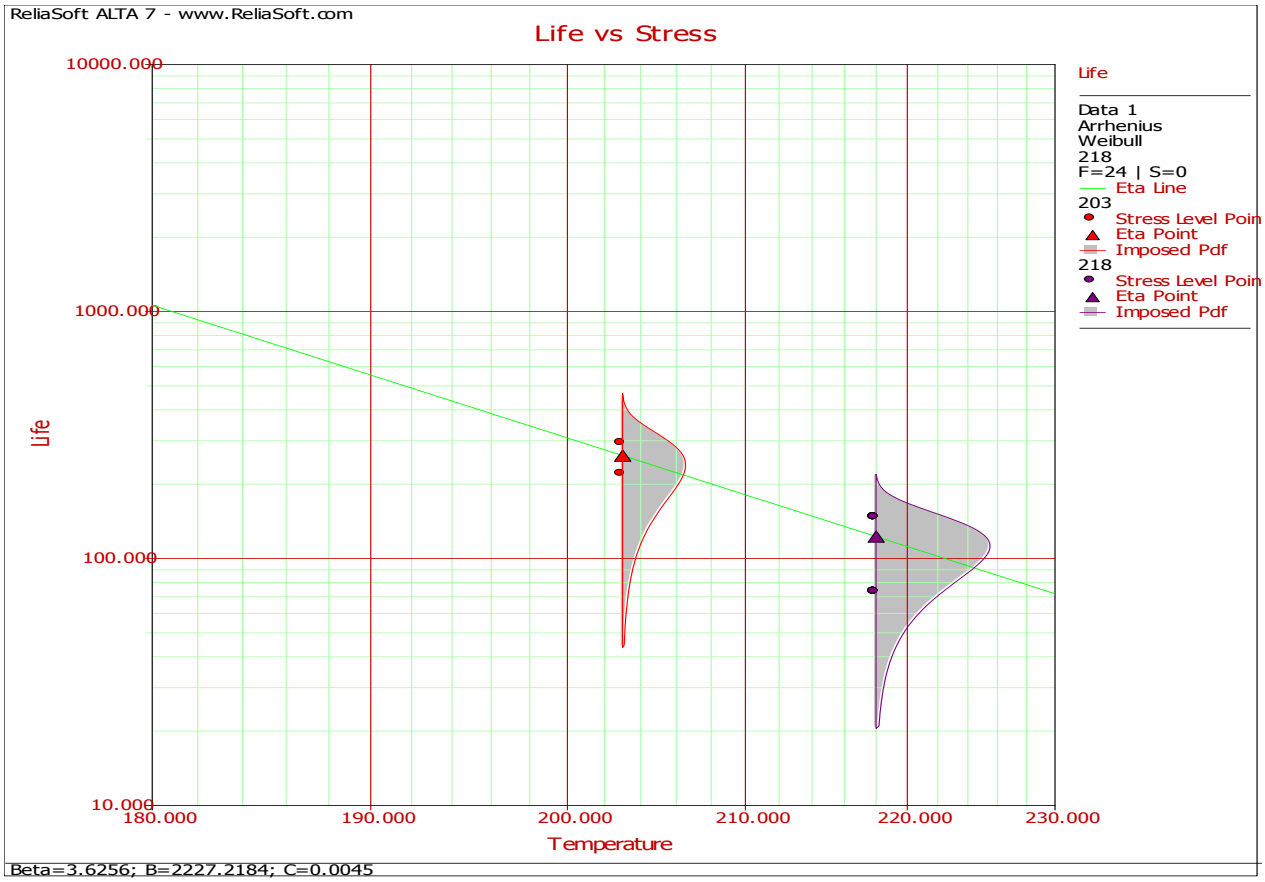

Figure 25: Life versus Stress Graph for Temperature.

An Arrhenius life equation can now be used to support solving for an acceleration factor. Based on the Arrhenius AF as presented in Chapter 2, the equation can be adopted to model the misalignment versus temperature relationship. Referring to *Equation 10*, the Arrhenius equation states;

$$AF = e^{\frac{Ea}{K}\left(\frac{1}{T_1}-\frac{1}{T_2}\right)} \qquad (10)$$

If the following assumptions are established:

- All lasers are built and aligned in a clean room environment under temperature controlled.
- Resonators are aligned and are fully functional at the diode set-point temperature/ resonator cavity temperature. The failure rate is zero at the completion of the build process.
- If a resonator is functional, there should be no changes to alignment and as a result the resonator operating temperature can be normalized in an equation or referenced as the baseline temperature T2.
- Assume that T1= Laser Cold Operating Temperature in Celsius = $T_{OE.}$
- Assume that T2= Resonator Operating Temp (~ Diode Temp) in Celsius = $T_{RO.}$

The Temperature Model for a flat – curve resonator:

$$AF = e^{\frac{Ea}{K}\left(\frac{1}{273+T_{OE}} - \frac{1}{273+T_{RO}}\right)} \quad (25)$$

The resonator used in this study was designed for operation at -55^0C. The diode operation temperature is 80^0 C. The proposed model was used to determine the AF due to temperature using equation (25).

Where:

T_{OE} = -55^0C: Cold temperature for laser operation.

T_{RO} = 80^0 C: Diode Operating temperature for design under study.

Ea = 0.1919 eV: Obtained from an earlier calculation in Table 37.

K =0.00008617 eV/K: Boltzmann constant from the Arrhenius Equation measured in Electron volts/ Kelvin.

Using Temperature Model developed for a flat – curve resonator:

$$AF = e^{\frac{0.1919}{0.00008617}\left(\frac{1}{273.16-55}-\frac{1}{273.16+80}\right)} \quad (26)$$

$$AF = 49.75$$

The calculated value of 49.75 indicates that the failure mode, (mirror misalignment) has a factor of 49.75 times at a temperature of -55^0C.

Vibration Model Development

FEA of Vibration contribution to misalignment

The resonator cavity was subjected to an FEA study to determine the natural resonant frequencies that can contribute to a linear displacement or shift of the resonator mirrors. The exercise is commonly referred to as a modal analysis. The performance of a modal analysis is applicable since this section of the research is focused on determining the effect of vibration to both short term and long term mirror misalignment measured as a linear displacement. "Modal analysis can be used to provide information concerning the natural frequencies, modal damping factors, and mode shapes of structures and machinery. This information can be obtained from

mathematical analysis of a structure's dynamic response derived from a set of equations and knowledge of its mass and stiffness distributions, (Crocker, 2007, p.432).

During the modal analysis process, a simulated resonator is subjected to a random vibration spectrum to identify the modal or resonant frequencies. There were 12 resonant frequencies identified during the analysis. The modal frequencies identified were then evaluated to determine the effect of mirror misalignment, specifically at which frequency was there the most distortion observed to the resonator bed that would cause M1 or M2 to become misaligned from the optical axis. The test plan implemented utilized a random vibration profile that covered the 12 modal frequencies across a 2Hz to 2 KHz range using accelerometers to measure the linear displacement of the mirrors.

The most common vibration measurement sensor used to measure linear displacement is an accelerometer. "It is an electronic device that measures the acceleration of an object when it is rigidly coupled to the object under evaluation" (The Eastman Kodak, 2004, p.620). The output from an accelerometer is an electrical pulse proportional to the surface acceleration or stimulation detected. High levels of amplification of the electrical signal are often required for recording or display of the pulsed data. Electrical signals are often calculated as the Root Mean Square, (RMS) since it provides a more accurate and stable representation of the signal data when compared to peak to peak data. The G_{RMS} is a calculated using the RMS signal data. Tri-axial accelerometers were chosen as the measurement devices to record the displacement of M1 and M2. "A tri-axial accelerometer combines three accelerometers mounted at right angles to each other in a convenient package" (The Eastman Kodak, 2004, p.620). Tri-axial accelerometers are intended for simultaneous measurement of vibration in 3 perpendicular axes.

Vibration Experiment

A test plan was developed to measure the linear displacement of M1 and M2 from the effects of vibration stimulation. ALTA™ was not used in this instance to generate a test plan since all units were subjected to the same vibration stimulation coupled. There were 6 units evaluated in the vibration experiment. For each case, individual "tri-axial" accelerometers were mounted to the M1 and M2 mirror mounts within the resonator cavity. The laser was then mounted to the vibration table and power was applied by the controller box to simulate an in-use temperature active condition. Once the diode and heat load temperatures reached their desired levels of 80 and 120°C, respectively, a random vibration profile from 2Hz to 2 KHz was applied over a 15 minute period from 1 to 10 G_{RMS}. This provided 60 data points for analysis further supporting the adequacy of using 6 samples.

Optical alignment checks were performed before and after each vibration test to ensure all torqued optical components remained intact pre and post vibration analysis. This step eliminated the possibility of loosened screws or mounted hardware that could contribute to mirror misalignment.

It should also be noted that both mirrors could potentially be angularly displaced from the optical axis as a result of a vibration stress. Unfortunately a test method to measure the angular displacement of M1 and M2 was not developed due to the unavailability of the required test equipment and the complexity of the test configuration. To accurately measure the angular displacement of the mirrors while the resonator was subjected to various vibration stresses is both a challenging and complex task since the required measurement accuracy is micro-radians of tilt. As a result, it was an assumed risk for the vibration experiment. Table 15 present the test

values obtained for vibration testing for linear displacement of M1versus changes to vibration input. The data indicates that S1 and S5 did not respond in the same manner as the other samples; an increase in vibration stimulation did not always result in an increased displacement.

Table 15: Measured Linear Displacement of M1(X axis shifts) versus Changes in Vibration Stress

		Linear Displacement of M1 in the X axis				
Vibration Level (Grms)	Sample 1 (μm)	Sample 2 (μm)	Sample 3 (μm)	Sample 4 (μm)	Sample 5 (μm)	Sample 6 (μm)
1	4.1148	31.75	11.0998	6.9088	27.686	25.654
2	6.1722	52.324	15.3924	33.02	51.562	44.704
3	13.2588	72.39	16.129	49.276	67.818	60.198
4	9.6774	89.916	21.5138	59.182	81.534	72.39
5	85.344	91.186	26.416	73.66	76.708	82.042
6	60.706	112.268	30.226	80.01	52.832	86.36
7	73.914	121.666	31.496	89.662	31.242	90.678
8	75.184	141.732	35.56	99.568	37.592	96.266
9	44.45	154.432	41.402	109.982	41.656	98.044
10	39.878	166.37	45.212	121.158	16.4592	108.712

There were experimental errors observed in the data from Samples 1 and 5. The bonding agent used to attach the tri-axial accelerometer to the mirror mount in Sample 1 was softened. This allowed the accelerometer to move during the test providing false displacement readings. An alternative adhesive was used on samples 2 to 6. The erroneous readings from Sample 5 were the result of the detachment/ reattachment process of the accelerometer. Using a stronger adhesive used for bonding to the mirror mount required additional effort. A new accelerometer was used for sample 6.

Vibration Data Analysis

Various level of mirror misalignment was observed at varying levels of vibration stimulus (G_{RMS}). The test data indicated the linear displacement of M1 ranged from a low of 6.9088µm (S4@ 1GRMS) to a high of 166.37µm (S2 @ 10 GRMS). A graphical comparison is shown in figure 26, which compares the linear displacement of M1 versus vibration input for across samples 2, 3, 4 and 6.

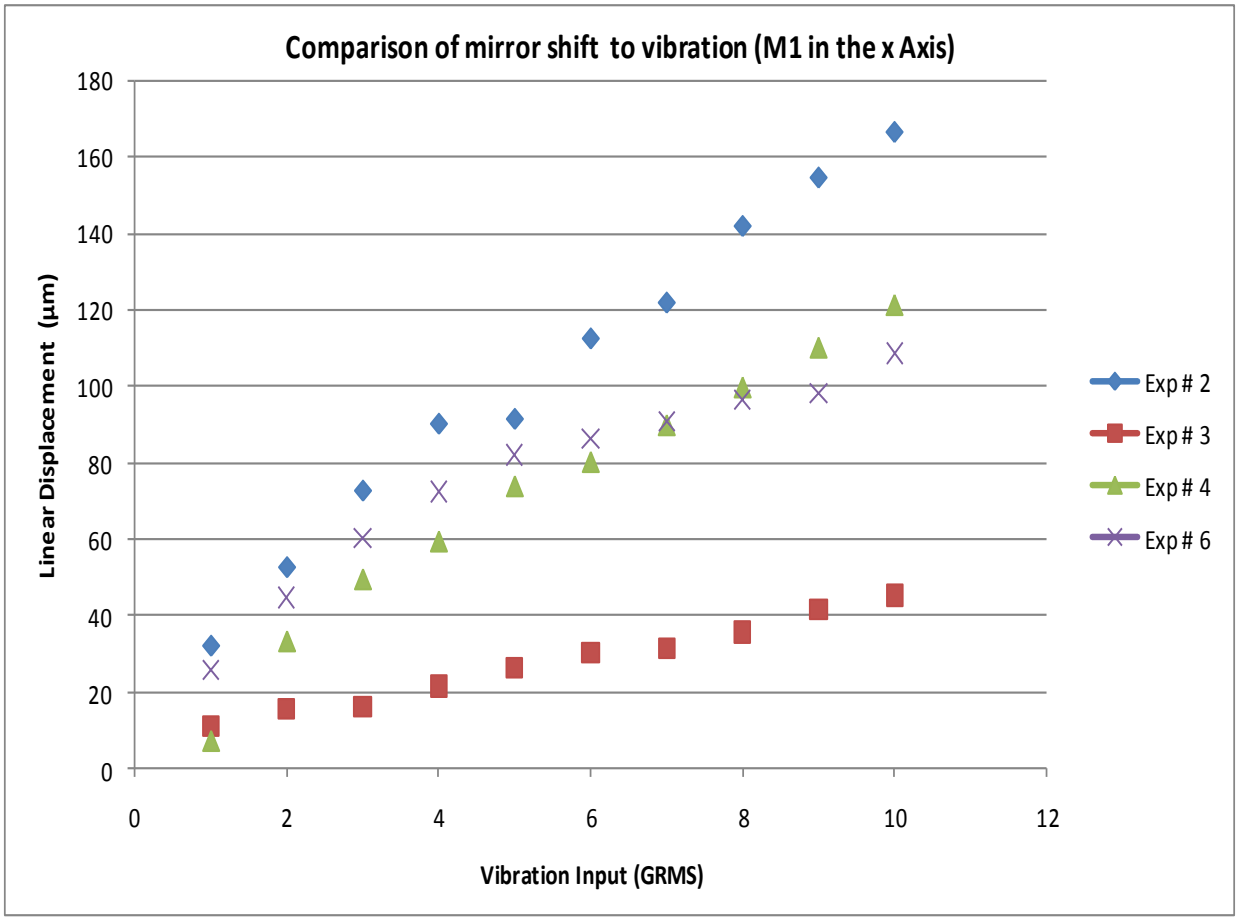

Figure 26: Linear displacement of M1 (X Axis) versus Vibration Strength

To support the development of a PoF vibration model, a failure limit was established similar to the temperature model. The failure limit defined in the thermal model is the reduction of the average output power by 10%. For consistency, the same failure limit was re-used as the standard approach for defining resonator failure.

The GLAD data indicated that the calculated average output power was 3.74W. A reduction by 10% to 3.36W of output power translated to a linear displacement of M1 equal to 82µm. The resonator under test is rated up to 5 G_{RMS} for retaining optical alignment. Generally a laser is not expected to show signs of degradation when the vibration limit is not exceeded. In cases where there were high vibration stresses applied as observed on samples 2, 4 and 6 the linear displacement measured exceeded the failure limit of 82µm which is an anticipated response.

Vibration Modeling

ALTA ™ was utilized to model the effects of resonator misalignment due to vibration stimulus to support the development of an acceleration model based on the IPL. Utilizing the features of ALTA for life distribution optimization based on test data supplied, a life distribution rank analysis was generated. The analysis indicated that the Weibull distribution was the best match based on the test data supplied.

The distribution rank selection is based on the goodness of the data fit and the calculated likelihood value, (LK Value). Using the test data collected, ALTA implemented the MLE to

estimate the parameters of the Weibull distribution. Identified in table 39 are the results from ALTA. The following model parameters are described:

- Model: Inverse Power Law. The model selected to measure the non-thermal accelerated stresses (vibration).
- Distribution: Weibull Life distribution selected.
- Analysis: MLE, life distribution parameter estimation method.
- Beta (β) = 2.7365. Slope of the line used to represent the failure rate of the Weibull distribution. Similar to the temperature model, the value indicates that the failure rate increases with time.
- K = Model constants generated by ALTA from the test data. K>0.
- n = Value of the life exponent. It is a measure of the effect of the stress on the life of the product.
- LK Value: Used to determine test data to model fit. A value close to zero is preferred when comparing different life distributions.
- Fail\ Susp: Number of test points entered and the associated test state (pass or fail).

Table 16: ALTA Results for Distribution Fitting of Misalignment Data across Different Vibration Input

Model:	Inverse Power Law
Distribution:	Weibull
Analysis:	MLE
Beta:	2.736591481
K:	0.041161486
n:	-0.707349032
LK Value:	-186.4991026
Fail \ Susp:	40 \ 0

ALTA calculated a value for n using the MLE to be -0.7073 *(Refer to table 38).* Unfortunately this value is misleading, (*a negative value*). A negative value indicates that the life of the unit is increasing as the stress increases, primarily because ALTA in this scenario equates life to linear displacement, *(refer to chapter 2 on the IPL).* It was shown experimentally that an increase in the vibration level resulted in an increase in the linear displacement. An increase in the linear displacement equates to an increase in the mirror misalignment ultimately causing a decrease in the average output power from the resonator. Thus an increase in life as represented by a negative life exponent (-0.7073) translate to an increase in linear displacement, which is counter intuitive since it is an increase in amount of mirror misalignment.

Instead, if the absolute value is used, the calculated value for the life exponent, (n) remains valid since n is a measure of the effect of the stress on the life of the unit. The life exponent used in this analysis is 0.7073.

The IPL AF was defined in chapter 2 as equation 7 which states:

$$AF = \left(\frac{V_A}{V_u}\right)^n \tag{27}$$

Instances where the use stress (V_u) can be selected to be zero for a particular environment is undesirable for calculating an acceleration factor. The approach adopted by the PCM is to normalize the ratio of the accelerated stress to use stress by the addition of 1 in the numerator and the denominator of the equation. The adoption of a similar normalization approach is feasible and does not invalidate the concept.

The revised Vibration Model for a flat – curve resonator is:

$$AF = \left(\frac{V_A+1}{V_u+1}\right)^n \tag{28}$$

If the Vibration AF Model is used to calculate the vibration impact on a flat - curve resonator with a stress level equal to 3.3 G_{RMS}, which is the default vibration level for a rotary wing aircraft as identified in Table 40 (an application of this laser).

Where:

V_A = Maximum applied stress applied to the resonator = 10 $_{GRMS}$

V_u = Use Stress = 3.3 $_{GRMS}$

The Vibration AF calculated using equation 28 is equal to

$$AF = \left(\frac{10+1}{3.3+1}\right)^{0.7073} \tag{29}$$

$$AF = 1.94$$

The calculated value of 1.94 indicates that the failure mode, (mirror misalignment) has a factor of 1.94 at a vibration level of 3.3 G_{RMS}. Table 17 is applicable for use in this research since literature on its accuracy and validity is available in the public domain. Additionally it has been validated for use by the RIAC for the 217 PLUS FR models. The environments listed in Table 17 are applicable to the laser FR model proposed.

Table 17: Environmental Stress Values

Environment	Vibration (GRMS)
Airborne	9
Airborne (Fixed Wing)	9
Airborne (Fixed Wing - Inhabited)	9
Airborne (Fixed Wing - Uninhabited)	9
Airborne (Missile)	10
Airborne (Missile - Flight)	1.3
Airborne (Missile- Launch)	16
Airborne (Rotary Wing)	3.3
Airborne (Rotary Wing - Inhabited)	3.3
Airborne (Rotary Wing -Uninhabited)	3.3
Airborne (Space)	0
Ground	0
Ground (Man Pack)	1
Ground (Mobile)	10
Ground Mobile (Heavy Wheeled)	10
Ground Mobile (Heavy Wheeled - Chassis Mount)	10
Ground Mobile (Heavy Wheeled - Engine Compartment)	10
Ground Mobile (Heavy Wheeled - Engine Mount)	10
Ground Mobile (Heavy Wheeled Instrument Panel Open)	10
Ground Mobile (Heavy Wheeled Instrument Panel Closed)	10
Ground Mobile (Heavy Wheeled - Trunk)	10
Ground Mobile (Light Wheeled)	4
Ground Mobile (Light Wheeled - Chassis Mounted)	4
Ground Mobile (Light Wheeled - Engine Compartment)	4
Ground Mobile (Light Wheeled - Engine Mounted)	4
Ground Mobile (Light Wheeled - Instrument Panel Open)	4
Ground Mobile (Light Wheeled- Instrument Panel Closed)	4
Ground Mobile (Light Wheeled - Trunk)	4
Ground Mobile (Tracked)	2
Ground (Stationary - Indoors)	0
Ground (Stationary - Outdoors)	0
Naval	0.7
Naval (Shipboard)	0.7
Naval (Shipboard - Sheltered)	0.7
Naval (Shipboard - Unsheltered)	0.7
Naval (Submarine)	1

DP FR Model Composition

The temperature and vibration acceleration models that were derived earlier (*Equations 24 & 28)* can be used to create an improved DP FR model based on the PoF methodology. In Chapter 2, new FR models that were based on the PoF methodology were discussed in detail. All the PoF FR models discussed, measured and represented the effects of temperature and vibration as "Pi Factors", (π_x). When temperature and vibration pi factors are combined with a base FR, a term referred to as the Environmental Factor is created. The Environmental Factor for the improved DP FR model will be represented as ($\pi_{E\ PoF}$).

The development of an environmental factor for new FR models such as the 217 PLUS and PCM FR models (*equations 14 & 17*) were completed similarly. It is the multiplication of the FR and pi factors. By adopting this approach, the base FR for temperature and vibration related failures will be defined as λ_B, the pi-factor for temperature obtained from the temperature acceleration model is defined as π_T and the pi-factor for vibration based on the vibration acceleration model is defined as π_V.

The equation for calculating the DP FR environmental factor is proposed as:

$$\pi_{E\ PoF} = \lambda_B * \pi_T * \pi_V \quad (30)$$

Referring to equations (25) and (28) respectively as defined earlier for reference:

$$\pi_{T=} e^{\frac{Ea}{K}\left(\frac{1}{273+T_{OE}}-\frac{1}{273+T_{RO}}\right)} \quad (25)$$

$$\pi_V = \left(\frac{V_A+1}{V_u+1}\right)^n \quad (28)$$

Nicholls (2007, p.20) identified that the base FR due to environmental factors, (λ_B) can be calculated using the following equation:

$$P_{FC} * \lambda_{obs} = \lambda_B * \pi_o \quad (31)$$

Where:

P_{FC} = Percentage of the failure rate attributable the operational failure causes.

λ_{obs} = Observed Failure rate percentage, (field data).

λ_B = Base failure rate to be derived.

π_o = Product of the Pi Factors, (π_T & π_V)

Solving for λ_B,

$$\lambda_{\boldsymbol{B}} = \frac{P_{FC} * \lambda_{OBS}}{\pi_o} \quad (31)$$

Nicholls (2007, p.20) further stated that it is feasible to use an adjustment factor (P_F) to address or scale the failure rate in instances where there are failed units that are unaccounted for within equation 32. This resulted in a new equation:

$$\lambda_{\boldsymbol{B}} = \frac{P_{FC} * \lambda_{OBS}}{\pi_o} * P_F \quad (32)$$

The use of P_F in the DP FR model is feasible since there is a difference observed in the failure rate due to operational causes (temperature and vibration) versus the field failure rate.

- The observed failure rate percentage based on field data for temperature and vibration failures, (λ_{obs}) was 42.8%.
- The percentage of failures attributed to operational causes was 60.16% (refer to Table 4).
- Using the Goal seek function in Microsoft Excel to solve for P_F, generated a solution of 1.4056.

The value for λ_B can be calculated by first solving for π_O

$$\pi_O = \pi_T * \pi_V = 1.94 * 49.75 = 96.5 \quad (33)$$

Substituting π_O in *Equation 33,*

$$\lambda_{\boldsymbol{B}} = \frac{0.6016 * 0.428}{96.5} * 1.4056 \quad (34)$$

$$\lambda_B = 3.75x10^{-3}$$

Using *Equation 30* to calculate the $\pi_{E\text{-}PoF}$

$$\pi_{E\ PoF} = 3.75x10^{-3} * 49.75 * 1.94 \quad (35)$$

$$\pi_{E\ PoF} = 0.3619$$

Comparing the MIL HDBK 217F environmental factor π_E versus $\pi_{E\text{-}PoF}$ for the same environmental application is 7 vs. 0.3619. The effect of using an environmental factor that is 19.4 times larger, (π_E) results in an inflated FR that masks true laser performance since the failure mechanisms are not accurately modeled.

DP FR Model Validation

Model validation is the most critical step in establishing credibility for a proposed model that has not yet been proven. A FR model that is based on the PoF methodology provides the ability to map a cause to an effect relationship and as a result establishes its accuracy based on the engineering analysis completed and the availability of field data for model comparison. Fundamentally, if the mechanisms that can cause a failure are understood, then accurate FR modeling of the effect results in the ability to derive an analytical solution that is representative system reliability.

A laser FR model is not a close end solution that guarantees a failure rate under all environments and circumstances. Instead, a laser FR model is a tool that provides the ability to compare different laser designs based on the intended application to determine how the correlation of temperature, vibration, number of optical surfaces, failures rates of the diode laser assembly, q switch and gain media all collectively interact to provide an estimate of anticipated performance, measured as the MTBF of the laser.

The proposed DP FR model is based on the MIL HDBK 217F Laser FR model with the inclusion of the following parameters:

- An environmental pi factor that represents the effects of temperature and vibration.
- Q Switch failure rate.

A Q switch is a critical component used in DP Laser designs yet it is unrepresented in the MIL-HDBK 217F laser FR model. Its fundamental function in a DP laser is to create a control mechanism that diffracts the beam out of the resonator thus prevents lasing from occurring until needed. The incorporation of the q switch FR within the proposed model is important since it is an electro-optical component with performance and limitation parameters established during its design and manufacturing.

The proposed model =

$$\lambda_p = (\lambda_{Pump} + \lambda_{Qswitch} + \lambda_{Media} + 16.3\,\pi_C\pi_{OS})\pi_{E-PoF} \quad (36)$$

Where:

λ_p = Laser FR

λ_{pump} = Pump Source FR

$\lambda_{q\ switch}$ = Q Switch FR

λ_{media} = Media FR

16.3 = Coupling Factor

π_C = Cleanliness Factor:

π_{OS} = Number of Active Optical surfaces.

$\pi_{E\text{ - }PoF}$ = Environmental factor

Where $\pi_{E\text{ - }PoF}$ = 0.3619 (*Refer to equation 36)*

To support model validation, a DP laser FR calculator was developed for comparing the predicted MTBF from the MIL HDBK 217F to the proposed FR model. The laser under evaluation is used in a pulse mode operation which is considered in the FR calculation. Additionally, the field data from the laser is recorded as the cumulative pulsed data. The FR comparison tables are identified as Table 18 and Table 19.

Table 18 is the DoD MIL HDBK 217F DP FR model that utilizes an overly aggressive π_E that does not accurately measure the effects of temperature and vibration nor includes a q switch FR.

Table 18: MIL HDBK 217F FR Model Sample Calculation

$\lambda_p = \lambda_{PUMP} + (\lambda_{MEDIA} + 16.3*\pi_c*\pi_{OS})\ \pi_E$ Failures/10^6 Hours		Values	Notes
λ_{PUMP}	Diode Bar Failure Rate	500	Mfg Test Data
λ_{MEDIA}	Media Failure Rate	0	Nd:YAG
16.3	Coupling Factor	16.3	Reliability Coupling Factor
π_c	Coupling Cleanliness Factor	30	Average Cleanroom Precaution
$\pi_{os(TOTAL)}$	Optical Surface Factor (Total Surface Count)	49	Total number of optical surfaces
π_E	Environment Factor : Provided by Mil Handbook	7	Airborne, Uninhabited, Cargo

	$\lambda_{OPTICS} = 16.3*\pi_c*\pi_{os}$	Pump
OPTICS	**Coupling Factor**	16.3
	π_c	30
	π_{os}	49
	λ_{OPTICS}	23961

$\lambda_{P\ (CONTINOUS)} =$	$(\lambda_{PUMP} +$	$\lambda_{MEDIA} +$	$\lambda_{OPTICS})\ *$	π_E
$\lambda_{P\ (CONTINOUS)} =$	500	0	23961	7
$\lambda_{P\ (CONTINOUS)} =$	171227			
$MTBF_{P\ (CONTINOUS)}$	5.84			

	Pulsed Impact	**Pulsed Impact**
PULSED IMPACT	**Period Description**	250 µsec @ 1KHz (Diode Pulse Rate)
	Time On (sec)	0.000250
	Cycles (Hz)	1000
	Pulse Impact (PI)	0.2500

$\lambda_{P\ (PULSED)} =$	$((\lambda_{(PUMP)} * PI) +$	$(\lambda_{MEDIA}) +$	$(\lambda_{OPTICS} * PI))$	π_E
$\lambda_{P\ (PULSED)} =$	125.00	0	5990.25	7
$\lambda_{P\ (PULSED)} =$	42806.75			
$MTBF_{(PULSED)}$	23.36			

Table 19: Proposed DP FR model that Utilizes a PoF Environmental Factor, π_{E-PoF}

$\lambda_P = \lambda_{PUMP} + (\lambda_{MEDIA} + 16.3*\pi_c*\pi_{OS})\ \pi_E$ Failures/10^6 Hours		Values	Notes
λ_{PUMP}	Diode Bar Failure Rate	500	Mfg Supplied
$\lambda_{QSWITCH}$	Q Switch Failure Rate	1000	Mfg Supplied
λ_{MEDIA}	Media Failure Rate	0	Nd:YAG
16.3	Coupling Factor	16.3	Reliability Coupling Factor
π_c	Coupling Cleanliness Factor	30	Average Cleanroom Precaution
$\pi_{OS(TOTAL)}$	Optical Surface Factor (Total Surface Count)	49	Total number of optical surfaces
π_E	Environment Factor	0.36193	Airborne, Rotary, Wing

	$\lambda_{OPTICS} = 16.3*\pi_c*\pi_{OS}$	Pump
	Coupling Factor	16.3
OPTICS	π_c	30
	π_{OS}	49
	λ_{OPTICS}	23961

π_E = Environmental Factor	$\pi_E = \lambda_B * \pi_T * \pi_V$	
Flat - Curve Resonator	Default Values	Notes
λ_B =	3.75E-03	Base failure rate for Flat Curve resonator
π_T =	49.75	Acceleration factor due to Temperature
π_V =	1.94	Acceleration factor due to Vibration
π_E =	**0.36193**	

$\lambda_{P\ (CONTINOUS)}$ =	(λ_{PUMP} +	$\lambda_{QSWITCH}$ +	λ_{MEDIA}	λ_{OPTICS}) *	π_E
$\lambda_{P\ (CONTINOUS)}$ =	500	1000	0	23961	0.36193125
$\lambda_{P\ (CONTINOUS)}$ =	9215.131556				
$MTBF_{P\ (CONTINOUS)}$	108.52				

	Pulsed Impact	**Pulsed Impact**
	Period Description	250 µsec @ 1KHz (Diode Pulse Rate)
PULSED IMPACT	**Time On (sec)**	0.000250
	Cycles (Hz)	1000
	Pulse Impact (PI)	0.2500

$\lambda_{P\ (PULSED)}$ =	((λ_{PUMP} * PI) +	($\lambda_{QSWITCH}$ * PI) +	(λ_{MEDIA} * PI) +	(λ_{OPTICS} * PI))	π_E
$\lambda_{P\ (PULSED)}$ =	125.00	250.00	0	5990.25	0.36193125
$\lambda_{P\ (PULSED)}$ =	2303.78				
$MTBF_{(PULSED)}$	434.07				

The use of the antiquated DoD model resulted in a predicted $MTBF_{(continuous)}$ of 5.84 hrs, with a $MTBF_{pulsed}$ of 23.36 hrs. This value clearly cannot represent the actual performance of the laser since it is a gross underestimation. In comparison, a PoF based model that accurately represents the environmental factor, (π_{E-PoF}) by including the effects of temperature and vibration, subsequently resulted in a predicted $MTBF_{(continuous)}$ of 108.52 hrs, with a $MTBF_{pulsed}$ of 434.07 hrs. Model validation is the comparison of projected to measured data.

A field life analysis of the lasers used in the FMEA process was completed to determine the correlation of the current field life measured as the MTTF of the laser versus the predicted MTBF which is determined using the predicted FR. The Minitab Statistical tool version 15 was used to perform the laser life distribution analysis. Minitab 15 is best suited to perform life data analysis because it supports mapping of a single set of data to multiple life distributions to maximize the line fit. Using the Least Squares Method, the best line fit of the field data was completed. The laser field data was compared to 11 life distributions to obtain the best data fit.

Figures 27, 28 and 29 are the Minitab results for the data life fit/ distribution mapping for the Weibull, Lognormal, Exponential, Log logistic, Smallest Extreme Value, Normal and Logistic distributions.

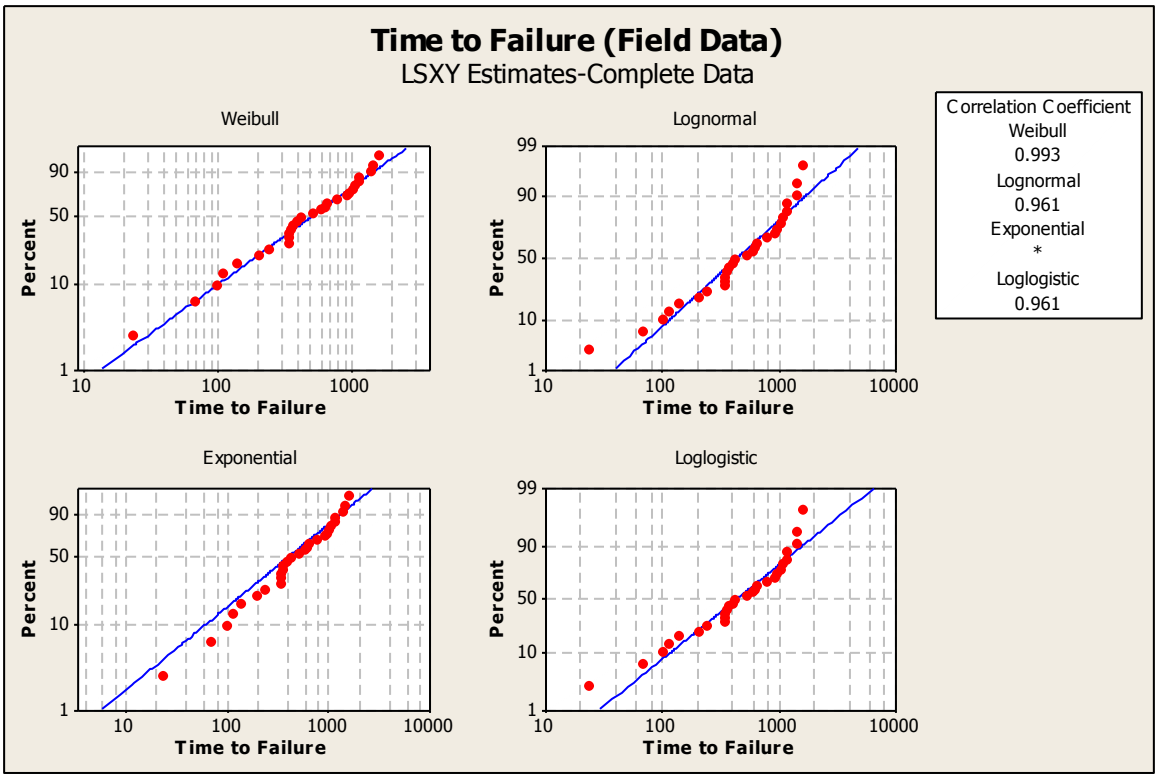

Figure 27: Time to Failure Distribution Mapping for the Weibull, Lognormal, Exponential and Log logistic Distributions

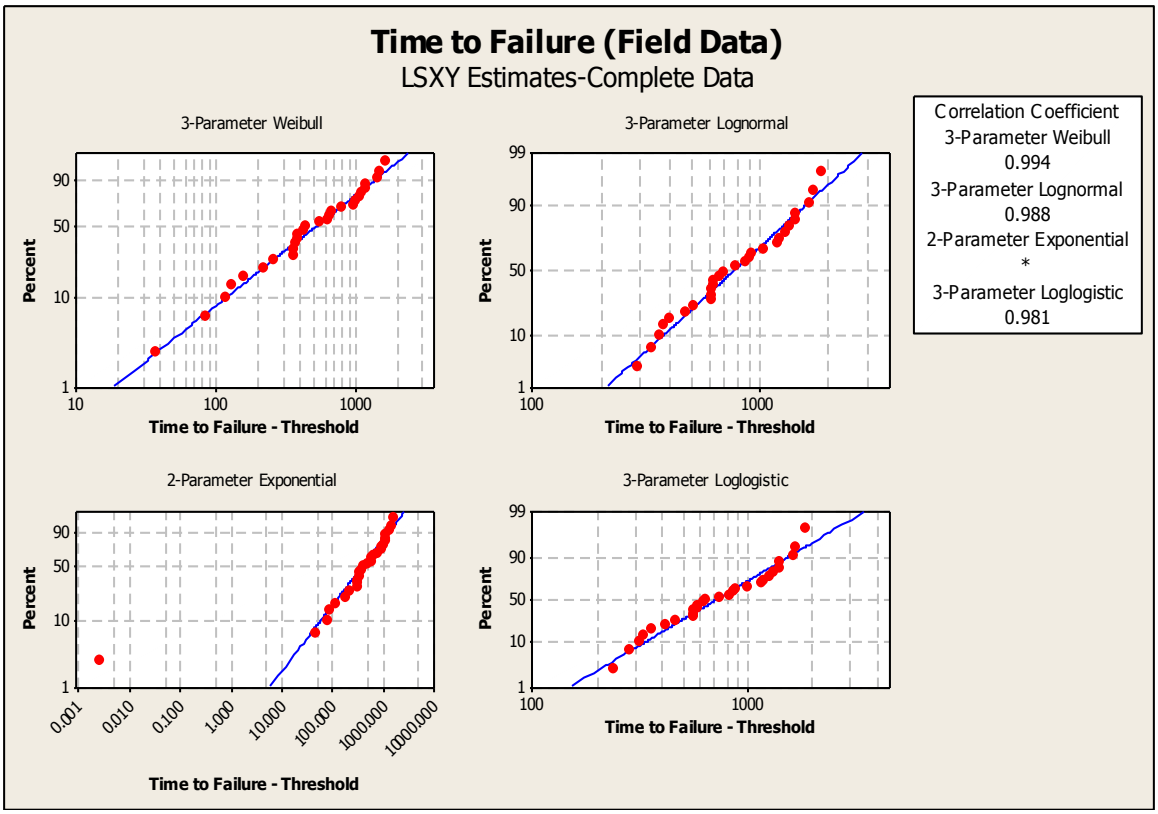

Figure 28: Time to Failure Distribution Mapping for the 3 Parameter Weibull, 3 Parameter Lognormal, 2 Parameter Exponential and 3 Parameter Log logistic distributions

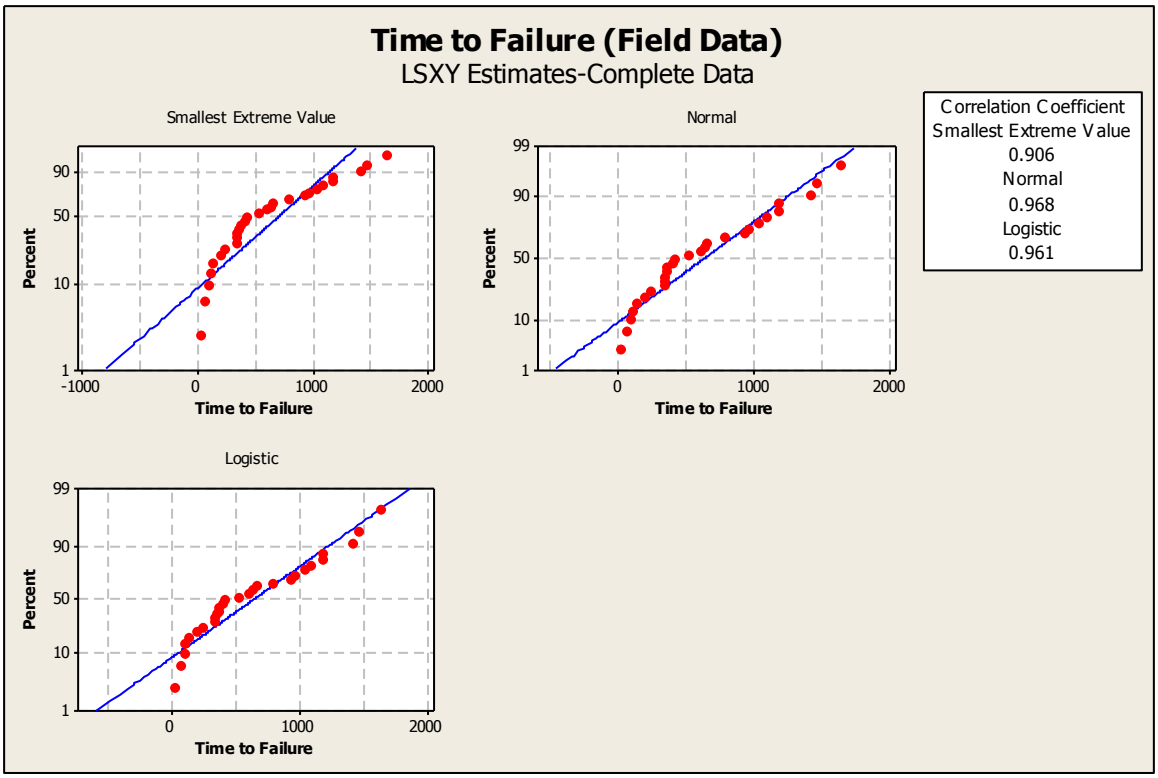

Figure 29: Time to Failure Distribution Mapping for the Smallest Extreme Value, Normal and Logistic Distributions

Table 20 is the Minitab results from the Goodness of Fit Test coupled with the Mean Time to Failure data for the individual distributions. There were two parameters from the Minitab analysis that were evaluated to determine the statistical confidence. The intent is to maximize both parameters for the most optimal solution:

1. Best data fit, the "Anderson Darling" statistic. The Anderson Darling statistic measures how well the data follows a particular distribution. The lower value the better the data fit. The 3 parameter Weibull distribution indicated an Anderson Darling Statistic of 0.639
2. The "Correlation Coefficient" is simply a regression line fit that attempts to maximize the value to 1. The 3 parameter Weibull distribution had a correlation coefficient of 0.994.

Based on the Anderson Daring Statistic and the Correlation Coefficient, Minitab generated an MTTF estimate for field data with 95% confidence of 449.22 hrs. When compared to the MTBF calculated using the proposed DP FR model an estimate of 434.07 hrs *(refer to table 42)* was calculated. This indicates that there is a strong relationship between the calculated values and the actual unit performance.

Table 20: Goodness of Fit and the MTTF for Field Data for a Flat – Curve Resonator/ Laser

Distrubtion	Anderson Darling Coefficient	Correlation Coefficient	Mean Time To Failure (MTTF)	Standard Error	Lower CI @ 95%	Upper CI @95%
Weibull	0.638	0.993	659.152	110.081	475.151	914.41
Lognormal	1.012	0.961	737.495	179.024	458.282	1186.82
Exponential	1.652	*	582.658	105.702	408.313	831.44
Loglogistic	1.042	0.961	829.274	263.089	474.643	1448.87
3-Parameter Weibull	0.639	0.994	648.623	101.737	449.223	848.02
3-Parameter Lognormal	0.715	0.988	650.287	104.817	444.85	855.72
3-Parameter Loglogistic	0.83	0.981	669.653	166.901	342.533	996.7
2-Parameter Exponential	1.475	*	593.203	104.057	420.62	836.6
Smallest Exterme Value	3.253	0.906	623.28	623.28	450.826	795.73
Normal	1.154	0.968	632.286	88.963	457.922	806.65
Logistic	1.256	0.961	632.286	91.889	452.186	812.39

CHAPTER FIVE: CONCLUSION

The previous chapters presented the methodology that was utilized to develop an improved laser FR model that provides the most accurate method to calculate the reliability of a DP laser that utilizes a flat - curve resonator. Chapter four described the simulations, experiments and analysis that were performed to ensure accuracy, reliability and credibility of the data used in the research to develop the model. The proposed model exceeds the capabilities of the current published DP laser FR model in MIL HDBK 217F Notice 2 since the effects of temperature and vibration were not accurately represented within that model. Environmental limiters (temperature and vibration induced failures) that reduce laser reliability are now measurable via the new environmental factor (π_{E-PoF}).

Results from the proposed model also show a strong correlation to the field reliability data for a DP flat - curve resonator. The data also indicated that laser field life can span a wide range of values, (MTBF) but the ability to tailor the FR model to the laser conditions of operation can identify areas of design improvements that are reliability opportunities. Jones and Hayes (1999) found in their research on circuit board reliability that there is still some inherent risk when comparing the output from a FR model, (MTBF or predicted reliability) to field data since early life product failure do occur in the field even after the post burn testing during the manufacturing processes. "Even if these considerations are taken into account, there is no guarantee that the field reliability is the same as that predicted because models are simple empirical approximations" (Jones & Hayes, 1999, p.127).

The approach used to develop the improved DR laser FR is consistent with the PoF models that are being developed by other organizations. Using the established practices of

accelerated life testing, life distribution analysis and proper acceleration model selection the foundation for creating a PoF model that is based on understanding the design, the use environment and the failure modes that occur during the life of the laser is achieved.

Research Limitations

Laser field failure data is very valuable yet unavailable in the public and research domain. Good data is primarily available within organizations that design, deploy and maintain lasers. Furthermore, many laser designs are considered proprietary and confidential since some are used in military applications hence specifics on reliability, failure rates and performance are not for disclosure.

The limitation of data availability was a factor experienced within this research. Literature reviews were not able to provide data on fielded DP lasers that could be as a reference to establish laser performance specifically the FR, failure mode comparison or reasons for laser failure. As a result, the approach adopted was to use the laser data supplied by Northrop Grumman since it was applicable and adequate for statistical analysis.

Researchers in addition to reliability practitioners have always struggled with the availability of field data because it is critical to model development. Primarily because any model that is developed requires validation and until validated the model will be of limited use until a comparison of field data versus predicted data is performed.

Research Contribution

This dissertation has opened many avenues for further research in the fields of:

- FR modeling of electro-optical systems.
- Methods to determine laser reliability utilizing the PoF methodology.
- Increasing the knowledge base of DP laser reliability over temperature and vibration.
- Laser failure mode analysis for resonator misalignment.

The ability to determine how environmental conditions such as temperature and vibration impact laser reliability has been theorized but was unproven until the creation of the new DP FR model in this research. The model created is based on established principles of laser design, statistical analysis and reliability engineering principles, thus establishing the credibility and accuracy of the model. The flexibility of the model lends itself to a variety of DP laser FR modeling applications. The research is a significant contribution to reliability engineers and laser researchers since the only DP laser FR model that was created addresses the basic elements of a laser yet the failure modes and mechanism, specifically resonator misalignment was not represented or calculated with the archaic FR model within MIL HDBK 217F Notice 2.

Another benefit of this research is utilizing the model for cost avoidance by laser purchasers such as the US military. Laser technology is being utilized in every aspect of the US military because of the inherent advantages that are offered by laser usage. Most military contractors are faced with the arduous task of designing a laser that meet and in some instances exceed the customer performance specification specifically for contract award. The ability to predict the reliability of a DP laser design prior to field deployment is a significant advantage to limiting

design and production costs. Currently, the inability to determine the predicted FR for a DP laser results in several design decisions being implemented, ultimately leading to an over designed, overpriced and over budget solution. The FR model proposed provides the mechanism for laser designers to create a design/solution that meets 80% of the customer performance requirements at 50% of the cost by making sensible tradeoffs. Accurate calculations of laser life (MTBF) allows the use of more commercially available components in the design and build processes thus reducing the need for custom fabricated components such as mirrors, lens, diodes and q-switches. Custom fabricated optical components are the primary drivers for higher laser manufacturing costs.

APPENDIX: RESONATOR TEMPERATURE TEST REPORTS

Table 21: Sample # 1- (Complete Laser) - Resonator Misalignment Test Report @ -70^{0}C

					S1*(-70 (^{0}C))											
						M1		M2								
Time (mins)	Cycle	Chamber Temp (^{0}C)	Diode Temp (^{0}C)	Heat Load (^{0}C)	Temp Controller	X	Y	X	Y	ΔX (arc min)	ΔY (arc min)	ΔX (μrad)	ΔY (μrad)	Change in ΔX (μrad)	Change in ΔY (μrad)	
0	1	25	25	-70	OFF	3.5	-13.75	-5	5.5	-1.5	-19.25	-436.332	-5599.598	0	0	
30	1	25	80	120	ON	3.5	-15	-5	4.5	-1.5	-19.5	-436.332	-5672.32	0	0	
60	2	-70	-70	-70	OFF	3.5	-12.5	-5	5.5	-1.5	-18	-436.332	-5235.988	0	363.61026	
90	2	-70	80	120	ON	4	-14.5	-5	4.5	-1	-19	-290.888	-5526.876	145.4441	145.4441	<-
120	3	-70	-70	-70	OFF	3.5	-12.5	-5	5.5	-1.5	-18	-436.332	-5235.988	0	363.61026	
150	3	-70	80	120	ON	4	-14	-5	4.75	-1	-18.75	-290.888	-5454.154	145.4441	218.16616	<-
180	4	-70	-70	-70	OFF	3.5	-12.5	-5	5.5	-1.5	-18	-436.332	-5235.988	0	363.61026	
210	4	-70	80	120	ON	4	-14	-5	4.75	-1	-18.75	-290.888	-5454.154	145.4441	218.16616	<-
240	5	-70	-70	-70	OFF	3.5	-12.5	-5	5.5	-1.5	-18	-436.332	-5235.988	0	363.61026	
270	5	-70	80	120	ON	4	-14	-5	4.75	-1	-18.75	-290.888	-5454.154	145.4441	218.16616	<-
300	6	-70	-70	-70	OFF	3.75	-12.5	-5	5.5	-1.25	-18	-363.61	-5235.988	72.722052	363.61026	
330	6	-70	80	120	ON	4	-14	-5	4.75	-1	-18.75	-290.888	-5454.154	145.4441	218.16616	<-
360	7	-70	-70	-70	OFF	3.75	-12.5	-5	5.5	-1.25	-18	-363.61	-5235.988	72.722052	363.61026	
390	7	-70	80	120	ON	4	-14	-5	4.75	-1	-18.75	-290.888	-5454.154	145.4441	218.16616	<-

Table 22: Sample # 2- Resonator Misalignment Test Report @ -70^{0}C

					S2 (-70 °C)											
Time	Cycle	Chamber Temp (°C)	Diode Temp (°C)	Heat Load (°C)	Temp Controller	M1		M2		ΔX (arc min)	ΔY (arc min)	ΔX (µrad)	ΔY (µrad)	Change in ΔX (µrad)	Change in ΔY (µrad)	
						X	Y	X	Y							
0	1	25	25	25	OFF	1.5	-1.5	0	0	1.5	-1.5	436.33	-436.33	0.00	0.00	
30	1	25	80	120	ON	1.75	-1.5	0	0	1.75	-1.5	509.05	-436.33	0.00	0.00	
60	2	-70	-70	-70	OFF	1.5	-1.5	0	0	1.5	-1.5	436.33	-436.33	0.00	0.00	
90	2	-70	80	120	ON	1.25	-2.5	0	0	1.25	-2.5	363.61	-727.22	-145.44	-290.89	<-
120	3	-70	-70	-70	OFF	1.5	-1.5	0	0	1.5	-1.5	436.33	-436.33	0.00	0.00	
150	3	-70	80	120	ON	1.25	-2.5	0	0	1.25	-2.5	363.61	-727.22	-145.44	-290.89	<-
180	4	-70	-70	-70	OFF	1.5	-1.5	0	0	1.5	-1.5	436.33	-436.33	0.00	0.00	
210	4	-70	80	120	ON	1.25	-2.5	0	0	1.25	-2.5	363.61	-727.22	-145.44	-290.89	<-
240	5	-70	-70	-70	OFF	1.5	-1.5	0	0	1.5	-1.5	436.33	-436.33	0.00	0.00	
270	5	-70	80	120	ON	1.25	-2.5	0	0	1.25	-2.5	363.61	-727.22	-145.44	-290.89	<-
300	6	-70	-70	-70	OFF	1.5	-1.5	0	0	1.5	-1.5	436.33	-436.33	0.00	0.00	
330	6	-70	80	120	ON	1.25	-2.5	0	0	1.25	-2.5	363.61	-727.22	-145.44	-290.89	<-
360	7	-70	-70	-70	OFF	1.5	-1.5	0	0	1.5	-1.5	436.33	-436.33	0.00	0.00	
390	7	-70	80	120	ON	1.25	-2.5	0	0	1.25	-2.5	363.61	-727.22	-145.44	-290.89	<-

Table 23: Sample # 1- (Complete Laser) - Resonator Misalignment Test Report @ -55^{0}C

S1* (-55 °C)

Time (mins)	Cycle	Chamber Temp (°C)	Diode Temp (°C)	Heat Load (°C)	Temp Controller	M1		M2		ΔX (arc min)	ΔY (arc min)	ΔX (µrad)	ΔY (µrad)	Change in ΔX (µrad)	Change in ΔY (µrad)	
						X	Y	X	Y							
0	1	25	25	25	OFF	6.5	-5	0	5	6.5	-10	1890.773	-2908.88	0	0	
30	1	25	80	120	ON	6.5	-5.25	0	5	6.5	-10.25	1890.773	-2981.6	0	0	
60	2	-55	-55	-55	OFF	6.5	-5	0	5	6.5	-10	1890.773	-2908.88	0	0	
90	2	-55	80	120	ON	6.25	-5.5	0	5	6.25	-10.5	1818.051	-3054.33	-72.72205218	-72.72205218	<-
120	3	-55	-55	-55	OFF	6.5	-5	0	5	6.5	-10	1890.773	-2908.88	0	0	
150	3	-55	80	120	ON	6.25	-5.5	0	5	6.25	-10.5	1818.051	-3054.33	-72.72205218	-72.72205218	<-
180	4	-55	-55	-55	OFF	6.5	-5	0	5	6.5	-10	1890.773	-2908.88	0	0	
210	4	-55	80	120	ON	6.25	-5.5	0	5	6.25	-10.5	1818.051	-3054.33	-72.72205218	-72.72205218	<-
240	5	-55	-55	-55	OFF	6.5	-5	0	5	6.5	-10	1890.773	-2908.88	0	0	
270	5	-55	80	120	ON	6.25	-5.5	0	5	6.25	-10.5	1818.051	-3054.33	-72.72205218	-72.72205218	<-
300	6	-55	-55	-55	OFF	6.5	-5	0	5	6.5	-10	1890.773	-2908.88	0	0	
330	6	-55	80	120	ON	6.25	-5.5	0	5	6.25	-10.5	1818.051	-3054.33	-72.72205218	-72.72205218	<-
360	7	-55	-55	-55	OFF	6.5	-5	0	5	6.5	-10	1890.773	-2908.88	0	0	
390	7	-55	80	120	ON	6.25	-5.5	0	5	6.25	-10.5	1818.051	-3054.33	-72.72205218	-72.72205218	<-

Table 24: Sample # 2- Resonator Misalignment Test Report @ -55^{0}C

					S2 (-55 °C)											
						M1		M2								
Time (mins)	Cycle	Chamber Temp (^{0}C)	Diode Temp (^{0}C)	Heat Load (^{0}C)	Temp Controller	X	Y	X	Y	ΔX (arc min)	ΔY (arc min)	ΔX (µrad)	ΔY (µrad)	Change in ΔX (µrad)	Change in ΔY (µrad)	
0	1	25	25	25	OFF	-0.5	-1.75	0	2	-0.5	-3.75	-145.444	-1090.83	0	0	
30	1	25	80	120	ON	-0.5	-2	0	2	-0.5	-4	-145.444	-1163.55	0	0	
60	2	-55	-55	-55	OFF	-0.75	-1.75	0	2	-0.75	-3.75	-218.166	-1090.83	72.72205	0	
90	2	-55	80	120	ON	-0.5	-2.25	0	2	-0.5	-4.25	-145.444	-1236.27	0	-72.7221	<-
120	3	-55	-55	-55	OFF	-0.75	-1.75	0	2	-0.75	-3.75	-218.166	-1090.83	-72.7221	0	
150	3	-55	80	120	ON	-0.75	-2.25	0	2	-0.75	-4.25	-218.166	-1236.27	-72.7221	-72.7221	<-
180	4	-55	-55	-55	OFF	-0.75	-1.75	0	2	-0.75	-3.75	-218.166	-1090.83	-72.7221	0	
210	4	-55	80	120	ON	-1	-2.25	0	2	-1	-4.25	-290.888	-1236.27	-145.444	-72.7221	<-
240	5	-55	-55	-55	OFF	-0.75	-1.75	0	2	-0.75	-3.75	-218.166	-1090.83	-72.7221	0	
270	5	-55	80	120	ON	-1	-2.25	0	2	-1	-4.25	-290.888	-1236.27	-145.444	72.72205	<-
300	6	-55	-55	-55	OFF	-0.75	-1.75	0	2	-0.75	-3.75	-218.166	-1090.83	-72.7221	0	
330	6	-55	80	120	ON	-1	-2.25	0	2	-1	-4.25	-290.888	-1236.27	-145.444	72.72205	<-
360	7	-55	-55	-55	OFF	-0.75	-1.75	0	2	-0.75	-3.75	-218.166	-1090.83	-72.7221	0	
390	7	-55	80	120	ON	-1	-2.25	0	2	-1	-4.25	-290.888	-1236.27	-145.444	72.72205	<-

Table 25: Sample # 3- Resonator Misalignment Test Report @ -55^{0}C

S3 (-55 ^{0}C)

Time (mins)	Cycle	Chamber Temp (^{0}C)	Diode Temp (^{0}C)	Heat Load (^{0}C)	Temp Controller	M1		M2		ΔX (arc min)	ΔY (arc min)	ΔX (μrad)	ΔY (μrad)	Change in ΔX (μrad)	Change in ΔY (μrad)	
						X	Y	X	Y							
0	1	25	25	25	OFF	-0.5	-1.75	0	2	-0.5	-3.75	-145.444	-1090.83	0	0	
30	1	25	80	120	ON	-0.5	-2	0	2	-0.5	-4	-145.444	-1163.55	0	0	
60	2	-55	-55	-55	OFF	-0.75	-1.75	0	2	-0.75	-3.75	-218.166	-1090.83	72.72205218	0	
90	2	-55	80	120	ON	-1	-2.5	0	2	-1	-4.5	-290.888	-1309	145.4441044	-145.4441044	<-
120	3	-55	-55	-55	OFF	-0.75	-1.75	0	2	-0.75	-3.75	-218.166	-1090.83	-72.72205218	0	
150	3	-55	80	120	ON	-1	-2.5	0	2	-1	-4.5	-290.888	-1309	-145.4441044	-145.4441044	<-
180	4	-55	-55	-55	OFF	-0.75	-1.75	0	2	-0.75	-3.75	-218.166	-1090.83	-72.72205218	0	
210	4	-55	80	120	ON	-1	-2.5	0	2	-1	-4.5	-290.888	-1309	-145.4441044	-145.4441044	<-
240	5	-55	-55	-55	OFF	-0.75	-1.75	0	2	-0.75	-3.75	-218.166	-1090.83	-72.72205218	0	
270	5	-55	80	120	ON	-1	-2.5	0	2	-1	-4.5	-290.888	-1309	-145.4441044	145.4441044	<-
300	6	-55	-55	-55	OFF	-0.75	-1.75	0	2	-0.75	-3.75	-218.166	-1090.83	-72.72205218	0	
330	6	-55	80	120	ON	-1	-2.5	0	2	-1	-4.5	-290.888	-1309	-145.4441044	145.4441044	<-
360	7	-55	-55	-55	OFF	-0.75	-1.75	0	2	-0.75	-3.75	-218.166	-1090.83	-72.72205218	0	
390	7	-55	80	120	ON	-1	-2.5	0	2	-1	-4.5	-290.888	-1309	-145.4441044	145.4441044	<-

Table 26: Sample # 4- Resonator Misalignment Test Report @ -55^{0}C

					S4 (-55 °C)											
						M1		M2								
Time (mins)	Cycle	Chamber Temp (°C)	Diode Temp (°C)	Heat Load (°C)	Temp Controller	X	Y	X	Y	ΔX (arc min)	ΔY (arc min)	ΔX (µrad)	ΔY (µrad)	Change in ΔX (µrad)	Change in ΔY (µrad)	
0	1	25	25	25	OFF	-0.75	-1.25	0	1.5	-0.75	-2.75	-218.166	-799.943	0	0	
30	1	25	80	120	ON	1	-1.5	0	1.5	1	-3	290.8882	-872.665	0	0	
60	2	-55	-55	-55	OFF	-1	-1.75	0	1.5	-1	-3.25	-290.888	-945.387	-72.72205218	-145.4441044	
90	2	-55	80	120	ON	-1.25	-2	0	1.5	-1.25	-3.5	-363.61	-1018.11	-654.4984696	-145.4441044	<-
120	3	-55	-55	-55	OFF	-1	-1.25	0	1.5	-1	-2.75	-290.888	-799.943	-72.72205218	0	
150	3	-55	80	120	ON	-1.25	-2	0	1.5	-1.25	-3.5	-363.61	-1018.11	-654.4984696	-145.4441044	<-
180	4	-55	-55	-55	OFF	-0.75	-1.25	0	1.5	-0.75	-2.75	-218.166	-799.943	0	0	
210	4	-55	80	120	ON	-1	-2	0	1.5	-1	-3.5	-290.888	-1018.11	-581.7764174	-145.4441044	<-
240	5	-55	-55	-55	OFF	-0.75	-1.25	0	1.5	-0.75	-2.75	-218.166	-799.943	0	0	
270	5	-55	80	120	ON	-1	-2	0	1.5	-1	-3.5	-290.888	-1018.11	-581.7764174	-145.4441044	<-
300	6	-55	-55	-55	OFF	-0.75	-1.25	0	1.5	-0.75	-2.75	-218.166	-799.943	0	0	
330	6	-55	80	120	ON	-1	-2	0	1.5	-1	-3.5	-290.888	-1018.11	-581.7764174	-145.4441044	<-
360	7	-55	-55	-55	OFF	-0.75	-1.25	0	1.5	-0.75	-2.75	-218.166	-799.943	0	0	
390	7	-55	80	120	ON	-1	-2	0	1.5	-1	-3.5	-290.888	-1018.11	-581.7764174	-145.4441044	<-

Table 27: Sample # 5- Resonator Misalignment Test Report @ -55^{0}C

S5 (-55 °C)

Time (mins)	Cycle	Chamber Temp (°C)	Diode Temp (°C)	Heat Load (°C)	Temp Controller	M1		M2		ΔX (arc min)	ΔY (arc min)	ΔX (µrad)	ΔY (µrad)	Change in ΔX (µrad)	Change in ΔY (µrad)	
						X	Y	X	Y							
0	1	25	25	25	OFF	0.5	-1.5	0	1	0.5	-2.5	145.4441	-727.221	0	0	
30	1	25	80	128	ON	0.5	-2.25	0.25	0.5	0.25	-2.75	72.72205	-799.943	0	0	
60	2	-55	-55	-55	OFF	0.5	-3.5	0	-0.75	0.5	-2.75	145.4441	-799.943	0	-72.72205218	
90	2	-55	80	124	ON	0.5	-5	0.5	-2	0	-3	0	-872.665	-72.72205218	-72.72205218	<-
120	3	-55	-55	-55	OFF	0.5	-3.5	0.25	-1	0.25	-2.5	72.72205	-727.221	-72.72205218	0	
150	3	-55	80	124	ON	0.5	-5.5	0.75	-2.25	-0.25	-3.25	-72.7221	-945.387	-145.4441044	-145.4441044	<-
180	4	-55	-55	-55	OFF	0.5	-3.5	0.25	-1	0.25	-2.5	72.72205	-727.221	-72.72205218	0	
210	4	-55	80	124	ON	0.5	-5.5	0.75	-2.25	-0.25	-3.25	-72.7221	-945.387	-145.4441044	-145.4441044	<-
240	5	-55	-55	-55	OFF	0.5	-3.5	0.25	-1	0.25	-2.5	72.72205	-727.221	-72.72205218	0	
270	5	-55	80	124	ON	0.5	-5.5	0.75	-2.25	-0.25	-3.25	-72.7221	-945.387	-145.4441044	-145.4441044	<-
300	6	-55	-55	-55	OFF	0.5	-3.25	0.25	-0.75	0.25	-2.5	72.72205	-727.221	-72.72205218	0	
330	6	-55	80	124	ON	0.5	-5.5	0.75	-2.25	-0.25	-3.25	-72.7221	-945.387	-145.4441044	-145.4441044	<-
360	7	-55	-55	-55	OFF	0.25	-4	0.25	-1.5	0	-2.5	0	-727.221	-145.4441044	0	
390	7	-55	80	124	ON	0.5	-5.5	0.75	-2.25	-0.25	-3.25	-72.7221	-945.387	-145.4441044	-145.4441044	<-

Table 28: Sample # 6- Resonator Misalignment Test Report @ -55^{0}C

					S6 (-55 °C)											
						M1		M2								
Time (mins)	Cycle	Chamber Temp (°C)	Diode Temp (°C)	Heat Load (°C)	Temp Controller	X	Y	X	Y	ΔX (arc min)	ΔY (arc min)	ΔX (µrad)	ΔY (µrad)	Change in ΔX (µrad)	Change in ΔY (µrad)	
0	1	25	25	25	OFF	0.25	-1.75	0	1	0.25	-2.75	72.72205	-799.943	0	0	
30	1	25	80	120	ON	0.25	-1.75	0	1	0.25	-2.75	72.72205	-799.943	0	0	
60	2	-55	-55	-55	OFF	0	-1.5	0	1	0	-2.5	0	-727.221	-72.72205218	72.72205218	
90	2	-55	80	120	ON	0	-2	0	1	0	-3	0	-872.665	-72.72205218	-72.72205218	<-
120	3	-55	-55	-55	OFF	0	-1.5	0	1	0	-2.5	0	-727.221	-72.72205218	72.72205218	
150	3	-55	80	120	ON	0	-2.25	0	1	0	-3.25	0	-945.387	-72.72205218	-145.4441044	<-
180	4	-55	-55	-55	OFF	0	-1.5	0	1	0	-2.5	0	-727.221	-72.72205218	72.72205218	
210	4	-55	80	120	ON	0	-2.25	0	1	0	-3.25	0	-945.387	-72.72205218	-145.4441044	<-
240	5	-55	-55	-55	OFF	0	-1.5	0	1	0	-2.5	0	-727.221	-72.72205218	72.72205218	
270	5	-55	80	120	ON	0	-2.25	0	1	0	-3.25	0	-945.387	-72.72205218	-145.4441044	<-
300	6	-55	-55	-55	OFF	0	-1.5	0	1	0	-2.5	0	-727.221	-72.72205218	72.72205218	
330	6	-55	80	120	ON	0	-2.25	0	1	0	-3.25	0	-945.387	-72.72205218	-145.4441044	<-
360	7	-55	-55	-55	OFF	0	-1.5	0	1	0	-2.5	0	-727.221	-72.72205218	72.72205218	
390	7	-55	80	120	ON	0	-2.25	0	1	0	-3.25	0	-945.387	-72.72205218	-145.4441044	<-

Table 29: Sample # 7- Resonator Misalignment Test Report @ -55^{0}C

S7 (-55 °C)

Time (mins)	Cycle	Chamber Temp (°C)	Diode Temp (°C)	Heat Load (°C)	Temp Controller	M1		M2		ΔX (arc min)	ΔY (arc min)	ΔX (µrad)	ΔY (µrad)	Change in ΔX (µrad)	Change in ΔY (µrad)	
						X	Y	X	Y							
0	1	25	25	25	OFF	-1.5	-0.5	0	2	-1.5	-2.5	-436.332	-727.221	0	0	
30	1	25	80	120	ON	-1.75	-0.5	0	2	-1.75	-2.5	-509.054	-727.221	0	0	
60	2	-55	-55	-55	OFF	-1.5	-0.5	0	2	-1.5	-2.5	-436.332	-727.221	0	0	
90	2	-55	80	120	ON	-2	-1	0	2	-2	-3	-581.776	-872.665	-72.72205218	-145.4441044	<-
120	3	-55	-55	-55	OFF	-1.5	-0.5	0	2	-1.5	-2.5	-436.332	-727.221	0	0	
150	3	-55	80	120	ON	-2	-1	0	2	-2	-3	-581.776	-872.665	-72.72205218	-145.4441044	<-
180	4	-55	-55	-55	OFF	-1.5	-0.5	0	2	-1.5	-2.5	-436.332	-727.221	0	0	
210	4	-55	80	120	ON	-2	-1	0	2	-2	-3	-581.776	-872.665	-72.72205218	-145.4441044	<-
240	5	-55	-55	-55	OFF	-1.5	-0.5	0	2	-1.5	-2.5	-436.332	-727.221	0	0	
270	5	-55	80	120	ON	-2	-1	0	2	-2	-3	-581.776	-872.665	-72.72205218	-145.4441044	<-
300	6	-55	-55	-55	OFF	-1.5	-0.5	0	2	-1.5	-2.5	-436.332	-727.221	0	0	
330	6	-55	80	120	ON	-2	-1	0	2	-2	-3	-581.776	-872.665	-72.72205218	-145.4441044	<-
360	7	-55	-55	-55	OFF	-1.5	-0.5	0	2	-1.5	-2.5	-436.332	-727.221	0	0	
390	7	-55	80	120	ON	-2	-1	0	2	-2	-3	-581.776	-872.665	-72.72205218	-145.4441044	<-

Table 30: Sample # 8- Resonator Misalignment Test Report @ -55^{0}C

					S8 (-55 °C)											
						M1		M2								
Time (mins)	Cycle	Chamber Temp (°C)	Diode Temp (°C)	Heat Load (°C)	Temp Controller	X	Y	X	Y	ΔX (arc min)	ΔY (arc min)	ΔX (µrad)	ΔY (µrad)	Change in ΔX (µrad)	Change in ΔY (µrad)	
0	1	25	25	25	OFF	-0.75	-1.75	0	2.5	-0.75	-4.25	-218.166	-1236.27	0	0	
30	1	25	80	120	ON	-0.75	-2	0	2.5	-0.75	-4.5	-218.166	-1309	0	0	
60	2	-55	-55	-55	OFF	-0.75	-1.75	0	2.5	-0.75	-4.25	-218.166	-1236.27	0	0	
90	2	-55	80	120	ON	-1	-2.25	0	2.5	-1	-4.75	-290.888	-1381.72	-72.72205218	-72.72205217	<-
120	3	-55	-55	-55	OFF	-0.75	-1.75	0	2.5	-0.75	-4.25	-218.166	-1236.27	0	0	
150	3	-55	80	120	ON	-1	-2.25	0	2.5	-1	-4.75	-290.888	-1381.72	-72.72205218	-72.72205217	<-
180	4	-55	-55	-55	OFF	-0.75	-1.75	0	2.5	-0.75	-4.25	-218.166	-1236.27	0	0	
210	4	-55	80	120	ON	-1	-2.25	0	2.5	-1	-4.75	-290.888	-1381.72	-72.72205218	-72.72205217	<-
240	5	-55	-55	-55	OFF	-0.75	-1.75	0	2.5	-0.75	-4.25	-218.166	-1236.27	0	0	
270	5	-55	80	120	ON	-1	-2.25	0	2.5	-1	-4.75	-290.888	-1381.72	-72.72205218	-72.72205217	<-
300	6	-55	-55	-55	OFF	-0.75	-1.75	0	2.5	-0.75	-4.25	-218.166	-1236.27	0	0	
330	6	-55	80	120	ON	-1	-2.25	0	2.5	-1	-4.75	-290.888	-1381.72	-72.72205218	-72.72205217	<-
360	7	-55	-55	-55	OFF	-0.75	-1.75	0	2.5	-0.75	-4.25	-218.166	-1236.27	0	0	
390	7	-55	80	120	ON	-1	-2.25	0	2.5	-1	-4.75	-290.888	-1381.72	-72.72205218	-72.72205217	<-

Table 31: Sample # 9- Resonator Misalignment Test Report @ -55^{0}C

S9 (-55 °C)

Time (mins)	Cycle	Chamber Temp (°C)	Diode Temp (°C)	Heat Load (°C)	Temp Controller	M1 X	M1 Y	M2 X	M2 Y	ΔX (arc min)	ΔY (arc min)	ΔX (μrad)	ΔY (μrad)	Change in ΔX (μrad)	Change in ΔY (μrad)	
0	1	25	25	25	OFF	0.25	-1.75	0	1	0.25	-2.75	72.72205	-799.943	0	0	
30	1	25	80	120	ON	0.25	-1.75	0	1	0.25	-2.75	72.72205	-799.943	0	0	
60	2	-55	-55	-55	OFF	0	-1.5	0	1	0	-2.5	0	-727.221	-72.7221	72.72205	
90	2	-55	80	120	ON	0	-2	0	1	0	-3	0	-872.665	-72.7221	-72.7221	<-
120	3	-55	-55	-55	OFF	0	-1.5	0	1	0	-2.5	0	-727.221	-72.7221	72.72205	
150	3	-55	80	120	ON	0	-2.25	0	1	0	-3.25	0	-945.387	-72.7221	-145.444	<-
180	4	-55	-55	-55	OFF	0	-1.5	0	1	0	-2.5	0	-727.221	-72.7221	72.72205	
210	4	-55	80	120	ON	0	-2	0	1	0	-3	0	-872.665	-72.7221	-72.7221	<-
240	5	-55	-55	-55	OFF	0	-1.5	0	1	0	-2.5	0	-727.221	-72.7221	72.72205	
270	5	-55	80	120	ON	0	-2	0	1	0	-3	0	-872.665	-72.7221	-72.7221	<-
300	6	-55	-55	-55	OFF	0	-1.5	0	1	0	-2.5	0	-727.221	-72.7221	72.72205	
330	6	-55	80	120	ON	0	-2	0	1	0	-3	0	-872.665	-72.7221	-72.7221	<-
360	7	-55	-55	-55	OFF	0	-1.5	0	1	0	-2.5	0	-727.221	-72.7221	72.72205	
390	7	-55	80	120	ON	0	-2	0	1	0	-3	0	-872.665	-72.7221	-72.7221	<-

Table 32: Sample # 10- Resonator Misalignment Test Report @ -55^{0}C

S10 (-55 °C)

Time (mins)	Cycle	Chamber Temp (°C)	Diode Temp (°C)	Heat Load (°C)	Temp Controller	M1 X	M1 Y	M2 X	M2 Y	ΔX (arc min)	ΔY (arc min)	ΔX (µrad)	ΔY (µrad)	Change in ΔX (µrad)	Change in ΔY (µrad)	
0	1	25	25	25	OFF	-0.5	-2.5	0	2.5	-0.5	-5	-145.444	-1454.44	0	0	
30	1	25	80	120	ON	-0.75	-2.5	0	2.5	-0.75	-5	-218.166	-1454.44	0	0	
60	2	-55	-55	-55	OFF	-0.5	-2.5	0	2.5	-0.5	-5	-145.444	-1454.44	0	0	
90	2	-55	80	120	ON	-0.5	-2.25	0	2.5	-0.5	-4.75	-145.444	-1381.72	72.72205218	72.72205218	<-
120	3	-55	-55	-55	OFF	-0.5	-2.5	0	2.5	-0.5	-5	-145.444	-1454.44	0	0	
150	3	-55	80	120	ON	-0.5	-2	0	2.5	-0.5	-4.5	-145.444	-1309	72.72205218	145.4441044	<-
180	4	-55	-55	-55	OFF	-0.5	-2.5	0	2.5	-0.5	-5	-145.444	-1454.44	0	0	
210	4	-55	80	120	ON	-0.5	-2	0	2.5	-0.5	-4.5	-145.444	-1309	72.72205218	145.4441044	<-
240	5	-55	-55	-55	OFF	-0.5	-2.5	0	2.5	-0.5	-5	-145.444	-1454.44	0	0	
270	5	-55	80	120	ON	-0.5	-2	0	2.5	-0.5	-4.5	-145.444	-1309	72.72205218	145.4441044	<-
300	6	-55	-55	-55	OFF	-0.5	-2.5	0	2.5	-0.5	-5	-145.444	-1454.44	0	0	
330	6	-55	80	120	ON	-0.5	-2	0	2.5	-0.5	-4.5	-145.444	-1309	72.72205218	145.4441044	<-
360	7	-55	-55	-55	OFF	-0.5	-2.5	0	2.5	-0.5	-5	-145.444	-1454.44	0	0	
390	7	-55	80	120	ON	-0.5	-2	0	2.5	-0.5	-4.5	-145.444	-1309	72.72205218	145.4441044	<-

Table 33: Sample # 11- Resonator Misalignment Test Report @ -55^{0}C

S11 (-55 °C)

Time (mins)	Cycle	Chamber Temp (°C)	Diode Temp (°C)	Heat Load (°C)	Temp Controller	M1		M2		ΔX (arc min)	ΔY (arc min)	ΔX (µrad)	ΔY (µrad)	Change in ΔX (µrad)	Change in ΔY (µrad)	
						X	Y	X	Y							
0	1	25	25	25	OFF	-0.5	-1.75	0	0	-0.5	-1.75	-145.444	-509.054	0	0	
30	1	25	80	120	ON	-0.5	-1.75	0	0	-0.5	-1.75	-145.444	-509.054	0	0	
60	2	-55	-55	-55	OFF	-0.5	-1.75	0	0	-0.5	-1.75	-145.444	-509.054	0	0	
90	2	-55	80	120	ON	-0.5	-1.25	0	0	-0.5	-1.25	-145.444	-363.61	0	145.4441044	<-
120	3	-55	-55	-55	OFF	-0.5	-1.75	0	0	-0.5	-1.75	-145.444	-509.054	0	0	
150	3	-55	80	120	ON	-0.5	-1.5	0	0	-0.5	-1.5	-145.444	-436.332	0	72.72205218	<-
180	4	-55	-55	-55	OFF	-0.5	-1.75	0	0	-0.5	-1.75	-145.444	-509.054	0	0	
210	4	-55	80	120	ON	-0.5	-1.5	0	0	-0.5	-1.5	-145.444	-436.332	0	72.72205218	<-
240	5	-55	-55	-55	OFF	-0.5	-1.75	0	0	-0.5	-1.75	-145.444	-509.054	0	0	
270	5	-55	80	120	ON	-0.5	-1.5	0	0	-0.5	-1.5	-145.444	-436.332	0	72.72205218	<-
300	6	-55	-55	-55	OFF	-0.5	-1.75	0	0	-0.5	-1.75	-145.444	-509.054	0	0	
330	6	-55	80	120	ON	-0.5	-1.5	0	0	-0.5	-1.5	-145.444	-436.332	0	72.72205218	<-
360	7	-55	-55	-55	OFF	-0.5	-1.75	0	0	-0.5	-1.75	-145.444	-509.054	0	0	
390	7	-55	80	120	ON	-0.5	-1.5	0	0	-0.5	-1.5	-145.444	-436.332	0	72.72205218	<-

Table 34: Sample # 12- Resonator Misalignment Test Report @ -55^{0}C

S12 (-55 °C)

Time (mins)	Cycle	Chamber Temp (°C)	Diode Temp (°C)	Heat Load (°C)	Temp Controller	M1 X	M1 Y	M2 X	M2 Y	ΔX (arc min)	ΔY (arc min)	ΔX (µrad)	ΔY (µrad)	Change in ΔX (µrad)	Change in ΔY (µrad)	
0	1	25	25	25	OFF	1	-1.5	0	1	1	-2.5	290.8882	-727.221	0	0	
30	1	25	80	120	ON	1	-1.75	0	1	1	-2.75	290.8882	-799.943	0	0	
60	2	-55	-55	-55	OFF	1	-1.5	0	1	1	-2.5	290.8882	-727.221	0	0	
90	2	-55	80	120	ON	1	-2	0	1	1	-3	290.8882	-872.665	0	-72.72205218	<-
120	3	-55	-55	-55	OFF	1	-1.5	0	1	1	-2.5	290.8882	-727.221	0	0	
150	3	-55	80	120	ON	1	-2	0	1	1	-3	290.8882	-872.665	0	-72.72205218	<-
180	4	-55	-55	-55	OFF	1	-1.5	0	1	1	-2.5	290.8882	-727.221	0	0	
210	4	-55	80	120	ON	1	-2	0	1	1	-3	290.8882	-872.665	0	-72.72205218	<-
240	5	-55	-55	-55	OFF	1	-1.5	0	1	1	-2.5	290.8882	-727.221	0	0	
270	5	-55	80	120	ON	1	-2	0	1	1	-3	290.8882	-872.665	0	-72.72205218	<-
300	6	-55	-55	-55	OFF	1	-1.5	0	1	1	-2.5	290.8882	-727.221	0	0	
330	6	-55	80	120	ON	1	-2	0	1	1	-3	290.8882	-872.665	0	-72.72205218	<-
360	7	-55	-55	-55	OFF	1	-1.5	0	1	1	-2.5	290.8882	-727.221	0	0	
390	7	-55	80	120	ON	1	-2	0	1	1	-3	290.8882	-872.665	0	-72.72205218	<-

Table 35: Sample # 13- Resonator Misalignment Test Report @ -55^{0}C

					S13 (-55 °C)											
						M1		M2								
Time (mins)	Cycle	Chamber Temp (°C)	Diode Temp (°C)	Heat Load (°C)	Temp Controller	X	Y	X	Y	ΔX (arc min)	ΔY (arc min)	ΔX (µrad)	ΔY (µrad)	Change in ΔX (µrad)	Change in ΔY (µrad)	
0	1	25	25	25	OFF	0.5	-2	0	2	0.5	-4	145.4441	-1163.55	0	0	
30	1	25	80	120	ON	0.25	-2	0	2	0.25	-4	72.72205	-1163.55	0	0	
60	2	-55	-55	-55	OFF	0.25	-1.75	0	2	0.25	-3.75	72.72205	-1090.83	-72.72205218	72.72205218	
90	2	-55	80	120	ON	0	-2.5	0	2	0	-4.5	0	-1309	-72.72205218	-145.4441044	<-
120	3	-55	-55	-55	OFF	0.25	-1.75	0	2	0.25	-3.75	72.72205	-1090.83	-72.72205218	72.72205218	
150	3	-55	80	120	ON	0	-2.5	0	2	0	-4.5	0	-1309	-72.72205218	-145.4441044	<-
180	4	-55	-55	-55	OFF	0.25	-1.75	0	2	0.25	-3.75	72.72205	-1090.83	-72.72205218	72.72205218	
210	4	-55	80	120	ON	0	-2.5	0	2	0	-4.5	0	-1309	-72.72205218	-145.4441044	<-
240	5	-55	-55	-55	OFF	0.25	-1.75	0	2	0.25	-3.75	72.72205	-1090.83	-72.72205218	72.72205218	
270	5	-55	80	120	ON	0	-2.5	0	2	0	-4.5	0	-1309	-72.72205218	-145.4441044	<-
300	6	-55	-55	-55	OFF	0.25	-1.5	0	2	0.25	-3.5	72.72205	-1018.11	-72.72205218	145.4441044	
330	6	-55	80	120	ON	0	-2.5	0	2	0	-4.5	0	-1309	-72.72205218	-145.4441044	<-
360	7	-55	-55	-55	OFF	0.25	-1.5	0	2	0.25	-3.5	72.72205	-1018.11	-72.72205218	145.4441044	
390	7	-55	80	120	ON	0	-2.5	0	2	0	-4.5	0	-1309	-72.72205218	-145.4441044	<-

Table 36: Sample # 14- Resonator Misalignment Test Report @ -55^{0}C

					S14 (-55 °C)											
						M1		M2								
Time (mins)	Cycle	Chamber Temp (°C)	Diode Temp (°C)	Heat Load (°C)	Temp Controller	X	Y	X	Y	ΔX (arc min)	ΔY (arc min)	ΔX (µrad)	ΔY (µrad)	Change in ΔX (µrad)	Change in ΔY (µrad)	
0	1	25	25	25	OFF	0.5	-1.5	0	1	0.5	-2.5	145.4441	-727.221	0	0	
30	1	25	80	120	ON	0.5	-1.75	0	1	0.5	-2.75	145.4441	-799.943	0	0	
60	2	-55	-55	-55	OFF	0.5	-1.5	0	1	0.5	-2.5	145.4441	-727.221	0	0	
90	2	-55	80	120	ON	0.25	-2	0	1	0.25	-3	72.72205	-872.665	-72.72205218	-72.72205218	<-
120	3	-55	-55	-55	OFF	0.5	-1.5	0	1	0.5	-2.5	145.4441	-727.221	0	0	
150	3	-55	80	120	ON	0.25	-2	0	1	0.25	-3	72.72205	-872.665	-72.72205218	-72.72205218	<-
180	4	-55	-55	-55	OFF	0.5	-1.5	0	1	0.5	-2.5	145.4441	-727.221	0	0	
210	4	-55	80	120	ON	0.25	-2	0	1	0.25	-3	72.72205	-872.665	-72.72205218	-72.72205218	<-
240	5	-55	-55	-55	OFF	0.5	-1.5	0	1	0.5	-2.5	145.4441	-727.221	0	0	
270	5	-55	80	120	ON	0.25	-2	0	1	0.25	-3	72.72205	-872.665	-72.72205218	-72.72205218	<-
300	6	-55	-55	-55	OFF	0.5	-1.5	0	1	0.5	-2.5	145.4441	-727.221	0	0	
330	6	-55	80	120	ON	0.25	-2	0	1	0.25	-3	72.72205	-872.665	-72.72205218	-72.72205218	<-
360	7	-55	-55	-55	OFF	0.5	-1.5	0	1	0.5	-2.5	145.4441	-727.221	0	0	
390	7	-55	80	120	ON	0.25	-2	0	1	0.25	-3	72.72205	-872.665	-72.72205218	-72.72205218	<-

Table 37: Sample # 15- Resonator Misalignment Test Report @ -55^{0}C

S15 (-55 °C)

Time (mins)	Cycle	Chamber Temp (°C)	Diode Temp (°C)	Heat Load (°C)	Temp Controller	M1		M2		ΔX (arc min)	ΔY (arc min)	ΔX (µrad)	ΔY (µrad)	Change in ΔX (µrad)	Change in ΔY (µrad)	
						X	Y	X	Y							
0	1	25	25	25	OFF	0.5	-1	0	1	0.5	-2	145.4441	-581.776	0	0	
30	1	25	80	120	ON	0.5	-1	0	1	0.5	-2	145.4441	-581.776	0	0	
60	2	-55	-55	-55	OFF	0	-0.75	0	1	0	-1.75	0	-509.054	-145.4441044	72.72205218	
90	2	-55	80	120	ON	0	-1.5	0	1	0	-2.5	0	-727.221	-145.4441044	-145.4441044	<-
120	3	-55	-55	-55	OFF	0.5	-1	0	1	0.5	-2	145.4441	-581.776	0	0	
150	3	-55	80	120	ON	0	-1.5	0	1	0	-2.5	0	-727.221	-145.4441044	-145.4441044	<-
180	4	-55	-55	-55	OFF	0.5	-0.75	0	1	0.5	-1.75	145.4441	-509.054	0	72.72205218	
210	4	-55	80	120	ON	0	-1.5	0	1	0	-2.5	0	-727.221	-145.4441044	-145.4441044	<-
240	5	-55	-55	-55	OFF	0.25	-0.5	0	1	0.25	-1.5	72.72205	-436.332	-72.72205218	145.4441044	
270	5	-55	80	120	ON	0	-1.5	0	1	0	-2.5	0	-727.221	-145.4441044	-145.4441044	<-
300	6	-55	-55	-55	OFF	0.25	-0.5	0	1	0.25	-1.5	72.72205	-436.332	-72.72205218	145.4441044	
330	6	-55	80	120	ON	0	-1.5	0	1	0	-2.5	0	-727.221	-145.4441044	-145.4441044	<-
360	7	-55	-55	-55	OFF	0.25	-0.5	0	1	0.25	-1.5	72.72205	-436.332	-72.72205218	145.4441044	
390	7	-55	80	120	ON	0	-1.5	0	1	0	-2.5	0	-727.221	-145.4441044	-145.4441044	<-

Table 38: Sample # 16- Resonator Misalignment Test Report @ -55^{0}C

S16 (-55 °C)

Time (mins)	Cycle	Chamber Temp (°C)	Diode Temp (°C)	Heat Load (°C)	Temp Controller	M1		M2		ΔX (arc min)	ΔY (arc min)	ΔX (µrad)	ΔY (µrad)	Change in ΔX (µrad)	Change in ΔY (µrad)	
						X	Y	X	Y							
0	1	25	25	25	OFF	0	-1.5	0	1	0	-2.5	0	-727.221	0	0	
30	1	25	80	120	ON	0	-1.5	0	1	0	-2.5	0	-727.221	0	0	
60	2	-55	-55	-55	OFF	0	-1.25	0	1	0	-2.25	0	-654.498	0	72.72205217	
90	2	-55	80	120	ON	0	-2	0	1	0	-3	0	-872.665	0	-145.4441044	<-
120	3	-55	-55	-55	OFF	0	-1.5	0	1	0	-2.5	0	-727.221	0	0	
150	3	-55	80	120	ON	0	-2	0	1	0	-3	0	-872.665	0	-145.4441044	<-
180	4	-55	-55	-55	OFF	0	-1.25	0	1	0	-2.25	0	-654.498	0	72.72205217	
210	4	-55	80	120	ON	0	-2	0	1	0	-3	0	-872.665	0	-145.4441044	<-
240	5	-55	-55	-55	OFF	0	-1.5	0	1	0	-2.5	0	-727.221	0	0	
270	5	-55	80	120	ON	0	-2	0	1	0	-3	0	-872.665	0	-145.4441044	<-
300	6	-55	-55	-55	OFF	0	-1.25	0	1	0	-2.25	0	-654.498	0	72.72205217	
330	6	-55	80	120	ON	0	-2	0	1	0	-3	0	-872.665	0	-145.4441044	<-
360	7	-55	-55	-55	OFF	0	-1.25	0	1	0	-2.25	0	-654.498	0	72.72205217	
390	7	-55	80	120	ON	0	-2	0	1	0	-3	0	-872.665	0	-145.4441044	<-

Table 39: Sample # 17- Resonator Misalignment Test Report @ -55^{0}C

S17 (-55 °C)

Time (mins)	Cycle	Chamber Temp (°C)	Diode Temp (°C)	Heat Load (°C)	Temp Controller	M1		M2		ΔX (arc min)	ΔY (arc min)	ΔX (µrad)	ΔY (µrad)	Change in ΔX (µrad)	Change in ΔY (µrad)	
						X	Y	X	Y							
0	1	25	25	25	OFF	0.5	-0.5	0	0	0.5	-0.5	145.4441	-145.444	0	0	
30	1	25	80	120	ON	0.5	-0.75	0	0	0.5	-0.75	145.4441	-218.166	0	0	
60	2	-55	-55	-55	OFF	0.5	-0.5	0	0	0.5	-0.5	145.4441	-145.444	0	0	
90	2	-55	80	120	ON	0.75	-1	0	0	0.75	-1	218.1662	-290.888	72.72205218	-72.72205218	<-
120	3	-55	-55	-55	OFF	0.5	-0.5	0	0	0.5	-0.5	145.4441	-145.444	0	0	
150	3	-55	80	120	ON	0.75	-1	0	0	0.75	-1	218.1662	-290.888	72.72205218	-72.72205218	<-
180	4	-55	-55	-55	OFF	0.5	-0.5	0	0	0.5	-0.5	145.4441	-145.444	0	0	
210	4	-55	80	120	ON	0.75	-1.25	0	0	0.75	-1.25	218.1662	-363.61	72.72205218	-145.4441044	<-
240	5	-55	-55	-55	OFF	0.5	-0.5	0	0	0.5	-0.5	145.4441	-145.444	0	0	
270	5	-55	80	120	ON	0.75	-1.25	0	0	0.75	-1.25	218.1662	-363.61	72.72205218	-145.4441044	<-
300	6	-55	-55	-55	OFF	0.5	-0.5	0	0	0.5	-0.5	145.4441	-145.444	0	0	
330	6	-55	80	120	ON	0.75	-1.25	0	0	0.75	-1.25	218.1662	-363.61	72.72205218	-145.4441044	<-
360	7	-55	-55	-55	OFF	0.5	-0.5	0	0	0.5	-0.5	145.4441	-145.444	0	0	
390	7	-55	80	120	ON	0.75	-1.25	0	0	0.75	-1.25	218.1662	-363.61	72.72205218	-145.4441044	<-

Table 40: Sample # 18- Resonator Misalignment Test Report @ -55^{0}C

S 18 (-55 °C)

Time (mins)	Cycle	Chamber Temp (°C)	Diode Temp (°C)	Heat Load (°C)	Temp Controller	M1		M2		ΔX (arc min)	ΔY (arc min)	ΔX (μrad)	ΔY (μrad)	Change in ΔX (μrad)	Change in ΔY (μrad)	
						X	Y	X	Y							
0	1	25	25	25	OFF	0	-1.75	0	0	0	-1.75	0	-509.054	0	0	
30	1	25	80	120	ON	0	-2	0	0	0	-2	0	-581.776	0	0	
60	2	-55	-55	-55	OFF	0	-1.75	0	0	0	-1.75	0	-509.054	0	0	
90	2	-55	80	120	ON	0	-2.25	0	0	0	-2.25	0	-654.498	0	-72.72205218	<-
120	3	-55	-55	-55	OFF	0	-1.5	0	0	0	-1.5	0	-436.332	0	72.72205218	
150	3	-55	80	120	ON	0	-2.25	0	0	0	-2.25	0	-654.498	0	-72.72205218	<-
180	4	-55	-55	-55	OFF	0	-1.5	0	0	0	-1.5	0	-436.332	0	72.72205218	
210	4	-55	80	120	ON	0	-2.25	0	0	0	-2.25	0	-654.498	0	-72.72205218	<-
240	5	-55	-55	-55	OFF	0	-1.5	0	0	0	-1.5	0	-436.332	0	72.72205218	
270	5	-55	80	120	ON	0	-2.25	0	0	0	-2.25	0	-654.498	0	-72.72205218	<-
300	6	-55	-55	-55	OFF	0	-1.5	0	0	0	-1.5	0	-436.332	0	72.72205218	
330	6	-55	80	120	ON	0	-2.25	0	0	0	-2.25	0	-654.498	0	-72.72205218	<-
360	7	-55	-55	-55	OFF	0	-1.5	0	0	0	-1.5	0	-436.332	0	72.72205218	
390	7	-55	80	120	ON	0	-2.25	0	0	0	-2.25	0	-654.498	0	-72.72205218	<-

Table 41: Sample # 19- Resonator Misalignment Test Report @ -55^{0}C

S19 (-55 °C)

Time (mins)	Cycle	Chamber Temp (°C)	Diode Temp (°C)	Heat Load (°C)	Temp Controller	M1		M2		ΔX (arc min)	ΔY (arc min)	ΔX (µrad)	ΔY (µrad)	Change in ΔX (µrad)	Change in ΔY (µrad)	
						X	Y	X	Y							
0	1	25	25	25	OFF	0.5	-2.75	0	0	0.5	-2.75	145.4441	-799.943	0	0	
30	1	25	80	120	ON	0.25	-3	0	0	0.25	-3	72.72205	-872.665	0	0	
60	2	-55	-55	-55	OFF	0.25	-2.5	0	0	0.25	-2.5	72.72205	-727.221	-72.72205218	72.72205218	
90	2	-55	80	120	ON	0	-3.25	0	0	0	-3.25	0	-945.387	-72.72205218	-72.72205217	<-
120	3	-55	-55	-55	OFF	0	-2.5	0	0	0	-2.5	0	-727.221	-145.4441044	72.72205218	
150	3	-55	80	120	ON	0	-3.25	0	0	0	-3.25	0	-945.387	-72.72205218	-72.72205217	<-
180	4	-55	-55	-55	OFF	0	-2.5	0	0	0	-2.5	0	-727.221	-145.4441044	72.72205218	
210	4	-55	80	120	ON	0	-3.25	0	0	0	-3.25	0	-945.387	-72.72205218	-72.72205217	<-
240	5	-55	-55	-55	OFF	0	-2.5	0	0	0	-2.5	0	-727.221	-145.4441044	72.72205218	
270	5	-55	80	120	ON	0	-3.25	0	0	0	-3.25	0	-945.387	-72.72205218	-72.72205217	<-
300	6	-55	-55	-55	OFF	0	-2.5	0	0	0	-2.5	0	-727.221	-145.4441044	72.72205218	
330	6	-55	80	120	ON	0	-3.25	0	0	0	-3.25	0	-945.387	-72.72205218	-72.72205217	<-
360	7	-55	-55	-55	OFF	0	-2.5	0	0	0	-2.5	0	-727.221	-145.4441044	72.72205218	
390	7	-55	80	120	ON	0	-3.25	0	0	0	-3.25	0	-945.387	-72.72205218	-72.72205217	<-

Table 42: Sample # 20- Resonator Misalignment Test Report @ -55^{0}C

S20 (-55 °C)

Time (mins)	Cycle	Chamber Temp (°C)	Diode Temp (°C)	Heat Load (°C)	Temp Controller	M1		M2		ΔX (arc min)	ΔY (arc min)	ΔX (µrad)	ΔY (µrad)	Change in ΔX (µrad)	Change in ΔY (µrad)	
						X	Y	X	Y							
0	1	25	25	25	OFF	0	-2.5	0	0	0	-2.5	0	-727.221	0	0	
30	1	25	80	120	ON	0	-2.5	0	0	0	-2.5	0	-727.221	0	0	
60	2	-55	-55	-55	OFF	-0.25	-2	0	0	-0.25	-2	-72.7221	-581.776	-72.72205218	145.4441044	
90	2	-55	80	120	ON	0	-2.75	0	0	0	-2.75	0	-799.943	0	-72.72205218	<-
120	3	-55	-55	-55	OFF	-0.25	-2	0	0	-0.25	-2	-72.7221	-581.776	-72.72205218	145.4441044	
150	3	-55	80	120	ON	0	-2.75	0	0	0	-2.75	0	-799.943	0	-72.72205218	<-
180	4	-55	-55	-55	OFF	0	-2	0	0	0	-2	0	-581.776	0	145.4441044	
210	4	-55	80	120	ON	-0.25	-2.75	0	0	-0.25	-2.75	-72.7221	-799.943	-72.72205218	-72.72205218	<-
240	5	-55	-55	-55	OFF	0	-2	0	0	0	-2	0	-581.776	0	145.4441044	
270	5	-55	80	120	ON	-0.25	-2.75	0	0	-0.25	-2.75	-72.7221	-799.943	-72.72205218	-72.72205218	<-
300	6	-55	-55	-55	OFF	-0.25	-2	0	0	-0.25	-2	-72.7221	-581.776	-72.72205218	145.4441044	
330	6	-55	80	120	ON	-0.25	-2.75	0	0	-0.25	-2.75	-72.7221	-799.943	-72.72205218	-72.72205218	<-
360	7	-55	-55	-55	OFF	-0.25	-2	0	0	-0.25	-2	-72.7221	-581.776	-72.72205218	145.4441044	
390	7	-55	80	120	ON	-0.25	-2.75	0	0	-0.25	-2.75	-72.7221	-799.943	-72.72205218	-72.72205218	<-

Table 43: Sample # 21- Resonator Misalignment Test Report @ -55^{0}C

S21 (-55 °C)

Time (mins)	Cycle	Chamber Temp (°C)	Diode Temp (°C)	Heat Load (°C)	Temp Controller	M1		M2		ΔX (arc min)	ΔY (arc min)	ΔX (μrad)	ΔY (μrad)	Change in ΔX (μrad)	Change in ΔY (μrad)	
						X	Y	X	Y							
0	1	25	25	25	OFF	0.5	-1.5	0	1	0.5	-2.5	145.4441	-727.221	0	0	
30	1	25	80	120	ON	0.5	-1.75	0	1	0.5	-2.75	145.4441	-799.943	0	0	
60	2	-55	-55	-55	OFF	0.5	-1.5	0	1	0.5	-2.5	145.4441	-727.221	0	0	
90	2	-55	80	120	ON	0.25	-2	0	1	0.25	-3	72.72205	-872.665	-72.72205218	-72.72205218	<-
120	3	-55	-55	-55	OFF	0.5	-1.5	0	1	0.5	-2.5	145.4441	-727.221	0	0	
150	3	-55	80	120	ON	0.25	-2	0	1	0.25	-3	72.72205	-872.665	-72.72205218	-72.72205218	<-
180	4	-55	-55	-55	OFF	0.5	-1.5	0	1	0.5	-2.5	145.4441	-727.221	0	0	
210	4	-55	80	120	ON	0.25	-2	0	1	0.25	-3	72.72205	-872.665	-72.72205218	-72.72205218	<-
240	5	-55	-55	-55	OFF	0.5	-1.5	0	1	0.5	-2.5	145.4441	-727.221	0	0	
270	5	-55	80	120	ON	0.25	-2	0	1	0.25	-3	72.72205	-872.665	-72.72205218	-72.72205218	<-
300	6	-55	-55	-55	OFF	0.5	-1.5	0	1	0.5	-2.5	145.4441	-727.221	0	0	
330	6	-55	80	120	ON	0.25	-2	0	1	0.25	-3	72.72205	-872.665	-72.72205218	-72.72205218	<-
360	7	-55	-55	-55	OFF	0.5	-1.5	0	1	0.5	-2.5	145.4441	-727.221	0	0	
390	7	-55	80	120	ON	0.25	-2	0	1	0.25	-3	72.72205	-872.665	-72.72205218	-72.72205218	<-

Table 44: Sample # 22- Resonator Misalignment Test Report @ -55^{0}C

S22 (-55 °C)

Time (mins)	Cycle	Chamber Temp (°C)	Diode Temp (°C)	Heat Load (°C)	Temp Controller	M1		M2		ΔX (arc min)	ΔY (arc min)	ΔX (μrad)	ΔY (μrad)	Change in ΔX (μrad)	Change in ΔY (μrad)	
						X	Y	X	Y							
0	1	25	25	25	OFF	0.5	1.75	0	0	0.5	1.75	145.4441	509.0544	0	0	
30	1	25	80	120	ON	0.5	1.75	0	0	0.5	1.75	145.4441	509.0544	0	0	
60	2	-55	-55	-55	OFF	0.75	2	0	0	0.75	2	218.16616	581.7764	72.72205218	72.72205218	
90	2	-55	80	120	ON	1	2	0	0	1	2	290.88821	581.7764	145.4441044	72.72205218	<-
120	3	-55	-55	-55	OFF	0.75	2	0	0	0.75	2	218.16616	581.7764	72.72205218	72.72205218	
150	3	-55	80	120	ON	1	2.25	0	0	1	2.25	290.88821	654.4985	145.4441044	145.4441044	<-
180	4	-55	-55	-55	OFF	0.75	2	0	0	0.75	2	218.16616	581.7764	72.72205218	72.72205218	
210	4	-55	80	120	ON	1	2.25	0	0	1	2.25	290.88821	654.4985	145.4441044	145.4441044	<-
240	5	-55	-55	-55	OFF	0.75	2	0	0	0.75	2	218.16616	581.7764	72.72205218	72.72205218	
270	5	-55	80	120	ON	1	2.25	0	0	1	2.25	290.88821	654.4985	145.4441044	145.4441044	<-
300	6	-55	-55	-55	OFF	0.75	2	0	0	0.75	2	218.16616	581.7764	72.72205218	72.72205218	
330	6	-55	80	120	ON	1	2.25	0	0	1	2.25	290.88821	654.4985	145.4441044	145.4441044	<-
360	7	-55	-55	-55	OFF	0.75	2	0	0	0.75	2	218.16616	581.7764	72.72205218	72.72205218	
390	7	-55	80	120	ON	1	2.25	0	0	1	2.25	290.88821	654.4985	145.4441044	145.4441044	<-

REFERENCES

Applied Optics Research. (Unknown). Maker of GLAD Laser and Physical Optics Software. 3/13/11, www.aor.com

Burger, L., Forbes, A. (2008). Porro Prism Resonators- A New Perspective. Optical Technologies for Arming, Safing, Fuzing, and Firing IV, Vol. 7070.

Crocker, M.J. (2007). Handbook of Noise and Vibration Control. John Wiley & Sons, Hoboken, New Jersey, Pg 432.

Cushing, M.J., Mortin, D.E., Stadterman, T.J., Malhot, A. (1993) Comparison of Electronics Reliability Assessment Approaches. IEEE Transactions on Reliability, Vol. 42, 542-546.

Denson, W.K., Keene, S., Caroli, J., (1998). A New System Reliability Assessment Methodology. Annual Reliability and Maintainability Symposium. IEEE.Pg.413-420.

Dylis, D.D., Priore, M.G., (2001). A Comprehensive Reliability Assessment Tool for Electronic Systems. Annual Reliability Maintainability Symposium. IEEE.Pg.308-313.

Groebel, D.J., Mettas, A., Sun, F., (2001). Determination and Interpretation of Activation Energy Using Accelerated- Test Data. Annual Reliability Symposium. IEEE.Pg. 58-61.

Hartler, G., (1986). Parameter Estimation for the Arrhenius Model. IEEE Transactions on Reliability, Vol. R35 N.4, 414-418.

Hauck, R., Kortz, H.P., Weber, H., (1980). Misalignment Sensitivity of Optical Resonators. Applied Optics, Vol. 19 N. 4.

Hodgson, N., Weber, H., (2005). Laser Resonator and Beam Propagation: Fundamentals, Advanced Concepts and Applications. New York, N.Y, Springer Publishing.

Ireson, G. W., Coombs, C. F., Moss, R. Y., (1988). Handbook of Reliability Engineering. New York, N.Y., McGraw- Hill.

Jones, J., Hayes, J., (1999). A Comparison of Electronic- Reliability Prediction Models. IEEE Transactions on Reliability, Vol. 48 N. 2, Pg 127-134.

Koechner, W., (2006). Solid State Laser Engineering. New York, N.Y., Springer Publishing.

Krasich, M., (2009). How to Estimate and Use MTTF/MTBF Would the Real MTBF Please Stand Up. Reliability and Maintainability Symposium, Pg 353-359.

Kurowki, P.M., (2004). Finite Element Analysis for Design Engineers. Warrendale, Pennsylvania, Society of Automotive Engineers. Inc.

Lee, J., Leung, C., (1988). Beam Pointing Direction Changes in a Misaligned Porro Prism Resonator. Applied Optics, Vol. 27 N. 13, Pg 2701-2707.

Liu, J., Li, G., Wang, C., Shao, Z., Jiang, M., (1999). Thermal Lens Stabilized Flat- Flat Resonator 15-W CW Nd; YVO4 Laser End Pumped by a Diode-Laser-Array. Proceedings of SPIE, Vol. 3862, Pg 267-269.

Magni, V., (1987). Multi- Element Stable Resonators Containing a Variable Lens. Journal of Optical Society of America, Vol. 4 N. 10 Pg 1962-1969.

Manthos, E., (2004). The Merits and Limitation of Reliability Predictions. Annual Reliability and Maintainability Symposium. IEEE, Pg. 352-357.

Mettas, A., Vassiliou, P., (2002). Modeling and Analysis of Time dependent Stress Accelerated Life Data. Annual Reliability and Maintainability Symposium. IEEE, Pg. 343-348.

McLeish, J. G., (2010). Enhancing MIL-HDBK-217 Reliability Predictions with Physics of Failure Methods. Annual Reliability and Maintainability Symposium. IEEE, Pg. 1-6.

McLeish, J. G., (2010). Transitioning to Physics of Failure Reliability Assessments for Electronics. March, 8, 2011, www.dfrsolutions.com/uploads/publications/2010-08_ISSAR.pdf

Mitchell, P. V., Griffith, P. B., Henderson, D. K., (2001). Fast Steering Mirrors Improve Active Beam Stabilization. January 10, 2011,www.optoelectronics-world.com

Myung, J., (2003). Tutorial on Maximum Likelihood Estimation. Journal of Mathematical, N. 47, Pg 90-100.

Nelson, W., (1990). Accelerated Testing: Statistical Models, Test Plans and Data Analyses. Hoboken, New Jersey, John Wiley and Sons.

Nelson, W., (1972). Graphical Analysis of Accelerated Life Test Data with the Inverse Power Law Model. IEEE Transactions on Reliability, Vol. R-21 N. 1, Pg 2-11.

Nicholls, D. (2007). What is 217Plus and where did it come from. Annual Reliability and Maintainability Symposium, IEEE. Pg.22-27.

Nicholls, D., (2007). An Introduction to the RIAC 217 PLUS Component Failure Rate Models. February 17, 2011, www.theriac.org/riacapps/journal/IntroductionTo217PlusComponentModels.pdf.com. Pg16-21

Nicholls, D., Avak, A., Mazurowski, J., (2008). Photonic Component and Subsystem Reliability. Avionics, Fiber- Optics and Photonics Technology Conference. IEEE. Pg 49-50.

Nicholls, D., Mazurowski, J., Avak, A., Hackert, M. (2010). Photonic Component and Subsystem Reliability Modeling. Annual Reliability and Maintainability Symposium. IEEE. Pg.1-6

Ozberkmen, Y. C., (1989). Fostering and Funding Military Laser R&D. Optics News, Pg. 16-19.

Perkins, J.F., Jones, R. W., (1984). Effect of Unstable Resonator Misalignment in the Cusping Domain. Applied Optics, Vol. 23 N. 2.

Pikey, W. D., (1997). Peterson's Stress Concentration Factors. Hoboken, New Jersey, John Wiley & Sons.

Rapaport, A., Weichman, L., Brickeen, B., Green, S., Bass, M., (2001). Laser Resonator Design Using Optical Ray Tracing Software: Comparisons with Simple Analytical Models and Experimental Results. IEEE Journal of Quantum Electronics, Vol. 37, Pg. 1401- 1408.

Thiraviam, A., Foley, T., Malone, L., (2010). Development of an Acceleration Model for Subsea Pressure. Annual Reliability and Maintainability Symposium IEEE. Pg. 1- 6

White, M., Bernstein, B., (2008). Microelectronics Reliability: Physics of failure Based Modeling and Lifetime Evaluation. December 2, 2010. www.Trs new.jpl.nasa.gov/dspace/bitstream/2014/40791/1/1/08-05.pdf.